2011

Continuous, Passive Liquid-Liquid Extraction and Emulsion Separation Within Microfluidic and Millifluidic Devices

Janet Tesfai
Bucknell University

I, Janet T. Tesfai, do grant permission for my thesis to be copied.

CONTINUOUS, PASSIVE LIQUID-LIQUID EXTRACTION AND EMULSION SEPARATION WITHIN MICROFLUIDIC AND MILLIFLUIDIC DEVICES

By

Janet T. Tesfai

A Thesis

Presented to the Faculty of

Bucknell University

In Partial Fulfillment of the Requirements for the Degree of

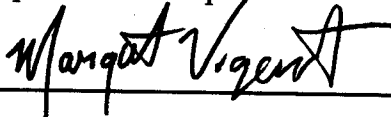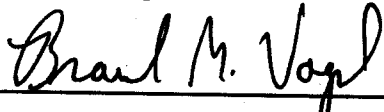Master of Science in Chemical Engineering

Approved:

_____
Adviser

_____
Department Chairperson

_____
Engineering Thesis Committee Member

_____
Engineering Thesis Committee Member

May 2011

Acknowledgments

I want to express my gratitude towards my advisor, Professor Erin Jablonski, for all her guidance and support during my years at Bucknell. Professor Jablonski's enthusiasm toward this project not only inspired me participate in this program but also made research an enjoyable experience. I would also like to thank my thesis committee members, Professor Brandon Vogel and Professor Margot Vigeant, for their assistance in developing and completing this thesis.

I would like to thank Professor William King and Professor Ryan Snyder for their assistance with data analysis, saving me countless hours of calculation by trial and error. I would also like to give thanks to Diane Hall for her assistance in the lab and Nancy Lamay for her never-ending supply of moral support.

Many thanks go to Renee Perry, the former graduate student working on this project, for bestowing me with all her knowledge and for her patience while training me. I want to thank my fellow graduate students for their support and for reminding me to persevere through the more trying times of this process.

Finally, I would like to thank my family for supporting me over the years. Their encouragement and belief in me made this achievement possible.

Table of Contents

List of Figures

List of Tables

Abbreviations

LLE - Liquid-liquid extraction

Irgacure 2959 - 4-(2-hydroxyethoxy)phenyl-(2-hydroxy-2-propyl) ketone

PEG-DA - Poly (ethylene glycol) - diacrylate

PDMS - Poly(dimethylsiloxane)

SAM - Self-assembled monolayer

TPM - 3-(trichlorosilyl)-propyl methacrylate

Abstract

Liquid-liquid extraction (LLE) is a method used to separate compounds based on their relative activity in two immiscible phases. However, conventional liquid-liquid extraction requires the use of large volumes of fluids to achieve separation, making this process undesirable for expensive materials. By significantly reducing the scale of liquid-liquid extraction to the micro- and milli-fluidic levels, this separation process can be made suitable for low volume, high value materials. A practical application of microfluidic liquid-liquid extraction is the passive separation and purification of biomolecules. Currently, other separation techniques risk degrading the biomolecule by heating (evaporation) or mechanical force (centrifugation) or result in the loss of product (filtration). Microfluidic extraction of a desired compound occurs by the parallel flow of an aqueous solvent against an organic solvent. An optical adhesive channel is created by photolithographic techniques and channel surface modification and a poly(ethylene glycol) hydrogel are used to stabilize the adjacent laminar flow of the two phases. The channel is treated with a solution containing a self-assembled monolayer in order for the hydrogel to adhere to the glass channel walls and to modify the channel with the deposition of less hydrophilic groups. The hydrogel is cured to define one wall of the optical adhesive channel. Due to hydrophilic interactions and weak non-polar interactions, respectively, the aqueous stream is stabilized along the hydrogel boundary and the organic stream is stabilized along the optical adhesive boundary, resulting in a stable interface for diffusion between the two immiscible liquids.

With a small adjustment to the position of the organic inlet needle, the device for liquid-liquid extraction can be applied to the separation of emulsions after formation within a microfluidic device. A major application of emulsion separation is wastewater treatment. Many large manufacturers, such as the petrochemical, pharmaceutical, and food industries produce large volumes of oily wastewater. Current methods of wastewater treatment have low efficiency and high operational costs. The device described above is able to achieve separation efficiencies of greater than 80%. By placing the organic inlet needle at the interface of the hydrogel and aqueous stream, the oil boundary layer surrounding each aqueous droplet is disrupted, allowing the aqueous droplet to migrate into the continuous water stream.

By scaling these separations up to the milli-fluidic scale, it is possible to maintain the benefits of microfluidic flow such as confined flow and mixing by diffusion while eliminating some of the disadvantages such as large pressure drops, low flow rates, and susceptibility to device damage by clogging.

Chapter 1. Overview

Microfluidics is a rapidly developing field with great potential to revolutionize how experiments are being performed by providing quicker results with higher throughput at lower costs[1]. Microfluidics is defined as the study of fluid flow in channels with dimensions on the sub-millimeter scale, where diffusion, surface/interfacial tension, and viscosity dominate the effects of gravity and inertia[2]. This thesis deals strictly with the flow of immiscible liquids. Two types of flow can result when dealing with the small scale flow of immiscible liquids: slug flow, the alternating flow of segmented fragments of immiscible fluids, and parallel flow, the side-by-side flow of immiscible fluids[3]. The capillary number can be used to determine the likelihood of slug and parallel flow. The capillary number is a ratio of viscous forces to interfacial tension and is defined as

$$Ca = \frac{viscous\ forces}{liquid - liquid\ interfacial\ tension} = \frac{\mu v}{\gamma}$$

where μ is viscosity, *v* is fluid velocity, and γ is interfacial tension. A capillary number less than 1 means the effects of interfacial tension dominate, resulting in a decrease in the interfacial area between the two immiscible phases. Whether a decrease in interfacial area results in slug flow or parallel flow is highly channel geometry dependent. Thus, a capillary number less than 1 can result in parallel or slug flow. A capillary number greater than 1 means the effects of viscosity dominate, resulting in parallel flow[3]. The Weber number is a ratio of a fluid's inertia to its interfacial tension and characterizes the interfacial stability between multiphase flow. This dimensionless value can be used to predict the disruption of an interface under strong inertial forces. The Weber number is defined as

$$We = \frac{inertial\ forces}{liquid - liquid\ interfacial\ tension} = \frac{\rho v^2 D_H}{\gamma}$$

$$D_H = \frac{4A}{P_W}$$

where ρ is the fluid density, D_H is the hydraulic diameter, A is the cross-sectional area, and P_W is the wetted perimeter. A Weber number less than 1 means the forces of interfacial tension are strong enough to maintain a stable interface between the two phases. A Weber number greater than 1 indicates that inertial forces dominate interfacial tension, resulting in turbulent and chaotic flow at the interface[3].

Fluid flow at the microfluidic scale results in confined flow due to the significant decrease in channel diameter, as characterized by a Reynolds number below 2000. Reynolds number for a non-circular conduit is defined as[4]

$$Re = \frac{inertial\ forces}{viscous\ forces} = \frac{\rho v D_H}{\mu}.$$

The numerator of the Reynolds number represents inertial forces while the denominator represents viscous forces. Thus, when a Reynolds number is greater than 2000 inertial forces dominate the flow regime and when a Reynolds number is below 2000, viscous forces dominate the flow regime, resulting in confined flow. Confined flow allows for separation and molecular transport to occur by diffusion rather than convective mixing[2]. The considerable decrease in fluid volume also results in an increased interfacial area-to-volume ratio allowing for a potential increase in mass transfer dependent upon channel geometry.

Milli-fluidics deals with fluid flow within channels whose critical dimensions are on the order of millimeters. Milli-fluidic operations are the intermediate between industrial processes and microfluidic processes. When moving down to the milli-fluidic scale from the industrial scale, benefits such as increased system control and faster performance time are achieved. Both of these advantages are due to the predictability of mixing and transport processes and the increase in interfacial area-to-volume ratio at the milli-scale. The uniformity of the process at this scale also results in a more consistent and reliable product when compared to the macroscale. Much like microfluidics, milli-fluidic operations offer the benefits of mixing by diffusion, control over heat transfer, and laminar flow. By increasing channel dimensions to the millimeter scale, the occurrence of solids-related damage in the form of fouling is decreased, the pressure drop over the length of the channel is decreased, and the processing capability of the device is increased[5].

This thesis explores the application of micro- and milli-fluidic devices for liquid-liquid extraction and water-in-oil emulsion separation. Emulsion separation is carried out at the milli-fluidic level and scaled up to determine the maximum emulsion processing capability of this separation method. Liquid-liquid extraction is carried out at the microfluidic level and scaled up to the milli-fluidic level, to maximize the interfacial area-to-volume ratio, resulting in greater extraction efficiency. The design of the micro- and milli-fluidic separation devices used in this thesis for emulsion separation and liquid-liquid extraction was proposed by Daniel Mayo and successfully applied to capsule separation by Renee N. Perry[6,7]. The ability of the separation device to separate

hydrophilic capsules led to the use of this separation device for the separation of emulsions[7]. Renee N. Perry demonstrated that it is possible to apply the separation device for emulsion breaking[7]. The idea of using a similar separation device design for liquid-liquid extraction and emulsion separation is explored and the efficiency of each system is quantified in this thesis.

Liquid-liquid extraction is a separation technique based on a compound's relative activity in two immiscible liquids, generally an aqueous solvent and organic solvent. The driving force for mass transfer is the difference in a compound's activity within those phases[8]. Conventional LLE functions on a density difference between the two immiscible phases as the driving force for countercurrent flow within a bubble column, requiring a density difference between the two immiscible solvents and a difference in the compound's concentration in the each of the immiscible solvents. The less dense phase enters at the bottom of the bubble column and flows upward while the denser phase enters at the top of the column and flows downward. Implementation of this mass transfer operation is time consuming, labor intensive, and results in the use of large volumes of material making it undesirable for the separation of low volume, high value materials[9]. The large volume of material could potentially be harmful to the operator and hazardous to the environment making it an undesirable option when toxic materials are being used[10].

An emulsion is a dispersion of liquid droplets in a continuous, immiscible, liquid medium[11]. An application of micro- and milli-fluidic devices that will be explored in this thesis is emulsion breaking. Emulsions requiring separation are often the byproduct of a

chemical production process and need to be separated for proper disposal or are the result of microreactor chemistry and need to be separated for product recovery. Microreactors are reactor systems with channel dimensions on the sub-micrometer to the sub-millimeter range used in various fields of science and engineering. These microreactors can be created by water-in oil emulsions, where oil serves as a boundary to diffusion, allowing the aqueous droplet to function as a self-contained reactor[12]. Once reactions are completed, it is necessary to recover the product within the microreactors.

By combining the fluid properties available at the micro- and milli-scale with separation techniques, separation can be achieved using a smaller volume of fluids resulting in lower solvent consumption, lower waste production, shorter analytical times, smaller space requirements, and lower energy consumption[13]. The potential for increased interfacial area-to-volume ratio based on channel geometry due to micro- and milli-fluidic flow can result in more efficient transport between the two liquid streams[2]. Micro- and milli-scale separation are accomplished by the co-current laminar flow of two immiscible fluids resulting in a pinned interface capable of behaving as a membrane for mass transfer, as shown in Figure 1.1[10]. Micro- and milli-scale liquid-liquid extraction can also be applied for the determination of mass transfer coefficients. The current use of conventional LLE to estimate mass transfer coefficients is unreliable due to many assumptions that are made when estimating the mass transfer area between the dispersed and continuous phases. Some of these assumptions are that all droplets are perfectly spherical, are the same size, and move at the same velocity[14]. Since the form of micro- and milli-fluidic extraction described here results in a well defined mass transfer interface

with known dimensions, it is a more dependable method for determining mass transfer coefficients.
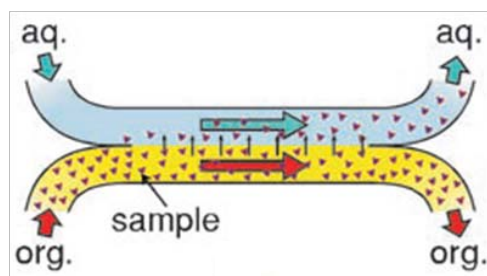
Figure 1.1. Co-current laminar flow[15].

This thesis explores the application of micro- and milli-fluidic devices for liquid-liquid extraction, mass transfer coefficient determination, and efficient emulsion separation. Furthermore, this thesis demonstrates the usefulness of milli-fluidic devices as a practical separation method. Milli-fluidic devices exhibit many of the beneficial fluid properties of microfludic devices while being able to process larger volumes of fluid per time. Milli-fluidic device dimensions are small enough that mixing occurs by diffusion, laminar flow occurs, and heat transfer can be easily controlled. By increasing the dimensions of the channel within the separation device to the millimeter scale, the occurrence of fouling is decreased and a larger volume of material can be processed per time[5].

1.1 References

(1) Clayton, J. Go with the Microflow. *Nature Methods.* **2005**, 2, 621-627.

(2) Atencia, J.; Beebe, D. J. Controlled Microfluidic Interfaces. *Nature.* **2005**, 437, 648-655.

(3) Dessimoz, A. L.; Cavin, L.; Renken, A.; Kiwi-Minsker, L. Liquid-liquid two-phase flow patterns and mass transfer characteristics in rectangular glass microreactors. *Chemical Engineering Science.* **2008**, 63, 4035-4044.

(4) Narayana, P. A. A.; Seetharamu, K. N. *Engineering Fluid Mechanics;* Alpha Science International: India, 2005.

(5) Jonsson, M.; Johnson, B. Millichannel Reactors: A Practical Middle Ground for Production. *Chemical Engineering*. **2009**, 116, 44-50.

(6) Mayo, D. Calcium alginate encapsulation and continuous separation of the capsules through co-laminar flow of immiscible fluids. Master's Thesis, Bucknell University, 2008.

(7) Perry, R. N. Continuous formation and separation of calcium-alginate capsules containing viable mammalian cells in microfluidic devices. Master's Thesis, Bucknell University, 2010.

(8) Treybal, R. E. *Mass-transfer Operations,* 3rd ed.; McGraw-Hill Book Company: Singapore, 1980.

(9) Sun, M.; Du, W.; Fang, Q.; Microfluidic Liquid-liquid Extraction System Based on Stopped-flow Technique and Liquid Core Waveguide Capillary. *Talanta.* **2006**, 70, 392-396.

(10) Silvestre, C. I. C.; Santos. J. L. M.; Lima, J. L. F. C.; Zagatto, E. A. G. Liquid-liquid Extraction in Flow Analysis: A Critical Review. *Analytica Chimica Acta*. **2009**, 652, 54-65.

(11) Derkach, S. R. Rheology of Emulsions. *Advances in Colloid and Interface Science*. **2009**, 151, 1-23.

(12) Ehrfeld, W; Hessel, V; Lowe, H. *Microreactors: New Technology for Modern Chemistry;* Wiley-VCH: Germany, 2000.

(13) Berduque, A.; O'Brien, J.; Alderman, J.; Arrigan, D. W. M. Microfluidic Chip for Electrochemically-modulated Liquid-Liquid Extraction of Ions. *Electrochemisty Communications*. **2008**, 10, 20-24.

(14) Saien, J.; Daliri, S.; Modelling Mass Transfer Coefficient for Liquid-liquid Extraction with the Interface Adsorption of Hydroxyl Ions. *Korean Journal of Chemical Engineering.* **2009**, 26, 963-968.

(15) Aota, A.; Nonaka, M.; Hibara, A; Kitamori, T. Countercurrent Laminar Microflow for Highly Efficient Solvent Extraction. *Angew. Chem. Int. Ed.* **2007**, 46, 878-880.

Chapter 2. Liquid-Liquid Extraction at the Micro- and Milli-fluidic Scale

2.1 Background

2.1.1 Conventional Liquid-Liquid Extraction

Liquid-liquid extraction is a separation technique utilizing two immiscible liquids, generally water and an organic solvent, for the removal of a desired compound, referred to as the solute. The solution containing the solute to be extracted is the feed and the solvent used to extract the solute is the extractant. The driving force for mass transfer is the difference in a compound's activity within those phases[1]. The extraction efficiency of the separation can be maximized by maximizing the interfacial area and decreasing the mass transfer resistance. Interfacial area can be increased by forming smaller droplets of the dispersed phase. However, droplet size must be balanced against throughput and emulsion formation. As the droplet size decreases, a smaller volume of feed can be supplied for extraction. Also, smaller droplets result in more stable emulsions which are more difficult to separate. Mass transfer resistance can be decreased by increasing temperature, resulting in lower fluid viscosity[2].

The types of extractors that can be used for extraction can be separated into four categories: mixers-settlers, centrifugal extractors, unagitated columns, and agitated columns. Mixer-settlers are tanks containing agitators. The feed solution containing the solute and the solvent for the extraction are supplied to the tank. The contents are then mixed and allowed to settle. The light phase is removed from the top of the tank and the heavy phase is removed from the bottom of the tank. Gravity settling based on the density difference between the two phases is the main separation mechanism in this

extraction method. In some cases, the mixer and settler are two separate vessels. Centrifugal extractors are made up of a series of perforated cylinders. The light and heavy phases are supplied to the outer and inner cylinders, respectively, while the cylinders are rotated. The two phases contact as they pass through the perforated cylinders. The main advantage of centrifugal extractors is the process' low residence time. A density difference is the mechanism for separation of the two immiscible phases. However, a large density difference is not required since a centripetal force is applied to accelerate separation. Unagitated columns function on differences in interfacial tension and density between the two immiscible phases for countercurrent flow within the column. The less dense phase enters at the bottom of the bubble column and flows upward while the denser phase enters at the top of the column and flows downward. The light phase and heavy phase are collected from the top and bottom of the column, respectively. A high interfacial tension between the two fluids would make it easier for droplets of the dispersed phase to coalesce prior to collection. To function well, unagitated columns require a significant difference between the density of the two immiscible solvents and the compound's concentration in the respective phases. Agitated columns typically use turbine impellers or rotating discs to maintain dispersions over a wider range of operating conditions. A high interfacial tension is still beneficial for effective droplet coalescence[3].

LLE is typically used to increase the concentration of a solute in a particular phase, for solvent recovery, or for product recovery. However, many of these conventional extraction methods require an additional separation step after extraction has

been completed to separate the resulting emulsion. Because of the necessity for an additional separation process after extraction, LLE is used when it is either the only method available or the most economical option[4]. Some situations when conventional LLE would be applied are for the separation of mixtures with similar boiling points, for the separation of heat-sensitive materials, and for the recovery of non-volatile compounds[2].

2.1.2 Micro- and Milli-fluidics

Microfluidics is the science of systems that manipulate small volumes of fluid, 10^{-9} to 10^{-8} liters, in channels with dimensions on the order of tens to hundreds of micrometers[5]. Microfluidics is a rapidly developing field with great potential to revolutionize how experiments are being performed by providing faster results with higher throughput at lower costs[6]. Microfluidic devices were initially fabricated from silicon and glass, materials that were successfully used to create microdevices in the fields of microelectronics and microelectromechanical systems. However, these materials were less appropriate for the applications of microfluidics, which require flexibility for micropumps and microvalves, transparency for optical detection, and a quick fabrication procedure. For these reasons, polymers eventually came to replace silicon and glass as the material of choice in microfluidic device fabrication. The most frequently used polymer for device fabrication is poly(dimethylsiloxane), PDMS. PDMS is a low cost, clear, flexible elastomer with strong adhesive properties, making it an ideal material for microfluidic applications. The procedure for creating a PDMS

microfluidic device is quick and can be completed in a few hours. First a master, or template, of the device design is created using a photoresist and photolithographic methods. The PDMS prepolymer and curing agent are combined and react, forming a cross-linked elastomer. The PDMS mixture is poured over the template and heat cured, resulting in a solid polymer slab with channels defined by the master. Due to the flexibility and low surface energy of the PDMS, the PDMS slab is easily peeled off the master without damage to the PDMS slab or the master. The slab can now be reversibly sealed to itself or a silicon, glass, or thermoplastic surface. Reversible seals are watertight but unable to withstand pressures greater than 5 psi. For an irreversible seal, the surface of the PDMS and the substrate are oxidized using air plasma and sealed. This sealing procedure is effective on glass, silicon, polystyrene, polyethylene, silicon nitride, and PDMS[7].

Although PDMS devices are convenient for many microfluidic applications, they are unsuitable for use with most organic solvents. When exposed to organic solvents, such as toluene, PDMS absorbs the solvent and swells. For applications involving harsh solvents, it is necessary to have a solvent resistant and transparent material and a low cost microfluidic fabrication technique with rapid prototyping. Harrison et al. developed a photolithographic method of microfluidic fabrication using two glass plates separated by spacers, a photomask, and a thiolene-based optical adhesive. Spacers, which define the channel width, are placed on either side of the glass plate. The optical adhesive is applied to the glass plate and the second glass plate is applied at a shallow angle to avoid air bubble formation. A photomask is applied to the second glass slide to define the

channel and the optical adhesive is exposed to UV light. If a negative tone photoresist is used, then the areas of optical adhesive which are exposed to UV light crosslink and harden. The areas shielded from UV exposure can then be removed by solvent injection. If a positive tone photoresist is used, then the areas of optical adhesive exposed to UV light become soluble to a developer solution. The excess photoresist is removed by immersion in a developer solution. This microfluidic fabrication technique created by Harrison et al. is capable of yielding channels from micrometers to millimeters deep. Unlike many other photolithographic methods, this technique is capable of producing a channel height gradient within a device[8].

Some current applications of microfluidics are in the fields of chemistry, biochemistry, and biology. In chemistry, these devices are often used to demonstrate principles of fluid flow and handle small scale reactions. In biochemistry, microfluidic devices are most often used for the bioanalysis of human bodily fluid samples and environmental samples. In biology, microfluidic devices are an ideal medium for cell growth and observation since devices are fabricated from transparent, low toxicity polymers[5].

Microfluidic devices are defined as devices with dimensions on the sub-millimeter scale[9]; while milli-scale devices have critical dimensions on the millimeter scale[10]. With fluid flow occurring in small channels, diffusion, surface/interfacial tension, and viscosity dominate the effects of gravity and inertia[11]. Three dimensionless numbers, as shown in Table 2.1, are significant in characterizing such small scale flows. The Reynolds number indicates whether flow within the channel will be laminar, Re < 2000,

or turbulent, Re > 2300. In micro- and milli-fluidic systems, laminar flow can generally be expected. There are two types of liquid-liquid two phase flow that can result when working with liquids at the micro- and milli-fluidic scales: slug flow and parallel flow. The capillary number can be used to predict the presence of such flow. A capillary number less than 1 indicates that the forces of interfacial tension dominate viscous forces, resulting in a decrease in the interfacial area. Depending on device geometry, a decrease in interfacial area could lead to slug flow or parallel flow. A capillary number greater than 1 results in parallel flow due to the viscous fluid's resistance to shear which extends the interface down the length of the channel. The Weber number is used to predict when inertial forces become so significant that they lead to instabilities at the interface of two-phase flow. A Weber number greater than 1 is indicative of flow instabilities.

Table 2.1. Summary of dimensionless quantities used to characterize small scale liquid flow.

Dimensionless Number	Ratio	Equation	Implications
Reynolds	$\dfrac{inertial\ forces}{viscous\ forces}$	$\dfrac{\rho v D_H}{\mu}$	Re < 2000 → laminar flow Re > 2300 → turbulent flow
Capillary	$\dfrac{viscous\ forces}{liquid-liquid\ interfacial\ tension}$	$\dfrac{\mu v}{\gamma}$	Ca < 1 → reduce interfacial area Ca > 1 → parallel flow
Weber	$\dfrac{inertial\ forces}{liquid-liquid\ interfacial\ tension}$	$\dfrac{\rho v^2 D_H}{\gamma}$	We < 1 → stable interface We > 1 → unstable interface

Both slug flow and parallel flow have advantages and disadvantages when used successfully for liquid-liquid extraction. An advantage of slug flow as a liquid-liquid contacting method is that it can result in increased mass transfer due to internal circulation within each liquid plug, as illustrated in Figure 2.1. This internal circulation is due to shear between the slower moving fluid at the channel wall and the fluid in the center of each slug. The circulation decreases the diffusion path for each solute molecule from half the length of each slug to the half the channel diameter[12]. The main disadvantage of slug flow is that it results in an emulsion of the immiscible liquids, requiring separation after extraction. Parallel flow is able to maintain separation of the immiscible liquids over the entire channel length but results in lower mass transfer rates, due to a decrease in the interfacial contact area. However, the lower mass transfer rate can be addressed by changing the device geometry to increase the interfacial area-to-volume ratio.
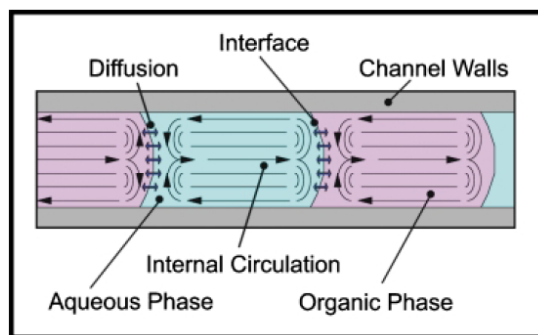
Figure 2.1. Internal circulation within immiscible slug flow[12].

While conventional LLE is beneficial when separating large volumes of fluid and microfluidic LLE is beneficial when separating extremely small volumes of fluid, this

research presents a middle ground that eliminates the additional separation step that is required with conventional LLE and allows for a larger processing capacity than microfluidic LLE. Implementation of a separation step after conventional LLE requires large unit operations, is time consuming, is labor intensive, and results in the use of large volumes of material making it undesirable for the separation of low volume, high value materials[13]. The large volume of material could potentially be harmful to the operator and hazardous to the environment making it an undesirable option when toxic materials are being used[14]. By reducing LLE to the micro- and milli-scale, the need for separation is eliminated because the immiscible streams do not mix at any point in the extraction process. By combining the properties of fluid flow at the micro- and milli- scale with LLE, separation can be achieved using smaller volumes of fluids, resulting in lower solvent consumption, lower waste production, shorter analytical times, smaller space requirements, and lower energy consumption[15]. The potential for increased interfacial area-to-volume ratio based on device geometry could also result in more efficient transport between the two liquid streams[11].

Micro- and milli-fluidic LLE is accomplished by the parallel flow of two immiscible fluids resulting in a pinned interface capable of behaving as a membrane for mass transfer, as shown in Figure 2.2[14]. Because the dimensions of the channel are known, the interfacial area over which mass transfer occurs is well defined making this separation technique a novel method of mass transfer determination. Conventional means of mass transfer estimation require significant assumptions to determine the contact area between the two immiscible phases. Some of these assumptions are that

droplets within the system are perfectly spherical, the interfacial area of droplets remains constant, droplets move through the column at the same velocity, and that all droplets are approximately the same size[16]. This separation method can be used to more accurately estimate mass transfer coefficients because the contact area of the two phases is well defined.
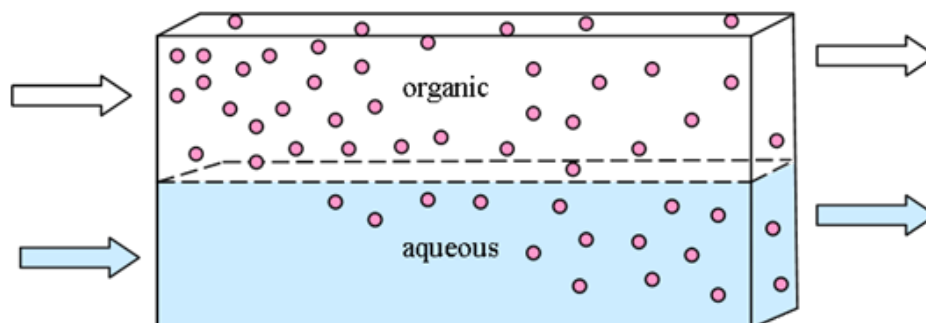
Figure 2.2. Parallel flow of two immiscible liquids within a micro- or milli-fluidic device resulting in a stable pinned interface.

Co-current and countercurrent laminar flow are currently being achieved within microfluidic devices using selective surface modification[17,18,19], a membrane for separation of the two immiscible liquids[20], or guide structures[21,22]. In selective surface modification, various compounds are used to treat the microchannel walls to obtain a hydrophobic or hydrophilic surface, generally by solution deposition[18]. In some cases, channel surfaces can even be modified to create superhydrophobic and superhydrophilic surfaces which are better at stabilizing parallel two-phase flows. Superhydrophobic surfaces can be created by combining nanoscale roughness with hydrophobic treatment. Superhydrophilic surfaces can be created by photocatalytic decomposition of deposited groups under controlled photoirradiation[19]. In membrane separation, a hydrophilic or

hydrophobic porous membrane physically prevents mixing of the aqueous and organic phases, while allowing the compound of interest to diffuse across the membrane[20]. The use of guide structures to stabilize parallel multiphase flow is widely used but it should be noted that as the height of the guide structure increases, the extraction efficiency decreases due to a decrease in interfacial area[21]. The method of fluidic separation explored in this thesis uses surface modification and a PEG-DA hydrogel to stabilize co-current laminar flow of two immiscible liquids. A thiolene-based optical adhesive channel enclosed between two glass slides is created using photolithography. The optical adhesive channel is then treated with a self-assembled monolayer, 3-(trichlorosilyl)-propyl methacrylate (TPM), to deposit less hydrophilic groups along the channel wall and to allow the hydrogel to adhere to channel walls. Adsorption of the trichlorosilane onto the hydroxylated glass surface occurs by multiple steps as shown in Figure 2.3. Hydrochloric acid is lost in the chemisorption of the trichlorosilane onto the hydroxylated glass surface. The remaining chlorides on each TPM molecule are lost as hydrochloric acid and replaced by hydroxyls from water present in solution. Finally, water is lost through a condensation reaction in the creation of Si-O-Si bonds between the TPM molecules resulting in the formation of a complete monolayer[23].
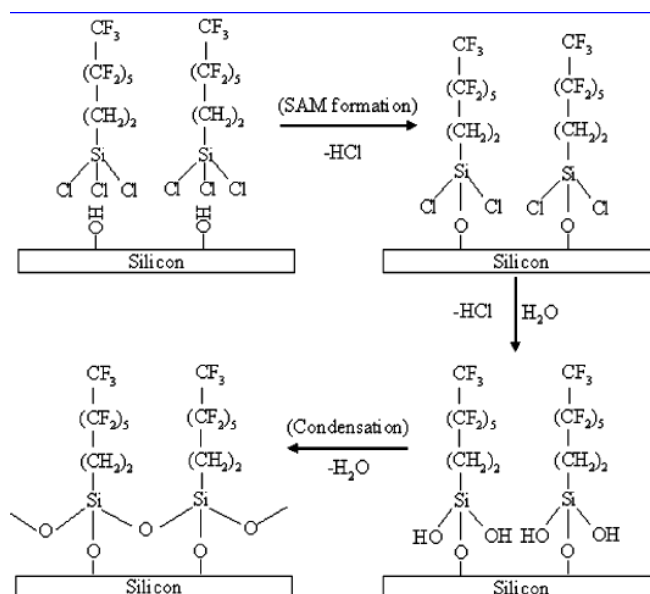
Figure 2.3. Adsorption of trichlorosilanes onto a hydroxylated silicon surface[23].

The deposition of these less hydrophilic TPM molecules helps stabilize organic flow along the optical adhesive boundary and allows the hydrogel to bond to the glass channel walls. It is necessary for the hydrogel to adhere to the channel walls through a chemical reaction with the TPM molecules to ensure that the aqueous phase flows through the crosslinked hydrogel network rather than around the hydrogel slab. The hydrogel layer is cured to define one side of the optical adhesive channel by free radical polymerization, initiated at each of the vinyl groups on PEG-DA monomers. During the polymerization, PEG-DA vinyl groups are able to react with the methacrylate group on TPM molecules, resulting in a chemical bond attaching the hydrogel layer to the glass slide. The chemical structures of a TPM molecule and a PEG-DA monomer are shown in Figure 2.4.
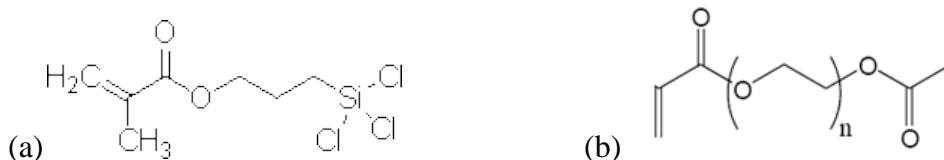
Figure 2.4. (a) Chemical structure of 3-(trichlorosilyl)-propyl methacrylate (TPM).

(b) Chemical structure of poly(ethylene glycol) diacrylate (PEG-DA).

The result of this procedure is a rectangular channel defined by two glass slides, a hydrogel boundary, and an optical adhesive boundary, as shown in Figure 2.5. All surfaces excluding the hydrogel boundary are treated with the less hydrophilic TPM solution. Flow of the aqueous stream is stabilized along the hydrogel boundary due to hydrophilic interactions and flow of the organic stream is stabilized along the optical adhesive boundary due to weak non-polar interactions. Once co-current laminar flow is stabilized, the rate of mass transfer can be manipulated by altering the flow rate of the aqueous and organic phases and/or the concentration of the compound of interest within the feed stream.
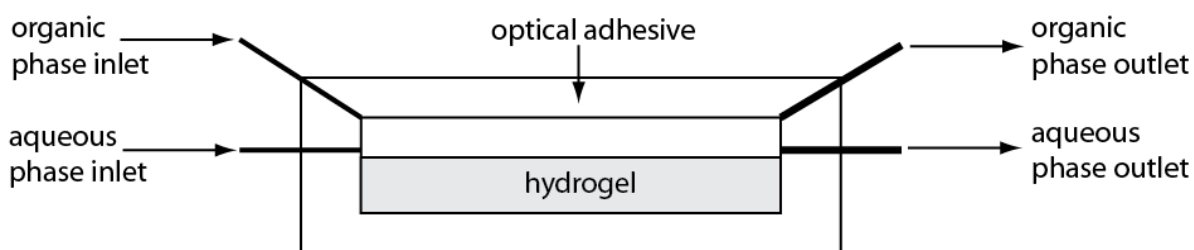
Figure 2.5. A rectangular channel defined by two glass slides, a hydrogel boundary,

and an optical adhesive boundary.

2.1.3 Rhodamine 6G

This thesis investigates micro- and milli-fluidic LLE with rhodamine 6G as the solute being extracted from the organic phase, pentanone, into an aqueous stream. The chemical structure of rhodamine 6G is shown in Figure 2.6. Rhodamine 6G is a synthetic dye compound with high photostability, high quantum yield, and low cost that is used in many applications as a water tracing agent, laser dye, and fluorescent marker. Furthermore, rhodamine 6G fluoresces making it easily detectable[24]. A well known phenomenon of this dye that has been studied for years is its tendency to dimerize in aqueous solutions even at dilute concentrations, sometimes forming higher order aggregates. Dimerization in aqueous solutions has been observed at concentrations as low as 10^{-5} M [25]. At sufficiently low concentrations, monomers of rhodamine 6G dominate. However, as rhodamine 6G concentration increases the presence of dimers and other higher order aggregates becomes more significant. A disadvantage of this dimerization phenomenon is that it reduces the laser dye efficiency since dimers do not contribute to light amplification but absorb radiation, resulting in a decrease in fluorescence intensity. An additional drawback of rhodamine 6G dimerization is that it is no longer possible to use Beer's law to correlate solution absorbance to solution concentration since the relationship is no longer linear[26]. The formation of dimers can be avoided by using non-aqueous solvents, by the addition of a surfactant such as triton-X100, by increasing temperature, or by decreasing rhodamine 6G concentration[24].
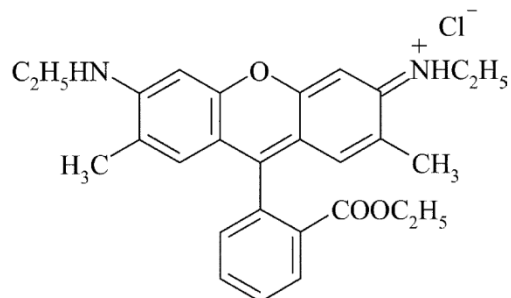
Figure 2.6. Chemical structure of rhodamine 6G.

Practical and advantageous applications of micro- and milli-fluidic LLE include the passive separation and purification of biomolecules[27], particle separation[28], and pharmaceutical product purification[29]. When performing these separations, the product of interest is generally present in such small quantities that conventional LLE is not an economical option[30]. Other current methods of separation are filtration, evaporation, and centrifugation[31]. Unfortunately, filtration can result in the loss of valued product due to size limitations[32], evaporation can denature heat sensitive molecules and cause agglomeration of molecules[30], and centrifugation can exert harsh forces that damage the product or result in low separation yield depending on the density difference between the carrier fluid and molecule of interest[33]. Recovery using chromatographic methods may also be an option, but column resins can be expensive and easily fouled[34]. For applications that require high separation efficiencies, this micro- and milli-fluidic separation method presents an additional benefit; the device geometry can be tailored to target specific efficiencies. Two options exist to increase the extraction efficiency. The channel length, defined as L in Figure 2.7, can be increased to allow for more extraction due to an increase in contact time and area between the two immiscible phases or the

channel height, h, can be decreased while the device width, w, is increased for a greater interfacial area-to-volume ratio allowing for more extraction to occur per volume of fluid processed. By shrinking LLE to the micro- and milli-scale, this separation method can be applied to a new class of applications, particularly in chemical and biomedical engineering.
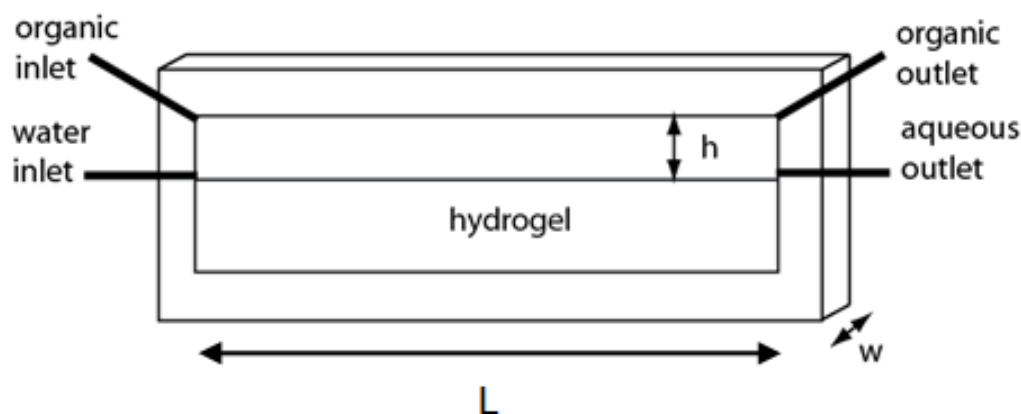
Figure 2.7. Schematic of LLE device.

Milli-fluidic devices also offer benefits over microfluidic devices by exhibiting many of the beneficial fluid flow properties of microfludic devices while being able to process larger volumes of fluid per time. Milli-fluidic device dimensions are small enough that mixing occurs by diffusion, there is laminar flow, and heat transfer can be easily controlled. By increasing the dimensions of the channel within the separation device to the millimeter scale the occurrence of fouling is decreased[10]. The method of LLE described here is low cost, small volume, and provides a platform for more accurate determination of the mass transfer coefficient of a system.

2.2 Materials

This section lists all materials used in the construction and use of the LLE device. The Materials section is separated into three parts: preparatory cleaning, LLE device fabrication, and experimental trials.

2.2.1 Preparatory Cleaning

The materials used to clean the glass slides prior to being used for LLE devices include acetone [Reochem Inc., >99% purity by weight], ethanol [Pharmco-Aaper, >99.98%], and delicate task wipers [Kimtech Sciences]. A Harrick Radio Frequency Plasma Cleaner was used with oxygen for cleaning purposes.

2.2.2 LLE Device Fabrication

The materials used to create the LLE devices include syringe needles [18 G x 3.8 cm and 21 G x 3.8 cm, Becton-Dickinson], poly (ethylene glycol)(diacrylate) (PEG-DA) [MW 575, Sigma Aldrich], 4-(2-hydroxyethoxy)phenyl-(2-hydroxy-2-propyl)ketone [Irgacure 2959, Ciba Specialty Chemicals], 3-(trichlorosilyl)-propyl methacrylate (TPM) [≥95 %, Fluka], hexane [Matheson Coleman and Bell], glass slides [76.2 mm x 25.4 mm x 1 mm, VWR], acetone [>99% purity by weight, Reochem Inc.], ethanol [>99 %, Pharmco-Aaper], Norland optical adhesive [NOA-81 resin, Norland Products Inc.], silicon spacers, and patterned transparencies. A Blak-Ray® Ultraviolet Lamp was used to provide long-wave (365 nm) ultraviolet light and a UVAB ST-513 UV Lightmeter was used to measure the intensity of the ultraviolet light source.

2.2.3 Experimental Trials

The materials used to conduct LLE trials include NE-300 Single Syringe Pumps [New Era Pump Systems Inc., Model No. NE-300, syringepump.com], silicone tubing [0.85 mm and 0.8 mm inner diameter, Cole-Parmer], rhodamine 6G [Fluka], syringes [25 mL luer-lock plastic syringes, National Scientific Company], and 2-pentanone [≥90 %, Sigma Aldrich].

2.3 Methods

The Methods section discusses the procedure used to create the LLE devices, how to operate the LLE devices, and how to take the measurements required for characterizing the LLE system. The methods section is separated into seven sections: preparatory cleaning, milli-fluidic LLE device fabrication, microfluidic LLE device fabrication, experimental trials, distribution coefficient study, interfacial tension measurements, and rhodamine 6G solubility.

2.3.1 Preparatory Cleaning

All glass slides are cleaned with acetone using a delicate task wiper and allowed to air dry. All glass slides are then wiped with ethanol to deposit a monolayer of hydroxyl groups along the surface of the glass slides. The presence of these hydroxyl groups will be necessary for the solution deposition of TPM molecules onto glass slides. The glass slides are placed in the plasma cleaner and cleaned with oxygen for 3 min to ensure removal of organic contaminants.

2.3.2 Milli-fluidic LLE Device Fabrication

Two silicon spacers, each 0.6 mm in width, were stacked at each corner of a clean glass slide, defining the width of the milli-fluidic LLE device. Optical adhesive was applied to the glass slide and a clean glass slide was carefully laid over the optical adhesive making sure not to create any air bubbles between the optical adhesive and glass slide. A photomask, shown in Figure 2.7, was placed over the second glass slide to define the optical adhesive channel.

Figure 2.7. LLE device photomask design.

The corners of the glass slides were covered to prevent curing of the silicon spacers and the entire assembly was exposed to UV light at an intensity of 1100 μW/cm^2 for 14 min. After 7 min of UV exposure the glass slides and optical adhesive assembly was rotated 180° to ensure even curing of the optical adhesive. A schematic of the assembly used to define the optical adhesive channel within the LLE device is shown in Figure 2.8.
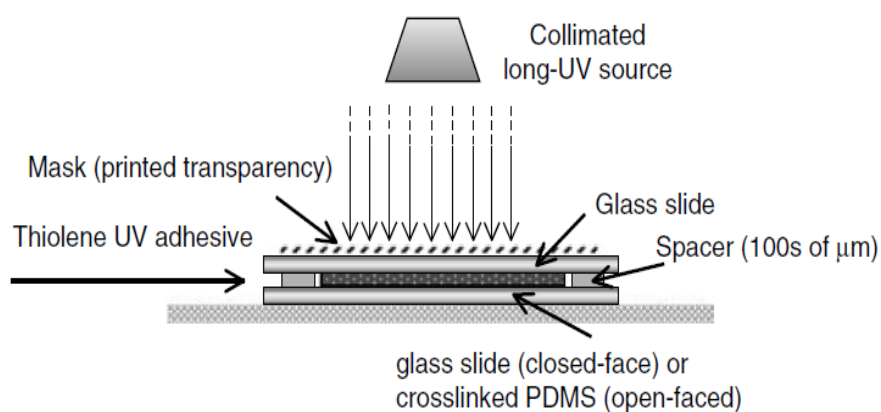
Figure 2.8. Assembly used to define optical adhesive boundary within device[8].

Once the curing of the optical adhesive was complete, the silicon spacers were removed and excess optical adhesive was removed with pressurized air, acetone, and ethanol. Needles, 21 G and 18 G in size, were cured into the inlets and outlets of the

device, respectively, using optical adhesive. The device was baked at 50 $^{\circ}$C for 12 h to increase the adhesion of the optical adhesive to the glass slide[8]. After baking, the glass slides were exposed to a 1mM solution of TPM in hexane for 25 min for deposition of a complete self-assembled monolayer. A hydrogel solution of 40 vol.% water, 60 vol.% PEG-DA, and 0.25 wt% Irgacure 2959 was injected into the optical adhesive channel. Opaque, black electrical tape was used as a photomask and applied to the device to define the hydrogel layer just below the aqueous inlet and outlet needles. The entire assembly was exposed to UV light at an intensity of 1100 µW/cm^2 for 14 min. The assembly was rotated 180° after 7 min of curing to ensure even curing of the hydrogel layer. Once hydrogel curing was complete, excess hydrogel solution was removed with deionized water. If devices are not used immediately, the channel is filled with water to prevent the hydrogel from dehydrating, wrapped in foil to prevent the hydrogel from curing as a result of stray UV radiation, and stored in the refrigerator to prevent thermal degradation of the PEG-DA.

2.3.3 Microfluidic LLE Device Fabrication

A microfluidic LLE device can be created using the above procedure by changing a few instructions. Instead of using two silicon spacers at each corner of a clean glass slide, use one silicon spacer. This results in a 0.6 mm thick LLE device. Due to the approximate 50% reduction in optical adhesive volume, the optical adhesive and hydrogel UV exposure times are reduced to 7 min at an UV intensity of 1100 µW/cm^2. Due to the decrease in channel width, 21 G needles are used as the inlets and outlets to

the LLE device. In order for the 21 G needles to fit between the two glass slides, they must be flattened slightly with a pair of pliers.

2.3.4 Experimental Trials

A calibration curve, shown in Figure 2.9, was created to correlate the rhodamine 6G/pentanone solution absorbance to the solution concentration using ultraviolet-visible (UV-Vis) spectroscopy. Solutions of rhodamine 6G in pentanone with concentrations ranging from 1.25 µg/ml to 100 µg/ml were used to generate the calibration curve. Concentrations within this range resulted in a linear trend, as shown by an R-squared value of 0.9993. The calibration curve is only valid in this linear region, pertaining to dilute solutions. This method is not valid for determining solution concentration based on absorbance values that fall outside of the linear region. Any points outside of the linear region are diluted to fall within this concentration range.
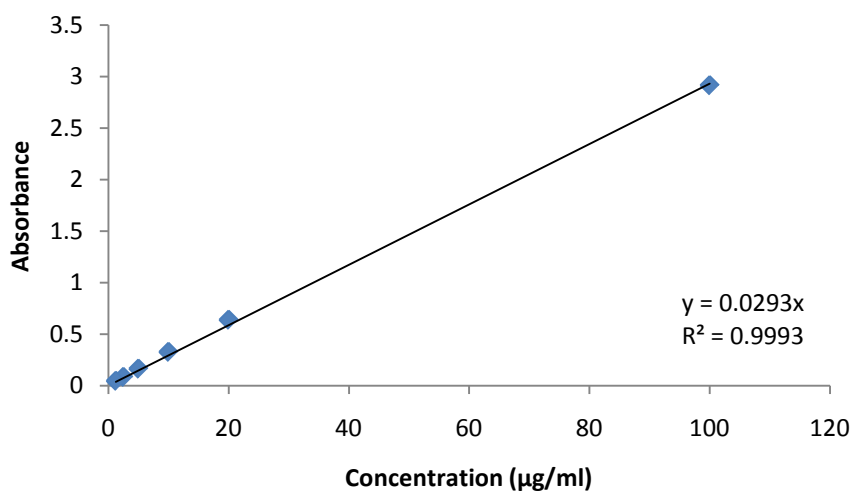
Figure 2.9. Calibration curve of rhodamine 6G in pentanone using UV-Vis spectroscopy.

A calibration curve could not be used to correlate absorbance readings to the concentration of rhodamine 6G in aqueous solutions due to the dye molecule's tendency to dimerize in aqueous solution. A significant effect of rhodamine 6G dimerization is that the solution no longer obeys Beer's law. Instead, an equation derived by Georges based on the assumption that rhodamine 6G monomers and dimers individually obey Beer's law was used to correlate aqueous solution absorbance to concentration[35]. Georges' equation for the total solution absorbance, A_t, is given as

$$A_t = \frac{l}{2}\left[\varepsilon_d C_t + (2\varepsilon_m - \varepsilon_d)\left(\frac{\sqrt{1 + 8K_d C_t} - 1}{4K_d}\right)\right]$$

where l is the optical path length (cm), ε_d is the dimer molar absorptivity (M^{-1}cm^{-1}), ε_m is the monomer molar absorptivity (M^{-1}cm^{-1}), K_d is the dimerization coefficient (M^{-1}), and C_t is the total solution concentration (M). The constants used for the calculation of the total concentration of rhodamine 6G in aqueous solution were determined to be $\varepsilon_m = 8.2\times10^4$ M^{-1}cm^{-1}, $\varepsilon_d = 3.1\times10^4$ M^{-1}cm^{-1}, and $K_d = 2150$ M^{-1} at a wavelength of 525 nm[35].

Silicone tubing was used to transfer solutions from syringes to the LLE device and from the LLE device to collection vessels. A septum design was used to prevent evaporation of pentanone from the collection vessel. Two layers of parafilm® were used to create a seal around the top of the vessel. A small hole was punctured in the parafilm® to connect the tubing to the collection vessel. A syringe was loaded with a rhodamine 6G/pentanone solution which was delivered to the upper inlet needle of the LLE device at a constant flow rate of 40 ml/h. The concentration of rhodamine 6G/pentanone solutions were varied between three concentrations which ranged from 1.01×10^{-4} g/ml to

1.64×10^{-3} g/ml. A second syringe was loaded with deionized water which was delivered to the lower inlet needle of the LLE device. The water flow rate was varied in increments of 10 ml/h between 10 ml/h and 40 ml/h. Samples of the pentanone inlet, and water and pentanone outlets were collected and their absorbances were measured using UV-Vis spectroscopy. Aqueous outlet concentrations were determined from Georges' equation; pentanone inlet and outlet concentrations were determined from a calibration curve. In many cases, the pentanone samples were diluted to obtain absorbance values within the linear region of the calibration curve (1.25 µg/ml to 100 µg/ml).

2.3.5 Distribution Coefficient Study

A distribution coefficient study was set up to investigate how rhodamine 6G distributes itself between pentanone and water at equilibrium. Solutions of 0.5×10^{-3} g/ml, 5×10^{-3} g/ml, and 50×10^{-3} g/ml of rhodamine 6G in pentanone were created. Each of the three solutions of varying concentration were combined with an equivalent volume of water in a separatory funnel and allowed to reach equilibrium overnight. A sample was taken from the organic and aqueous phase of each separatory funnel. The concentration of each sample was determined by UV-Vis spectroscopy. This procedure was repeated three times at each concentration to determine statistical significance.

2.3.6 Interfacial Tension Measurements

The interfacial tension between water and solutions of rhodamine 6G/pentanone at various concentrations were determined using a KSV Sigma 703D manual tensiometer. It was necessary that the instrument be turned on for at least 30 min prior to use and be

calibrated using the pre-weighed calibration weight. The density of each phase was measured using the glass density measurement probe. The glass probe was cleaned with deionized water and acetone and placed on the balance hook. A clean sample container containing the solution to be measured was placed on the sample stage. The balance was tared while the glass probe was exposed to the atmosphere so that the density of air, approximately 0.0012 g/ml, was shown on the display screen. The sample stage was raised to immerse the glass probe in the solution. The density of the solution was reported on the display screen. This procedure for density measurement was repeated three times for each solution.

The interfacial tension was measured with a DuNouy ring. The DuNouy ring was submerged in acetone and hexane and burned to remove all contaminants. The ring was carefully placed on the balance hook, making sure not to deform the ring or touch the base of the ring. The instrument was set to the uncorrected DuNouy mode and the density difference between the heavy and light phase of the solutions was input. The heavy phase, water, was transferred to a clean beaker and the balance was tared. The ring was submerged in the heavy phase and the maximum value was reset using the "clear max" button. The light phase, rhodamine 6G in pentanone solution, was carefully added over the heavy phase. The stage was slowly lowered, dragging the ring through the heavy phase and into the light phase. When the meniscus "hanging" from the ring collapses, the maximum interfacial tension is reported on the display screen. This procedure for interfacial tension measurement was repeated three times for each combination of rhodamine 6G/pentanone solution and water.

2.3.7 Rhodamine 6G Solubility Study

A solubility study was set up to determine the solubility limit of rhodamine 6G in pentanone since this value has never been reported in studies. An excess of rhodamine 6G was loaded into 100 mL of pentanone and allowed to dissolve overnight in a sealed container at 25 $^{\circ}$C. A sample was drawn from the surface of the solution to avoid the excess rhodamine 6G that accumulated at the base of the container. The concentration of the solution was determined by UV-Vis spectroscopy and is assumed to be an approximation of solubility limit of rhodamine 6G in pentanone at room temperature.

2.4 Results

2.4.1 Device Design

The procedure and design of the LLE device required some adjustments in order to consistently stabilize co-current laminar flow over the entire length of the channel. A 1 mM solution of TPM in ethanol was initially used to deposit a self-assembled monolayer on the interior of the device channel by solution deposition. A complete monolayer of TPM is expected to result in a contact angle around 70°. The ethanolic solution produced an incomplete monolayer with a contact angle of $\approx$ 59°. A complete monolayer of TPM would better stabilize flow of the organic phase over the entire channel length. The formation of an incomplete monolayer was due to reactions between the hydroxyl group in ethanol and TPM molecules. By the time the TPM solution was exposed to the hydroxylated surface of the glass slides, much of it had already reacted. To prevent premature reaction of the TPM molecules, the ethanol solution was replaced with a hydrocarbon solvent. Hexane was selected because it is one of the few hydrocarbon solvents known not to degrade the optical adhesive structure during short time exposure. A TPM study was conducted to determine the optimum soak time resulting in complete monolayer coverage. Table 2.2 shows the resulting contact angles with varying TPM/hexane solution soak time. Based on the TPM study, the optimal soak time is 25 minutes. Based on the results of the TPM study, a 1 mM solution of TPM in hexane was used to deposit a self-assembled monolayer resulting in a contact angle of 71.4 ± 0.8^o.

Table 2.2. Contact angle as a function of varying soak times in TPM/hexane

solution.

Soak Time (min)	Trial 1 (^{o})	Trial 2 (^{o})	Trial 3 (^{o})	Average (^{o})
10	68.06	73.09	69.36	70 $\pm$ 3
15	69.75	71.28	71.14	70.7 $\pm$ 0.8
20	70.25	69.03	69.65	69.6 $\pm$ 0.6
25	71.36	70.61	72.11	71.4 $\pm$ 0.8
30	71.15	69.37	68.87	69.8 $\pm$ 1

Slight changes were made to the LLE device design to allow for better separation of the organic and aqueous streams at the device outlets. The initial design, shown in Figure 2.10, relied on stable co-current laminar flow of the two immiscible streams over the entire length of the channel and collected the outlets from the upper and lower outlets at the end of the channel.

Figure 2.10. Initial LLE device photomask.

However, co-current laminar flow of the aqueous and organic streams was only stable over the first three quarters of the channel and changed to slug flow over the last quarter of the device channel, resulting in organic flow exiting the aqueous outlet. Because of

this complication, it was necessary to alter the device design to ensure stable parallel flow over the entire channel length. The device channel was shortened slightly and hydrogel was cured around the aqueous outlet needle in an attempt to discourage organic contamination of the aqueous outlet stream. Figure 2.11 demonstrates how the hydrogel was cured around the aqueous outlet.
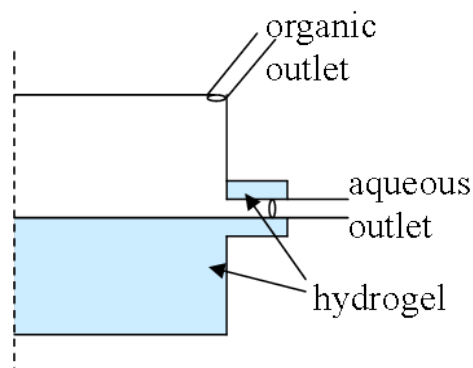
Figure 2.11. Schematic of new device design with hydrogel surrounding aqueous outlet.

The presence of hydrogel around the aqueous outlet is especially important at lower water flow rates since the water stream is significantly thinner, making it more difficult to achieve a pure aqueous outlet sample. The final LLE device design, shown in Figure 2.12, allowed hydrogel to be cured around the aqueous outlet needle. The height of the hydrogel was also decreased in the final LLE design because little hydrogel was necessary to stabilize parallel flow of the immiscible fluids.

Figure 2.12. Final LLE extraction device photomask.

2.4.2 Liquid-Liquid Extraction

The solubility of rhodamine 6G in water is cited as 0.02 mol/L, corresponding to a solubility of 9.58×10^{-3} g/ml[25]. The solubility of rhodamine 6G in pentanone was determined experimentally. An excess of rhodamine 6G was loaded into pentanone and allowed to dissolve over a two day period at 25 $^{\circ}$C. Excess rhodamine 6G remained undissolved and settled out of solution. The final concentration of the solution was determined using UV-Vis spectroscopy. The solubility of rhodamine 6G in pentanone and water are shown in Table 2.3.

Table 2.3. Solubility of rhodamine 6G at 25 $^{\circ}$C.

Solvent	Solubility $\times$ 10^{-3} (g/ml)
Water	9.58
Pentanone	1.64

The distribution coefficient for a system of two immiscible fluids is a ratio of the concentration of a solute in the organic phase to the concentration of a solute in the aqueous phase at equilibrium[36]. The distribution coefficient of rhodamine 6G, with

pentanone as the organic phase, was determined at room temperature. Because rhodamine 6G has a tendency to dimerize in aqueous solutions, the distribution coefficient for this system changes with variations in concentration. The distribution coefficient of rhodamine 6G at each concentration was repeated three times to determine statistical significant and is shown in Table 2.4. As the concentration of rhodamine 6G in the system increases, the distribution coefficient decreases. This is because at higher rhodamine 6G concentrations, more rhodamine 6G is dimerizing in the aqueous phase. As rhodamine 6G dimerizes, it decreases the effective concentration of rhodamine 6G in the aqueous phase allowing more rhodamine 6G to migrate from the organic phase into the aqueous phase. So as the rhodamine 6G concentration increases, the concentration of rhodamine 6G in the organic phase decreases and the concentration of rhodamine 6G in the aqueous phase increases, resulting in a lower distribution coefficient.

Table 2.4. Distribution coefficient of rhodamine 6G as a function of concentration at 25 ^{o}C.

Concentration $\times 10^{-3}$ (g/ml)	Distribution Coefficient
50	2.29 ± 0.03
5	3.2 ± 0.7
0.5	9 ± 4

Continuous LLE, with water as the extractant, was accomplished on the micro- and milli- scale through stabilization of the aqueous phase using a PEG hydrogel as shown in Figure 2.13.
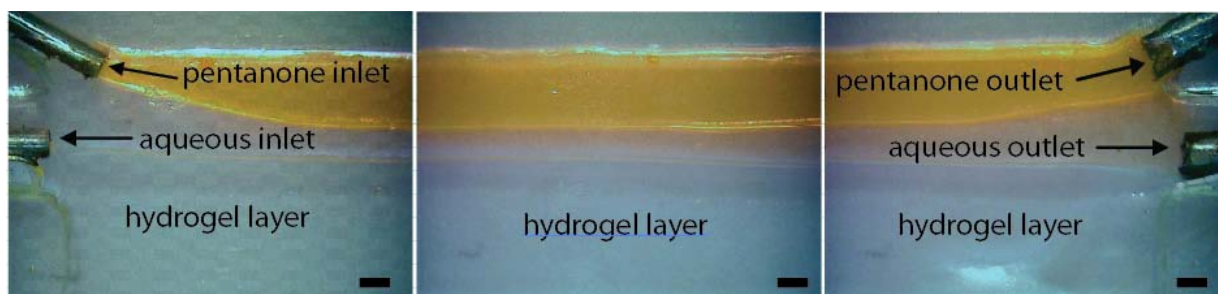
Figure 2.13. Continuous co-current laminar flow of rhodamine 6G/pentanone (orange stream) against water stabilized by surface modification and a hydrogel slab within a microfluidic device at water and pentanone flow rates of 40 ml/h and 30 ml/h, respectively. (a) inlet. (b) center. (c) outlet. (scale bar: 800 µm)

In order to demonstrate the stability of the interface between the two immiscible phases within the LLE device, the Weber number and capillary number were calculated for various flow rates and concentrations. The average Weber number and capillary number were calculated for each stream and averaged to characterize flow at each set of conditions. The average Weber number and average capillary number at the micro- and milli-fluidic scales are summarized in Table 2.5. All flow conditions resulted in Weber numbers less than 1, indicating a stable interface between two-phase flow. All flow conditions resulted in capillary numbers less than 1, resulting in a decrease in interfacial area. For the channel geometry explored in this thesis, parallel flow resulted in a decrease in interfacial area. This is because the channel width is so small compared to the channel height that slug flow would result in a greater interfacial area per volume of fluid.

Table 2.5. Average Weber and capillary numbers at the micro- and milli-fluidic scale at various concentrations and flow rates.

	Weber Number	Capillary Number
Microfluidic	3.23×10^{-2}	1.04×10^{-3}
Milli-fluidic	1.38×10^{-2}	5.22×10^{-4}

As shown in Table 2.4, an increase in the device width from the microfluidic scale to the milli-fluidic scale results in a decrease in the Weber number and capillary number. This is due to the decrease in the linear velocity of each stream when the device width is increased. It was found that both the Weber number and the capillary number increased with increasing flow rates due to an increase in the linear velocity of each stream. It was found that there was a decrease in the Weber number and capillary number with increasing rhodamine 6G concentration. This is due to the surfactant behavior of the amphiphilic dye molecule which causes a decrease in the interfacial tension. Rhodamine 6G's surfactant behavior is discussed in further detail later in the LLE results section.

From inlet and outlet concentration values, it is possible to calculate a mass transfer coefficient (k) for the system by conducting a mass balance on the presence of rhodamine 6G in the pentanone stream. The following overall mass balance on rhodamine 6G in the pentanone stream was initially used to calculate an estimate of the mass transfer coefficient

$$\dot{Q}_p C_{in,p} - \dot{Q}_p C_{out,p} - kwL \frac{\left(C_{in,p} - (C_{out,p} - C_{out,w})\right)}{\ln \left(\dfrac{C_{in,p}}{C_{out,p} - C_{out,w}}\right)} = 0$$

where $\dot{Q}_p$ is the pentanone flow rate (ml/s), $C_{in,p}$ is the inlet pentanone concentration (g/ml), $C_{out,p}$ is the outlet pentanone concentration (g/ml), w is the distance between the two glass slides (milli-fluidic: 0.12 cm; microfluidic: 0.06 cm), and L is the channel length (cm). To obtain a more accurate value of the mass transfer coefficient, changes in concentration throughout the length of the channel were taken into account using a differential mass balance. This was accomplished by numerical solution of the following differential mass balance on rhodamine 6G in the pentanone stream

$$\frac{dC_p}{dz} = -\frac{kw}{\dot{Q}_p}(C_p - C_w)$$

where dz is the length of each differential slice of the organic and aqueous streams (cm) and C_p and C_w are the average concentrations of rhodamine 6G in each differential slice of the organic and aqueous streams, respectively (g/ml). Matlab was used to solve the differential mass balance with the mass transfer coefficient estimated from the overall mass balance as an initial estimate of the mass transfer coefficient. For many of the experimental trials explored in this thesis, the mass transfer coefficient calculated based on the overall mass balance and differential mass balance do not vary significantly. However, as the concentration difference between organic and aqueous streams increases, the mass transfer coefficient obtained from the overall mass balance model will deviate more from the mass transfer coefficient obtained from the differential mass balance since a larger concentration gradient will be present as a function of channel length. In such a

case, the differential mass balance yields a more accurate approximation of the mass transfer coefficient. Table 2.6 summarizes the mass transfer coefficients determined by the differential mass balance for the micro- and milli-fluidic systems.

Table 2.6. Mass transfer coefficients determined by the differential mass balance for the micro- and milli-fluidic systems.

Mass Transfer Coefficients $\times\ 10^{-3}$ (cm/s)	
Microfluidic Scale	1.38 ± 0.49
Milli-fluidic Scale	2.10 ± 0.99

For this particular LLE system, it was necessary to take into consideration the mutual solubility of pentanone and water when modeling the extraction of rhodamine 6G. Pentanone has a solubility of 4.3 mass% in water at 25 $^{\circ}$C [37]. Because pentanone is in an environment in which it is exposed to air, pentanone is already saturated with water. Thus, it is not necessary to account for the extraction of water into the pentanone stream. Water has a solubility of 3.3 mass% in pentanone at 25 $^{\circ}$C [38]. It is necessary to account for the extraction of pentanone into the water stream because not doing so results in an overestimation of the concentration of rhodamine 6G in the pentanone stream. The following procedure was followed to offset pentanone extraction. When a pentanone outlet sample was collected, it was diluted to fall within the linear region of the calibration curve. The absorbance of this diluted pentanone outlet sample was converted to a concentration based on the pentanone calibration curve. A pentanone mass solubility of 4.3 mass% was converted to a pentanone solubility of approximately 5 vol.%. The rate

of pentanone extraction is dependent on the volume of water to which it is exposed. Based on the volume of water that flowed through the device for liquid-liquid extraction, the volume of pentanone extracted into the water stream was calculated. The volume of pentanone extracted into the water stream was subtracted from the total volume of pentanone that flowed through the device for liquid-liquid extraction. This value is the volume of pentanone that corresponds to the pentanone outlet concentration and was multiplied by the pentanone outlet concentration to determine the mass of rhodamine 6G in the outlet pentanone sample. The mass of rhodamine 6G was divided by the total volume of pentanone that flowed through the device and multiplied by the dilution factor resulting in a pentanone concentration that accounts for pentanone extraction into the aqueous stream. This procedure was a method of correcting the pentanone outlet concentration to account for the pentanone that was extracted into the aqueous phase. An example calculation of this procedure is shown below.

Example calculation accounting for solubility of pentanone in aqueous phase:

$$pent.\,absorbance\ =\ 1.076$$

$$pent.\,concentration\ =\ \frac{1.076}{29299\frac{ml}{g}} = 3.67 \times 10^{-5}\frac{g}{ml}$$

$$pent.\,extraction\ volume = 0.05 \times 10\frac{ml}{h} \times 0.246h = 0.123\ ml$$

$$pent.\,total\ volume = 40\frac{ml}{h} \times 0.246h = 9.84\ ml$$

$$mass\ of\ R6G = pent.concentration$$
$$\times (pent.total\ volume - pent.extraction\ volume)$$

$$= 3.67 \times 10^{-5} \frac{g}{ml} \times (9.84ml - 0.123ml)$$

$$= 3.57 \times 10^{-4} g$$

$$adjusted\ pent.concentration = \frac{mass\ of\ R6G}{total\ volume\ of\ pent.} \times dilution\ factor$$

$$= \frac{3.57 \times 10^{-4} g}{9.84ml} \times 16$$

$$= 5.80 \times 10^{-4} \frac{g}{ml}$$

A one sample t-test was used to determine if variations in aqueous flow rate and rhodamine 6G/pentanone solution concentration have a statistically significant impact on the mass transfer coefficient (α=0.05). It was found that there is no statistically significant difference in mass transfer coefficient measured in milli-fluidic and microfluidic devices due to changes in water flow rate or rhodamine 6G/pentanone solution concentration when compared to a mean mass transfer coefficient of 1.72×10^{-3} cm/s with α=0.05. Tables 2.7 and 2.8 show the water flow rates and concentrations that were examined and the resulting t and p values, respectively.

Table 2.7. t and p values showing there is no statistically significant difference in mass transfer coefficient due to changes in water flow rate when compared to a mean mass transfer coefficient of 1.72×10^{-3} cm/s and α=0.05.

Microfluidic				
Water Flow Rate (ml/hr)	Sample Size	Sample Mean Mass Transfer Coefficient X 10^{-3} (cm/s)	t value	p value
10	10	1.19	-0.82	0.43
20	10	1.31	-0.65	0.53
30	10	1.43	0.40	0.70
40	10	1.58	1.61	0.14
Milli-fluidic				
Water Flow Rate (ml/hr)	Sample Size	Sample Mean Mass Transfer Coefficient X 10^{-3} (cm/s)	t value	p value
10	9	2.27	0.82	0.44
20	9	1.62	-1.73	0.12
30	9	1.77	-1.19	0.27
40	9	2.74	1.52	0.17

Table 2.8. t and p values showing there is no statistically significant difference in mass transfer coefficient due to changes in rhodamine 6G/pentanone solution concentration when compared to a mean mass transfer coefficient of 1.72 x10^{-3}cm/s and α=0.05.

Microfluidic				
Rhodamine 6G/pentanone Concentration x 10^{-4} (g/ml)	Sample Size	Sample Mean Mass Transfer Coefficient X 10^{-3} (cm/s)	t value	p value
1.01	12	1.32	-0.34	0.74
5.82	12	1.59	1.75	0.11
9.65	16	1.26	-1.20	0.25
Milli-fluidic				
Rhodamine 6G/pentanone Concentration x 10^{-4} (g/ml)	Sample Size	Sample Mean Mass Transfer Coefficient X 10^{-3} (cm/s)	t value	p value
2.68	12	1.74	-1.14	0.28
6.19	12	2.40	1.12	0.29
16.4	12	2.15	0.20	0.85

Variations in aqueous flow rate have no impact on the mass transfer coefficient at both the micro- and milli-fluidic levels. This behavior is expected because for all aqueous flow rates that allow the stabilization of co-current laminar flow, the concentration of rhodamine 6G in the aqueous stream is sufficiently low that the concentration difference at the aqueous/organic interface is relatively unchanged. The concentration of the rhodamine 6G/pentanone solution has no impact on mass transfer coefficient at the

micro- and milli-fluidic level. However, because rhodamine 6G is an amphiphilic molecule, it is expected that at high concentrations the molecule acts like a surfactant and stabilizes the pentanone-aqueous interface. This phenomenon was verified through measurements of interfacial tension between rhodamine 6G/pentanone and aqueous phases. As shown in Figure 2.14, an increase in rhodamine 6G concentration resulted in a decrease in interfacial tension.
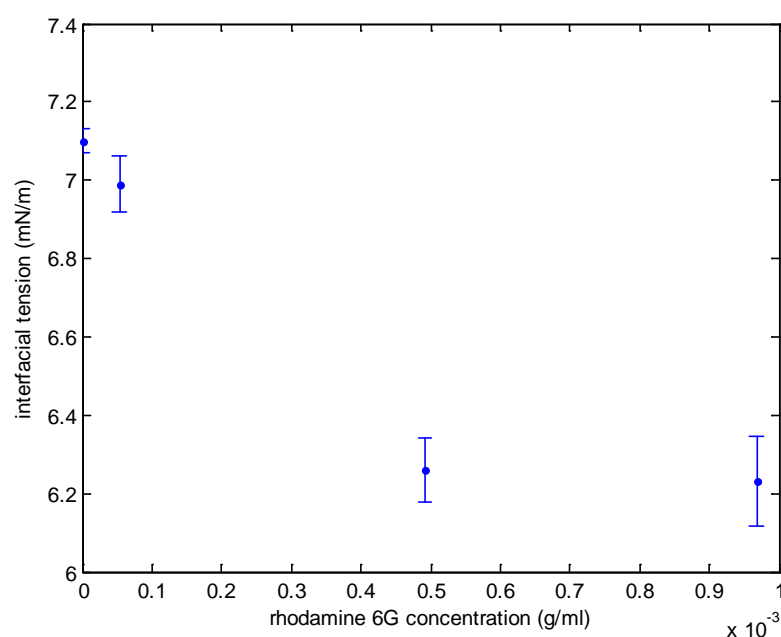
Figure 2.14. Interfacial tension between rhodamine 6G/pentanone and water as a function of rhodamine 6G/pentanone concentration.

As a result of this interfacial stabilization, the curvature of the interface changes. An increase in interfacial curvature leads to an increase in the interfacial area available for mass transfer. The effect of rhodamine 6G's surfactant behavior is small but as the width of the device decreases, the change in interfacial curvature plays a more significant role

since it results in a larger percent increase in interfacial area as shown in Figure 2.15. In

the differential mass balance on rhodamine 6G in the pentanone stream, this decrease in

channel width would be manifested as a decrease in the value of *w*, which is nominally

the distance between the two glass surfaces. Based on this phenomenon, milli-fluidic

liquid-liquid extraction is a more reliable method of mass transfer coefficient estimation.
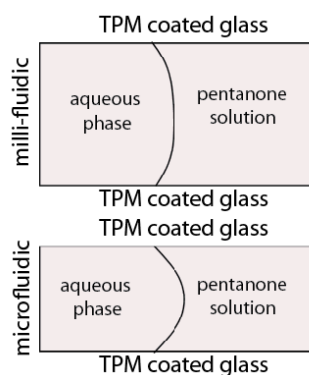
Figure 2.15. Cross-section of milli- and microfluidic device demonstrating a greater

percent increase in interfacial area with changes in curvature at the microfluidic

scale.

The extraction efficiency of micro- and milli-fluidic extraction were determined

according to the following equation

$$extraction\ efficiency = \frac{C_{in,p} - C_{out,p}}{C_{in,p}} \times 100.$$

The average extraction efficiency for micro- and milli-fluidic liquid-liquid extraction

over a 5 cm channel length were $5 \pm 3\%$ and $11 \pm 5\%$, respectively. The increase in milli-

fluidic extraction efficiency to approximately double the extraction efficiency at the

microfluidic level is due to the increase in channel width. When moving from the microfluidic to milli-fluidic level, the channel width was doubled. The channel length required to achieve 90% extraction efficiency was calculated using the overall mass balance with the log mean concentration difference of rhodamine 6G in each of the streams as the driving force for mass transfer. It was assumed that the concentration of rhodamine 6G at the aqueous outlet was zero because the mass transfer rate of rhodamine 6g was slow and the water stream was moving fast enough to remove all of it. The channel lengths required for 90% extraction efficiency are 362 cm and 128 cm at the micro- and milli-fluidic scales, respectively.

The mass transfer coefficient of the pentanone-rhodamine 6G-water system was also determined theoretically for comparison against experimental values. The Stokes-Einstein equation can be used for the estimation of diffusion coefficients in liquid systems containing spherical particles. This equation assumes the solute, rhodamine 6G, has a spherical structure and the solute is larger than the solvent, pentanone, so that changes in a solute's velocity due to collisions with the solvent can be neglected. The calculation of mass transfer coefficients is done with respect to the organic phase based on the assumption that the majority of mass transfer limitations are encountered when transporting the rhodamine 6G molecule to the organic-aqueous interface. The Stokes-Einstein equation is

$$D = \frac{kT}{6\pi\eta r}$$

where D is the diffusion coefficient, k is Boltzmann's constant, T is the absolute temperature, η is the liquid viscosity, and r is the particle radius[39]. The radius of a rhodamine 6G molecule was calculated to be 4.66 Å based on a molar volume of 424 Å^3. The equation derived for diffusion of a gas into a falling film according to penetration theory, shown below, was used to calculate the theoretical mass transfer coefficient for the pentanone-rhodamine 6G-water system

$$k = 2\sqrt{\frac{Dv_o}{\pi L}}$$

where v_o is superficial velocity and L is channel length. In this model, the pentanone phase containing rhodamine 6G is represented by the gas and the aqueous phase is represented by the falling film. Penetration theory functions on the assumptions that the thickness of the falling film is sufficiently thick that it does not become saturated with the gas and that the molecules at the interface are constantly being replenished. The theoretical mass transfer coefficients that result from these calculations are 1.57×10^{-3} cm/s at the microfluidic scale and 1.11×10^{-3} cm/s at the milli-fluidic scale. Both of these values fall just within the standard deviation of the experimental mass transfer coefficients. The good agreement between the theoretical values and the experimental values demonstrate that this method of liquid-liquid extraction is a reliable method of mass transfer coefficient determination.

2.5 References

(1) Treybal, R. E. *Mass-transfer Operations,* 3rd ed.; McGraw-Hill Book Company: Singapore, 1980.

(2) Cusack, R. W.; Fremeaux, P.; Glatz, D. A Fresh Look At Liquid-Liquid Extraction (Part 1). *Chemical Engineering.* **1991**, 98, 66-76.

(3) Ricci, L. *Separation Techniques 1: Liquid-liquid Systems;* McGraw-Hill: New York, 1980.

(4) McKetta, J. J. *Unit Operations Handbook Volume 1: Mass Transfer*; Marcel Dekker: New York, 1993.

(5) Whitesides, G. M. The origins and the future of microfluidics. *Nature*. **2006**, 442, 368-372.

(6) Clayton, J. Go with the microflow. *Nature Publishing Group*. **2005**, 2, 621-627.

(7) McDonald, J. C.; Whitesides, G. M. Poly(dimethylsiloxane) as a Material for Fabricating Microfluidic Devices. *Accounts of Chemical Research.* **2002**, 35, 491-499.

(8) Harrison, C.; Cabral, J.T.; Stafford, C. M.; Karim, A.; Amis, E. J. A rapid prototyping technique for the fabrication of solvent-resistant structures. *Journal of Micromechanics and Microengineering.* **2004**, 14, 153-158.

(9) Barbic, M.; Mock, J.J.; Gray, A.P.; Schultz, S. Electromagnetic Micromotor for Microfluidics Applications. *Appl. Phys. Lett.* **2001**, 79, 1399-1401.

(10) Jonsson, M.; Johnson, B. Millichannel Reactors: A Practical Middle Ground for Production. *Chemical Engineering*. **2009**, 116, 44-50.

(11) Atencia, J.; Beebe, D. J. Controlled Microfluidic Interfaces. *Nature.* **2005**, 437, 648-655.

(12) Burns, J. R.; Ramshaw, C. The intensification of rapid reactions in multiphase systems using slug flow in capillaries. *The Royal Society of Chemistry.* **2001**, 1, 10-15.

(13) Sun, M.; Du, W.; Fang, Q.; Microfluidic Liquid-liquid Extraction System Based on Stopped-flow Technique and Liquid Core Waveguide Capillary. *Talanta.* **2006**, 70, 392-396.

(14) Silvestre, C. I. C.; Santos. J. L. M.; Lima, J. L. F. C.; Zagatto, E. A. G. Liquid-liquid Extraction in Flow Analysis: A Critical Review. *Analytica Chimica Acta*. **2009**, 652, 54-65.

(15) Berduque, A.; O'Brien, J.; Alderman, J.; Arrigan, D. W. M. Microfluidic Chip for Electrochemically-modulated Liquid-Liquid Extraction of Ions. *Electrochemisty Communications*. **2008**, 10, 20-24.

(16) Saien, J.; Daliri, S.; Modelling Mass Transfer Coefficient for Liquid-liquid Extraction with the Interface Adsorption of Hydroxyl Ions. *Korean Journal of Chemical Engineering.* **2009**, 26, 963-968.

(17) Zhao, B.; Moore, J. S.; Beebe, D. J. Surface-directed Liquid Flow Inside Microchannels. *Science.* **2001**, 291, 1023-1026.

(18) Aota, A.; Nonaka, M.; Hibara, A; Kitamori, T. Countercurrent Laminar Microflow for Highly Efficient Solvent Extraction. *Angew. Chem. Int. Ed.* **2007**, 46, 878-880.

(19) Aota, A.; Kitamori, T. Microunit Operations and Continuous Flow Chemical Processing. *Advances in Chemical Engineering*. **2010**, 38, 1-36.

(20) Cai, Z.; Fang, Q,; Chen, H.; Fang, Z. A Microfluidic Chip Based Liquid-Liquid Extraction System with Microporous Membrane. *Analytica Chimica Acta*. **2006**, 556, 151-156.

(21) Tokeshi, M.; Minagawa, T.; Kitamori, T. Integration of a Microextraction System on a Glass Chip: Ion-Pair Solvent Extraction of Fe(II) with 4,7-Diphenyl-1, 10-phenanthrolinedisulfonic Acid and Tri-n-octylmethylammonium Chloride. *Analytical Chemistry.* **2000**, 72, 1711-1714.

(22) Maruyama, T.; Matsushita, H.; Uchida, J.; Kubota, F.; Kamiya, N.; Goto, M. Liquid Membrane Operationse in a Microfluidic Device for Selective Separation of Metal Ions. *Analytical Chemistry.* **2004**, 76, 4495-4500.

(23) Jung, G.; Li, Z.; Wu, W.; Chen, Y.; Olynick, D. L.; Wang, S.; Tong, W.M.; Williams, R.S. Vapor-Phase Self-Assembled Monolayer for Improved Mold Release in Nanoimprint Lithography. *Langmuir.* **2005,** 21, 1158-1161.

(24) Ghasemi, J.; Niazi, A.; Kubista, M. Thermodynamics study of the dimerization equilibria of rhodamine B and 6G in different ionic strengths by photometric titration and chemometrics method. *Spectrochimica Acta.* **2005**, 62, 649-656.

(25) Lu, Y.; Penzkofer, A. Absorption Behavior of Methanolic Rhodamine 6G Solutions at High Concentration. *Chemical Physics*. **1986**, 107, 175-184.

(26) Toptygin, D.; Packard, B. X.; Brand, L. Resolution of absorption spectra of rhodamine 6G aggregates in aqueous solution using the law of mass action. *Chemical Physics Letters.* **1997**, 277, 430-435.

(27) Blankenstein, G.; Larsen, U. D. Modular Concept of a Laboratory on a Chip for Chemical and Biochemical Analysis. *Biosensors and Bioelectronics*. **1998**, 13, 427-438.

(28) Sai, Y.; Yamada, M.; Yasuda, M.; Seki, M.; Continuous Separation of Particles Using a Microfluidic Device Equipped with Flow Rate Control Valves. *Journal of Chromatography A*. **2006**, 1127, 214-220.

(29) Dusseault, J.; Tam, S.; Menard, M.; Polizu, S.; Jourdan, G.; Yahia, L.; Halle, J. Evaluation of Alginate Purification Methos: Effect on Polyphenol, Endotoxin, and Protein Contamination. *Wiley Periodicals, Inc.* **2005**, 243-251.

(30) Garcia, A. A.; Bonen, M. R.; Ramirez-Vick, J.; Sadaka, M.; Vuppu, A. *Bioseparation Process Science;* Blackwell Science: Malden, 1999.

(31) Sivasankar, B. *Bioseparations: Priniciples and Techniques*. Prentice Hall of India: New Delhi, 2005.

(32) Matteson, M. J.; Orr, C. *Filtration: Priniciples and Practices*, 2nd ed.; Marcel Dekker: New York, 1987.

(33) Mironov, V.; Kasyanov, V.; Zheng Shu, X.; Eisenberg, C.; Eisenberg, L.; Gonda, S.; Trusk, T.; Markwald, R. R.; Prestwich, G. D. Fabrication of Tubular Tissue Constructs by Centrigual Casting of Cells Suspended in an In Situ Crosslinkable Hyaluronan-gelatin Hydrogel. *Biomaterials.* **2005**, 26, 7628-7635.

(34) Howe, K. J.; Clark, M. M. Fouling of Microfiltration and Ultrafiltration Membranes by Natural Waters. *Environ. Sci. Technol.* **2002**, 36, 3571-3576.

(35) Georges, J. Deviations from beer's law due to dimerization equilibria: theoretical comparison of absorbance, fluorescence and thermal lens measurements. *Spectrochimica Acta.* **1995**, 6, 985-994.

(36) Sangster, S. *Octanol-Water Partition Coefficients: Fundamentals and Physical Chemistry.* John Wiley & Sons: New York, 1997.

(37) *2-Pentanone*; U.S. Department of Health and Human Services: Washington, D.C., September 17, 2010.

(38) Stephenson, R. M. Mutual Solubilities: Water-Ketones, Water-Ethers, and Water-Gasoline-Alcohols. *Journal of Chemical Engineering Data.* **1992**, 37, 80-95.

(39) Cussler, E. L. *Diffusion: Mass Transfer in Fluid Systems*. Cambridge University Press: Cambridge, 1997.

Chapter 3: Emulsion Separation at the Milli-fluidic Scale

3.1 Background

3.1.1 Emulsion Formation

An emulsion is a dispersion of liquid droplets in a continuous, immiscible, liquid medium. Emulsions are most frequently encountered in the pharmaceutical, metallurgical, and food industries where they are used to prevent degradation or control time release properties, used as a coolant, and used to affect the product's texture or another physical property, respectively [1].

The most frequently employed industrial methods of emulsion formation can be separated into four categories: rotor-stator systems, high-pressure systems, membrane systems, and ultrasonic systems. These four methods of emulsion formation are illustrated in Figure 3.1. Rotor-stator systems use inertia during turbulent flow or shear stresses during laminar flow to induce droplet breakup of the dispersed phase, resulting in droplets with diameters as small as 1 µm. High-pressure systems use inertial forces, shear stresses, and cavitation to create droplet disruption and can result in emulsions with droplet diameters as small as 0.2 µm. In membrane systems, the dispersed phase is pressed through a microporous glass or ceramic membrane, resulting in droplets as small 0.2 µm in diameter. On the other side of the membrane, the continuous phase flows along the membrane and surrounds each droplet. Little stress is applied during this emulsion formation process making this method suitable for stress-sensitive products. In ultrasonic systems, an ultrasonic sonotrode causes droplet break up by microturbulences and

cavitation. Rotor-stator and high-pressure systems are high throughput systems and thus are suitable for industrial production. Membrane and ultrasonic systems, however, are better suited for laboratory scale production[2].
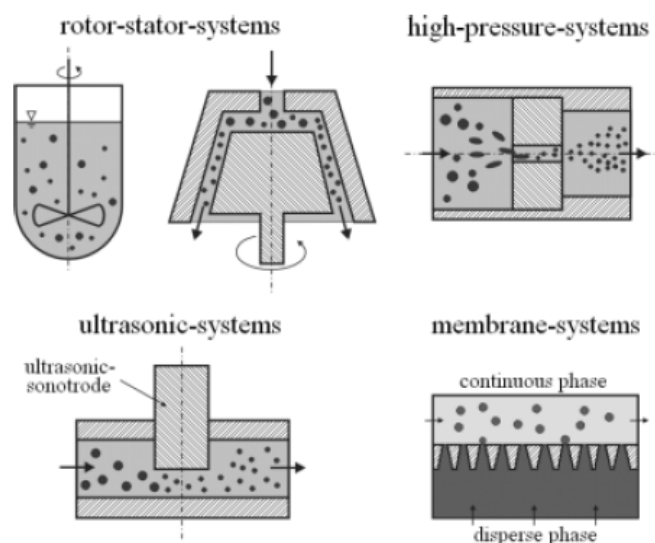
Figure 3.1. Four typical methods of emulsification[2].

A method of emulsion formation that is becoming increasingly popular is emulsion formation within microfluidic devices. The formation of emulsions with droplets on the sub-millimeter scale can be accomplished through the use of micro- and milli-fluidic devices by employing a cross-flow shear method at a T-junction or flow focusing geometry[3]. A T-junction device joins two immiscible phases at a perpendicular intersection forcing droplets of one phase to break off into a continuous phase. Flow focusing devices force the droplet forming stream through a small orifice shielded by continuous flow where shear forces cause the stream to break into droplets[4]. In this thesis, emulsions were formed using the cross-flow shear method within a T-junction

microfluidic device as shown in Figure 3.2, where water is the dispersed phase and oil is the continuous phase. The shear force that results when the water and oil streams collide at the T-junction causes droplets of water to break off into the continuous oil phase[4]. The surface chemistry of the channel plays a large role in the resulting emulsion by dictating which immiscible phase is the continuous phase and which is the dispersed phase. A hydrophobic channel wall results in a water-in-oil emulsion while a hydrophilic channel wall results in an oil-in-water emulsion. This well-controlled method of emulsion formation allows for highly reproducible emulsion formation with uniform droplet size. The ratio of water flow rate to oil flow rate can be varied to change droplet size. The ratio of water to oil flow rate can be scaled up to increase emulsion formation rate while maintaining droplet size[5].
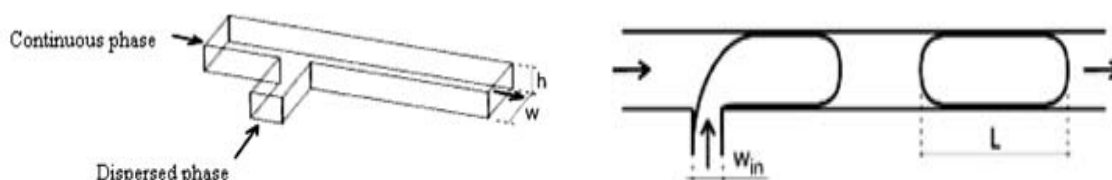
Figure 3.2. Emulsion formation within a T-junction microfluidic device[4].

3.1.2 Emulsion Separation

Oily wastewater streams are the result of many large industries, such as the petrochemical, pharmaceutical, and food industries[6]. Emulsion formation is particularly common as a result of petroleum production, when water and oil are present in oil reservoirs and water-in-oil emulsions are formed when shear forces accumulate during the oil extraction process[7]. It is necessary to separate emulsions formed as a result of

industrial production processes to ensure proper disposal and prevent environmental pollution. Current methods of emulsion separation consist of gravity separation, skimming, air flotation, and the addition of demulsifying agents. Gravity separation, the most common form of emulsion separation, depends on the density difference between the two immiscible phases, making it a poor choice for emulsions where there is only a slight difference in density between the dispersed and continuous phases. Longer retention times are required to increase separation efficiency. Skimming refers to natural separation of immiscible phases by gravity followed by removal of the lower density material by either a rotating drum or a scraper. In air flotation, a separation method that is generally used when gravity separation is ineffective, air bubbles are injected into the emulsion. The organic phase adheres to the air bubbles and floats to the surface as a foam. The foam is then skimmed from the surface[8]. The use of demulsifying agents to induce emulsion separation can in some cases promote the formation of an invert emulsion[9]. Limitations of these conventional emulsion separation methods include low efficiency and high operating costs[6].

Emulsions are also the result of microreactor systems. Microreactors are reactor systems with fluid channel dimensions on the sub-micrometer to the sub-millimeter range, generally created by flow focusing or T-junction devices[10]. These miniaturized reactors are a novel method for consistently creating small volumes of a product with both high purity and high yields, ideal for producing nanoparticles and biomolecules[11,12,13]. Furthermore, the chemical composition of microreactors is easily controlled by changes in feed flow rates[14]. Reactions progress to completion quickly due to the use of small

volumes, allowing for mixing by diffusion, and due to the internal mixing present in droplets because of viscosity and surface tension effects[11,14]. Microreactors are also suitable for safe execution of highly exothermic reactions that are usually too dangerous to carry out at the macroscale due to difficulties controlling heat transfer[14]. These microreactors can be created by water-in-oil emulsions, where oil serves as a boundary to diffusion, allowing the aqueous droplet to function as a self-contained reactor[10]. Once reactions are completed, it is necessary to recover the product within the microreactors.

Milli-scale separation devices can be applied to the separation of oil and water emulsions, specifically for purification in petroleum production and wastewater treatment, as well as microreactor recovery methods. By eliminating the need for demulsifiers and the wait associated with gravity separation, the method of emulsion separation explored in this thesis allows for more rapid and more reliable emulsion separation. The passive emulsion separation method described here has demonstrated separation efficiencies of greater than 80% and can be applied to further purify industrial waste streams. Furthermore, the milli-fluidic separation method described here provides a method for extracting the material contained within microreactors into a continuous aqueous stream.

Current research in the field of emulsion separation has shown success separating emulsions on the microfluidic scale by application of an external electrical field[15,16], use of optically induced dielectrophoresis (ODEP)[17], and use of a pore comb structure for capillary phase separation[18]. In previous work, an aqueous stream was flowed parallel to an oil stream containing aqueous droplets and an externally applied electrical signal was

used to cause aqueous droplets to merge with the continuous aqueous stream for emulsion separation. Below a certain threshold voltage, the aqueous droplets are not affected by the flow of the aqueous stream. However, droplet coalescence with the aqueous stream is induced when the electric field increases above the threshold voltage[15]. Other researchers have used ODEP for the size-based separation of an oil-in-water emulsion containing parent and satellite droplets. A negative ODEP force was used to repel oil droplets. As a beam of light was moved from right to left across the microfluidic chip, oil droplets migrated to the left. The speed each droplet moved was dependent upon the radius of the oil droplet, resulting in size-based droplet separation[17]. Angelescu et al. applied a hydrophobic PDMS pore comb structure for the passive, continuous separation of oil droplets from a continuous water stream. Though effective, the process was difficult to control due to pressure fluctuations within the microfluidic device which caused part of the aqueous stream to enter the hydrophobic pore comb structure. These fluctuations could be avoided by decreasing the pore comb diameter. However, a decrease in pore comb diameter makes the device even more susceptible to compromise by deposits and is difficult to achieve by current fabrication techniques[18]. The method of emulsion separation discussed in this thesis aims to provide a passive method of emulsion separation that is less likely to encounter solids related damage due to the increase in channel dimensions to the milli-scale. For milli-scale separation to be applicable on a large scale for industrial extractions, arrays of these separation devices should be assembled and operated in parallel. Research in the integration of microfluidic device networks has shown this is feasible and demonstrates robustness to process conditions[19].

Placement of the emulsion inlet needle is a critical factor in the efficiency of emulsion separation because the needle must interface with the hydrogel in a way that deforms each droplet of the dispersed phase and disrupts the boundary layer surrounding each droplet as it enters the emulsion separation device. If the needle interfaces with the hydrogel layer in a manner that allows a droplet to pass through without being deformed, then it is unlikely that the aqueous droplet will enter the aqueous phase. Instead, the droplet will move within the organic phase along the organic-aqueous interface. At high enough water flow rates, the shear from the aqueous stream against the emulsion inlet needle can also deform the droplet enough to disrupt the oil boundary layer surrounding each aqueous droplet. However, this situation is harder to control and is a less reliable method of emulsion separation. An illustration of the separation device demonstrating the location of the emulsion inlet needle is shown in Figure 3.3. Once the boundary layer surrounding each aqueous droplet is disrupted, the aqueous droplet is free to enter the continuous aqueous phase along the hydrogel boundary while the oil phase migrates towards the continuous oil stream along the optical adhesive boundary of the device channel. Because the co-current laminar flow of the oil and water streams is stabilized due to the presence of the hydrogel layer and channel surface modifications, there is perfect separation at the outlet of the emulsion separation device.
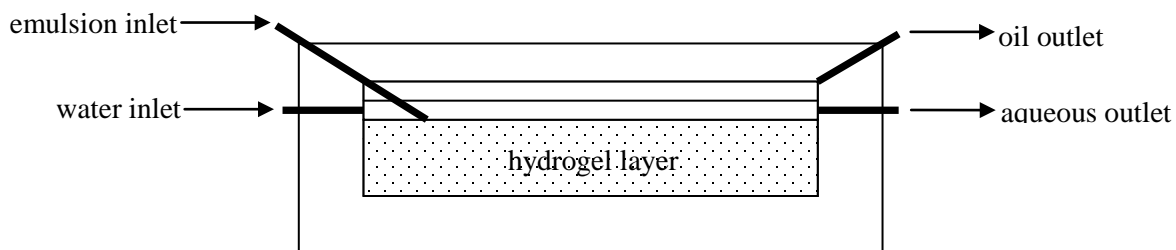
Figure 3.3. Schematic of the emulsion separation device demonstrating the location of the emulsion inlet needle.

Once emulsion separation has been accomplished at the micro- and milli-fluidic levels, the separation process will be scaled up to allow for separation at process scale flow rates. This will demonstrate the feasibility of this separation method in industrial settings. Scale up of the emulsion separation device was successfully accomplished, attaining a maximum emulsion flow rate of 3 ml/min, while maintaining greater than 80% emulsion separation efficiency. The scale up was accomplished by increasing the device width to approximately 2 mm and by increasing the device channel height to approximately 10 mm. As the dimensions of the device increase, higher flow rates are possible while maintaining more laminar flow. Such laminar flow is necessary to ensure efficient emulsion separation at process scale emulsion flow rates. An increase in device dimensions also allows for an increase in flow rates while maintaining a smooth liquid-liquid interface.

This chapter details the usefulness of milli-fluidic devices as a practical separation method. Milli-fluidic devices exhibit many of the beneficial fluid properties of microfluidic devices while being able to process larger volumes of fluid per time. Milli-

fluidic device dimensions are small enough that mixing occurs by diffusion, laminar flow occurs, and heat transfer can be easily controlled. By increasing the dimensions of the channel within the separation device to the millimeter scale the occurrence of solids-related damage is decreased and the pressure drop over the length of the channel is decreased. This pressure drop is especially significant in viscous fluids[20].

3.2 Materials

This section lists all materials used in the construction and use of the emulsion formation device and emulsion separation device. This part is separated into four sections: preparatory cleaning, emulsion formation device fabrication, emulsion separation device fabrication, and experimental trials.

3.2.1 Preparatory Cleaning

The materials used to clean the glass slides prior to being used for emulsion formation and separation devices include acetone [>99% purity by weight, Reochem Inc.], ethanol [>99.98%, Pharmco-Aaper], and delicate task wipers [Kimtech Sciences]. A Harrick Radio Frequency Plasma Cleaner was used with oxygen for cleaning purposes.

3.2.2 Emulsion Formation Device Fabrication

The materials used to create the emulsion separation device include a Sylgard® 184 silicone elastomer kit [Dow-Corning], nonsterile, blunt-end pipetting hub needles [35.6 x 10.2 cm, Cole Parmer Instrument Co.], poly(tetrafluoroethylene) (Teflon) tubing [Cole-Parmer], glass slides [3 in. x 1 in. x 1 mm, VWR], thiolene optical adhesive [NOA-81 resin, Norland Products Inc.], patterned transparencies, ethanol [>99.98%, Pharmco-Aaper], and acetone [>99%, Reochem Inc.]. A Blak-Ray® Ultraviolet Lamp was used to provide long-wave (365 nm) ultraviolet light and a UVAB ST-513 UV Lightmeter was used to measure the intensity of the ultraviolet light source.

3.2.3 Emulsion Separation Device Fabrication

The materials used to create the emulsion separation device are glass slides [3 in x 1 in x 1 mm, VWR], silicon spacers, thiolene optical adhesive [NOA-81 resin, Norland Products Inc.], patterned transparencies, ethanol [>99.98%, Pharmco-Aaper], acetone [>99%, Reochem Inc.], 3-(trichlorosilyl)-propyl methacrylate (TPM) [≥95 %, Fluka], hexane [Matheson, Coleman & Bell], poly(ethylene glycol)(diacrylate) (PEG-DA) [MW 575, Sigma Aldrich], 4-(2-hydroxyethoxy)phenyl-(2-hydroxy-2-propyl)ketone [Irgacure 2959, Ciba Specialty Chemicals], and needles [18 G x 3.8 cm and 21 G x 3.8 cm, Becton-Dickinson]. A Blak-Ray® Ultraviolet Lamp was used to provide long-wave (365 nm) ultraviolet light and a UVAB ST-513 UV Lightmeter was used to measure the intensity of the ultraviolet light source.

3.2.4 Experimental Trials

The materials used to conduct emulsion separation trials include high oleic sunflower oil (P82% oleic acid), Sudan IV [Sigma], mineral oil [Sigma Aldrich], methylene blue dye [Sigma Aldrich], crystal violet dye [Baker], dextran from *Leuconostoc mesenteroides* [MW 35,000–45,000, Sigma], 24 mL luer-lock plastic syringes [Henke Sass Wolf], silicone tubing [0.85 mm and 0.8 mm inner diameter, Cole-Parmer], and NE-300 Single Syringe Pumps [New Era Pump Systems Inc., Model No. NE-300, syringepump.com].

3.3 Methods

3.3.1 Emulsion Separation

This section discusses the procedure used to create the emulsion formation device and emulsion separation device and how to operate them. This part is separated into four sections: preparatory cleaning, emulsion formation device fabrication, emulsion separation device fabrication, and experimental trials.

3.3.1.1 Preparatory Cleaning

All glass slides are cleaned with acetone using a delicate task wiper and allowed to air dry. All glass slides are then wiped with ethanol to deposit a monolayer of hydroxyl groups along the surface of the glass slides. The presence of these hydroxyl groups will be necessary for solution deposition of a TPM monolayer. The glass slides are placed in the plasma cleaner and cleaned with oxygen for 3 min to ensure removal of organic contaminants.

3.3.1.2 Emulsion Formation Device Fabrication

A T-junction master slide was created to serve as a template for the emulsion formation device. A glass slide was placed over a pool of optical adhesive so that the glass slide was in complete contact with the optical adhesive. A photomask patterned with a T-junction channel design, as shown in Figure 3.4, was placed over the glass slide and the assembly was exposed to UV light at an intensity of 3700 μW/cm^2 for 4 min. The glass slide was then cleaned with pressurized air, acetone, and ethanol to remove any

excess optical adhesive. The master slide was UV post cured for 10 min at a UV intensity of 3700 μW/cm^2 and baked at 50 ^{o}C for 4 h. The result is a master slide with a T-junction design outlined in optical adhesive.

Figure 3.4. T-junction emulsion formation photomask design.

To create the emulsion formation device, a mixture of the PDMS elastomer base and 10 wt% curing agent was vigorously mixed for 5 min. This mixing is necessary for the silicon hydride groups in the curing agent to react with the vinyl groups present in the base to form the crosslinked polymer[21]. The T-junction master slide was surrounded with aluminum foil with the optical adhesive design exposed and the PDMS mixture was applied. The entire assembly was degassed in a vacuum desiccator until all air bubbles were eliminated. A thin layer of the PDMS mixture was applied evenly to a clean glass slide. The PDMS coated glass slide and PDMS coated T-junction master slide were baked at 70 ^{o}C for 2 h to cure the PDMS polymer. After curing, the patterned PDMS slab was carefully removed from the master slide and placed on a clean piece of foil with the design facing down. The inlet and outlet ports were excavated using blunt-end pipetting hub needles and the edges of the PDMS slab were trimmed using a razor. Both the PDMS coated glass slide and the PDMS slab were exposed to oxygen plasma for 5 min.

Immediately after exposure to oxygen plasma, the two PDMS parts were pressed together resulting in an irreversible seal. The result of this procedure is a hydrophobic PDMS channel approximately 800 µm in height and 1100 µm in width.

3.3.1.3 Emulsion Separation Device Fabrication

The emulsion separation device was created in a UV sensitive setting to prevent unwanted curing of the optical adhesive and hydrogel layer within the device. Two silicon spacers, each 0.6 mm thick, were stacked at each corner of a clean glass slide. Optical adhesive was applied to the glass slide and a second glass slide was laid carefully on top of the optical adhesive. The glass slide was applied at an angle so that no air bubbles became trapped between the optical adhesive and glass slide. A photomask, as shown in Figure 3.5, was laid on top of the glass slides to define the optical adhesive channel.

Figure 3.5. Emulsion separation device photomask design.

The corners of the glass slides were covered to prevent curing of the spacers to the glass slides and the entire assembly was exposed to UV light at an intensity of 1100 $\mu W/cm^2$ for 14 min. After 7 min of exposure the assembly was rotated 180° to ensure even curing of the entire device. After UV curing, the spacers were removed and the optical adhesive

channel was cleaned with pressurized air, acetone, and ethanol. Needles, 21G and 18G in size, were cured into the inlets and outlets of the device, respectively, using optical adhesive. Larger outlets needles are necessary to maintain stable co-current laminar flow within the device by facilitating removal of the oil phase. The device was baked at 50 $^{\circ}$C for 12 h to increase the adhesion of the optical adhesive to the glass slide[22].

After baking, the glass slides are exposed to a solution of 1 mM TPM in hexane for 25 min for deposition of a complete self-assembled monolayer. The TPM solution deposits less hydrophilic groups along the channel to help stabilize organic flow along the optical adhesive boundary and enables the hydrogel layer to bond to the glass slide as described in the overview. It is necessary for the hydrogel layer to bond to the glass slide to allow for stable co-current laminar flow by ensuring that water flows through the hydrogel rather than around it. Excess self-assembled monolayer was removed by rinsing with hexane. The channel is dried with pressurized air. A hydrogel solution of 40 vol.% water, 60 vol.% PEG-DA, and 0.25 wt% Irgacure 2959 was injected to fill the channel. Opaque, black electrical tape served as a photomask and was applied to define the hydrogel layer just below the aqueous inlet and outlet locations. The device and photomask are exposed to UV light at an intensity of 1100 μW/cm^2 for 14 min. After 7 min of UV exposure the device is rotated 180° to ensure even curing. Once curing is complete, excess hydrogel solution was removed with deionized water and the upper inlet needle was pushed to the surface of the hydrogel layer so that approximately 30% to 50% of the needle opening is embedded in the hydrogel layer. If devices are not used immediately, the channel is filled with water to prevent the hydrogel from dehydrating,

wrapped in foil to prevent the hydrogel from curing as the result of stray UV radiation, and stored in the refrigerator to prevent thermal degradation of the PEG-DA.

3.3.1.4 Experimental Trials

Syringes were loaded with aqueous solutions of methylene blue (1.78×10^{-4} g/ml), crystal violet (1.2×10^{-4} g/ml), or dextran and methylene blue (0.03 g/ml and 1.78×10^{-4} g/ml, respectively); sunflower oil or mineral oil; and deionized water. The dextran solution was dyed using methylene blue so that droplets of the dextran solution entering the aqueous phase within the emulsion separation device were visible. Within the T-junction device, aqueous droplets break off into the continuous oil phase. The outlet of the emulsion formation T-junction device was connected to the upper inlet of the emulsion separation device and deionized water was transported to the lower inlet of the emulsion separation device at a flow rate of 10 ml/h. Aqueous solution and oil flow rates supplied to the emulsion formation device were varied to achieve aqueous: oil flow rate ratios ranging from 0.4 to 2.5. This experimental setup is shown in Figure 3.6.
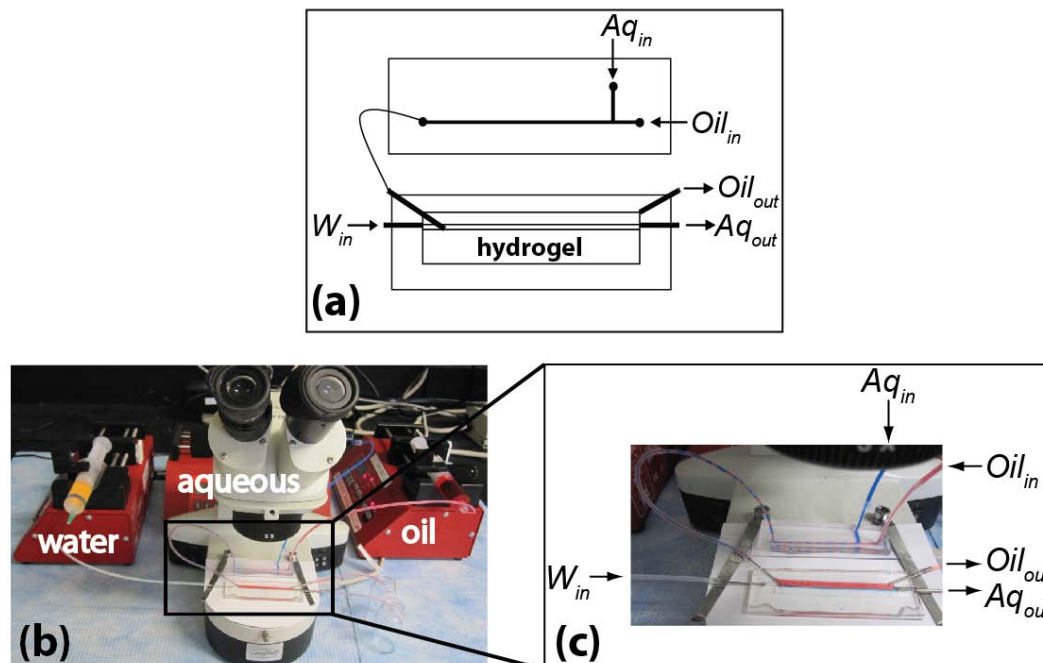
Figure 3.6. (a) Schematic of emulsion formation and separation devices were Aq_{in}

and Aq_{out} are aqueous inlet and outlet, Oil_{in} and Oil_{out} are oil inlet and outlet, and

W_{in} is the water inlet. (b) Emulsion formation and separation experimental setup. (c)

Enlarged image of T-junction emulsion formation and separation devices shown in

(b).

3.3.1.5 Interfacial Tension Measurements

The interfacial tension between high oleic sunflower oil and each of the aqueous

solutions (crystal violet, methylene blue, dextran + methylene blue) and between mineral

oil and aqueous methylene blue solution were determined using a KSV Sigma 703D

manual tensiometer. It was necessary that the instrument be turned on for at least 30 min

prior to use and be calibrated using the pre-weighed calibration weight. The density of

each phase was measured using the glass density measurement probe. The glass probe was cleaned with deionized water and acetone and placed on the balance hook. A clean sample container with the solution to be measured was placed on the sample stage. The balance was tared while the glass probe was exposed to the atmosphere so that the density of air, approximately 0.0012 g/ml, was shown on the display screen. The sample stage was raised to immerse the glass probe in the solution. The density of the solution was reported on the display screen. This procedure for density measurement was repeated three times for each solution.

The interfacial tension was measured with a DuNouy ring. The DuNouy ring was submerged in acetone and hexane and burned to remove all contaminants. The ring was carefully placed on the balance hook, making sure not to deform the ring or touch the base of the ring. The instrument was set to the uncorrected DuNouy mode and the density difference between the heavy and light phase of the solutions was input. The heavy phase, the aqueous solution, was transferred to a clean beaker and the balance was tared. The ring was submerged in the heavy phase and the maximum value was reset using the "clear max" button. The light phase, high oleic sunflower oil or mineral oil, was carefully added over the heavy phase. The stage was slowly lowered, dragging the ring through the heavy phase and into the light phase. When the meniscus "hanging" from the ring collapses, the maximum interfacial tension is reported on the display screen. This procedure for interfacial tension measurement was repeated three times for each combination of aqueous solution and high oleic sunflower oil and repeated three times for aqueous methylene blue solution and mineral oil.

3.3.2 Emulsion Separation Scale Up

For the emulsion separation scale up project, the same T-junction device was used to create the emulsion. The aqueous and oil flow rates to the emulsion formation device were increased while maintaining the aqueous: oil flow ratio at 1. The procedure for creating the emulsion separation device remained the same with the exception of the number of spacers used to separate the two glass slides, the UV intensity, the UV cure times, and the photomask used to define the optical adhesive channel. Table 3.1 summarizes the procedural differences in fabricating each of the emulsion separation scale-up devices.

Table 3.1. Summary of procedural differences for emulsion separation scale-up

device fabrication where channel length was held constant at 50 mm.

Width × height (mm × mm)	Number of Spacers	Optical Adhesive Cure Intensity ($\mu W/ cm^2$)	Optical Adhesive Cure Time (min)	Hydrogel Cure Intensity ($\mu W/ cm^2$)	Hydrogel Cure Time (min)	Photomask Design
1.2 × 3	2	1100	14	1100	14	Figure 3.7
1.8 × 3	3	1300	60	1300	15	Figure 3.7
1.8 × 6	3	1300	60	1300	15	Figure 3.8
1.8 × 10	3	1300	60	1300	15	Figure 3.9

The number of spacers used in device fabrication sets the width of the separation device. In the emulsion separation scale-up project, the number of spacers varied between 2 spacers, resulting in a 1.2 mm wide channel, and 3 spacers, resulting in a 1.8 mm wide

channel. The UV intensity was increased from 1100 µW/ cm^2 for the 2 spacer devices to 1300 µW/ cm^2 for the 3 spacer devices to ensure more effective curing. The cure times for the optical adhesive and hydrogel vary with device width because a greater width requires more time for the UV rays to penetrate into the width of the device. Finally, the photomask design was altered to increase the height of the channel and to ensure good outlet separation over a variety of flow conditions. Poor outlet separation results in the formation of an emulsion at the device outlet instead of generating pure aqueous and organic streams. For the emulsion separation scale-up, the channel length remained unchanged because length is not a significant factor in emulsion separation or in determination of flow limitations. Figures 3.7 through 3.9 show the various photomasks that were used to define the optical adhesive channel in each of the emulsion separation scale-up devices.

Figure 3.7. Emulsion separation scale-up photomask resulting in ~ 3 mm channel height.

Figure 3.8. Emulsion separation scale-up photomask resulting in ~ 6 mm channel height.

Figure 3.9. Emulsion separation scale-up photomask resulting in ~ 10 mm channel height.

Additional changes were made in device design to ensure good separation of the organic and aqueous stream at device outlets. This became especially important at higher emulsion flow rates as good outlet separation became more difficult to maintain. The aqueous outlet needle was manually crimped approximately 15 times along the length of the needle using pliers. The degree of crimping required to maintain good outlet separation at various emulsion flow rates was determined by trial and error.

3.4 Results

3.4.1 Emulsion Separation

The PDMS T-junction emulsion formation devices had channels 800 µm tall and 1100 µm wide. The height and width of the channel establish to some extent the size of droplets. The emulsion formation device consistently created a water-in-oil emulsion where droplet volume was determined by the relative aqueous and oil flow rates.

The resulting milli-fluidic emulsion separation device sustained co-current laminar flow of two immiscible fluids and efficient emulsion separation. Co-current laminar flow occurred immediately upon entering the emulsion separation device and was sustained throughout the length of the device. The Weber number for the various emulsion separation systems was calculated to demonstrate the interfacial stability of two-phase flow. The Weber numbers ranged from 3.29×10^{-4} to 1.14×10^{-3}, demonstrating the interfacial stability of two-phase flow. A Weber number greater than 1 would demonstrate interfacial turbulence and instability. The capillary number for the various emulsion separation systems was calculated to demonstrate stable parallel flow. The capillary number ranged from 3.54×10^{-3} to 9.51×10^{-3}. Such low capillary numbers demonstrate the significance of forces of interfacial tension over forces of viscosity, resulting in a decrease in interfacial area. Due to channel dimensions (a much smaller channel width than channel height), the smallest interfacial area per volume of fluid occurs by parallel flow of the two immiscible liquids.

To demonstrate the robustness of the emulsion separation device, several oil/aqueous systems were used. In each system, different water-soluble solutes were loaded into the aqueous stream entering the emulsion formation device. High oleic sunflower oil and mineral oil were used as the continuous phase; water soluble solutes selected for this study were methylene blue, crystal violet, and dextran. Emulsion separation was effective for various aqueous/oil interfacial tensions and flow rate ratios, and emulsion separation can be applied successfully for the separation of emulsions within this range with this device design.

3.4.1 High oleic sunflower oil/aqueous emulsions

The aqueous solutions and oil were delivered to the inlets of the T-junction device; the aqueous: oil flow rate ratio and thus the aqueous droplet sizes, were varied as shown in Table 3.2. The interfacial tension measured between each of the aqueous solutions and sunflower oil is given in Table 3.3.

Table 3.2. Aqueous solution flow rates and aqueous: oil flow rate ratios for

emulsion formation devices. Droplet lengths (mm) for aqueous solutions as

dispersed phase in high oleic sunflower oil.

Dispersed aqueous phase solute	Flow rate (ml/h)	Aqueous: oil flow rate ratio	Droplet length (mm)
Crystal violet	3	0.4	1.9
	10	2.5	3.6
Dextran + methylene blue	3	0.6	1.8
	10	2.5	3.4
Methylene blue	3	0.6	2.2
	10	2.5	4.2

Table 3.3. Interfacial tension between aqueous solutions and high oleic

sunflower oil.

Dispersed aqueous phase solute	Interfacial tension (mN/m)
Crystal violet	9.66 ± 0.45
Dextran + methylene blue	12.32 ± 0.74
Methylene blue	15.83 ± 1.58

The emulsion that was formed within the T-junction device at aqueous and oil

flow rates of 3 ml/h and 7 ml/h, respectively, for the aqueous/oil system with the lowest

interfacial tension (sunflower oil and aqueous crystal violet solution), is shown in Figure

3.10b. When transferred to the emulsion separation device (Figure 3.10c), the emulsion

was separated with 91 ± 7 vol.% efficiency. Figure 3.10c shows a satellite aqueous droplet, 172.1 µm in diameter, which was unable to be separated into the aqueous stream.
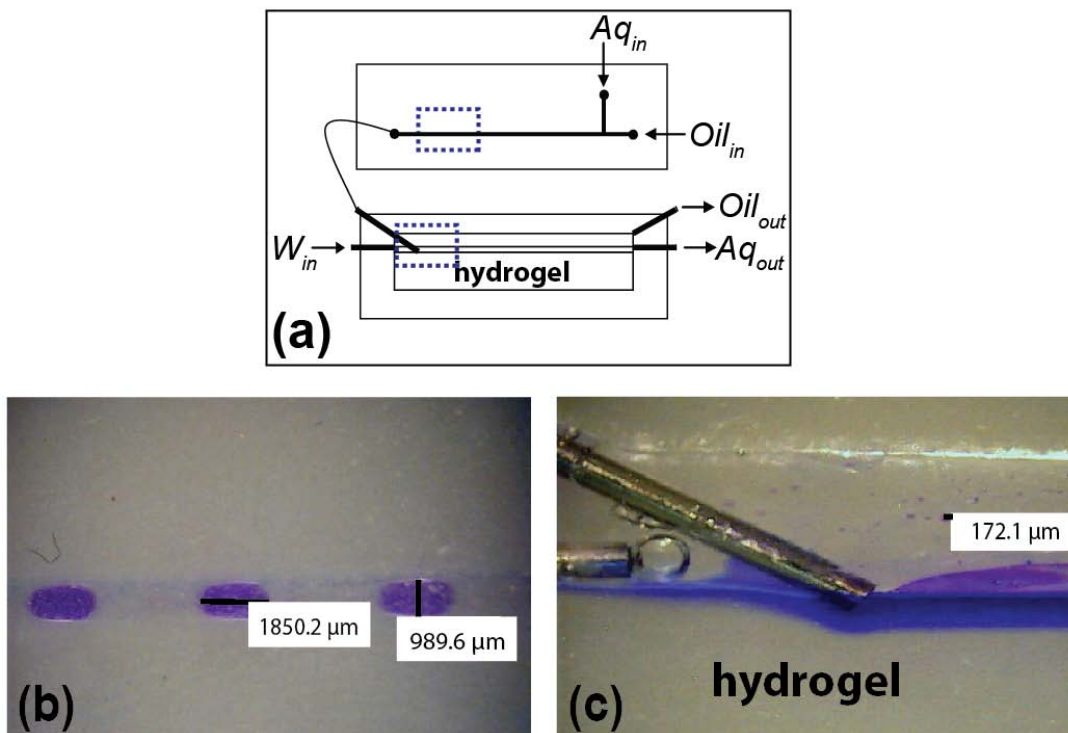

Figure 3.10. (a) Schematic of emulsion formation and separation devices, with (b) and (c) image locations indicated by dashed boxes. (b) Formation of aqueous droplets containing crystal violet within a continuous sunflower oil stream. (c) Separation of aqueous crystal violet droplets from emulsion into a continuous aqueous stream.

The efficiency of the separation was determined by obtaining a timed sample of the oil stream outlet. The expected sample volume was calculated based on the oil volume flow rate and sample time. This value was compared to the actual sample volume and any discrepancy was assumed to be caused by the presence of aqueous droplets that remained

in the oil stream. Oleic acid is insoluble in water and therefore oil losses due to transfer to the water stream were neglected. The difference between the oil sample volume and the expected oil volume was compared to the total volume of aqueous solution dispensed to determine the separation efficiency. There were no visible leaks from the devices even after long experimental times, and no visible oil layer at the surface of the aqueous outlet collection vial. Efficiency measurements were repeated three times at each set of flow rates for each system. The few aqueous droplets that were unable to be separated out of the emulsion were on the order of 100 µm in diameter (typically satellite droplets from the T-junction device). As shown, only a few small satellite aqueous droplets were unable to be separated from the emulsion (droplets shown in Figures 3.10c, 3.11c, 3.12b).

For the aqueous solution of dextran and methylene blue (dextran-mb), Figure 3.11a shows the emulsion that resulted at dextran-mb solution and sunflower oil flow rates of 3 ml/h and 5 ml/h, respectively. The emulsion separation device (Figure 3.11b) was able to separate this emulsion with 90 ± 10 vol.% efficiency. Figure 3.11c shows a satellite aqueous droplet, 150.6 µm in diameter, which was unable to be separated into the continuous aqueous phase. The sunflower oil has been dyed red in this system for clarity and to distinguish from the system where the aqueous phase contains only methylene blue.
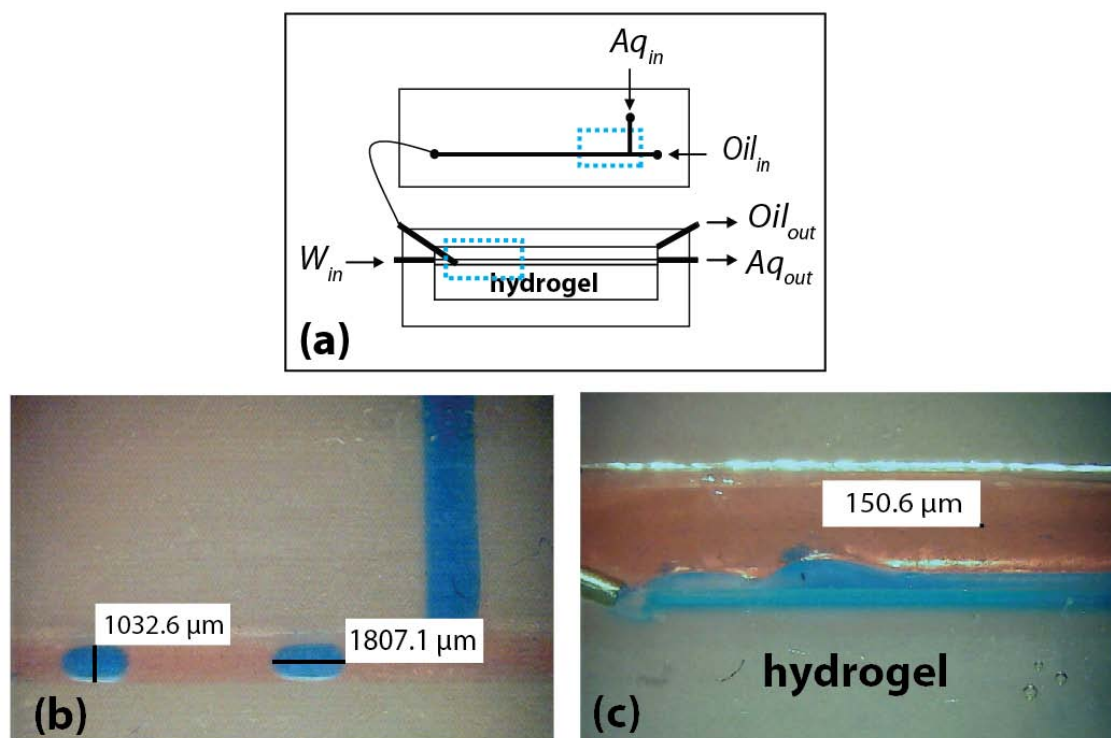
Figure 3.11. (a) Schematic of emulsion formation and separation devices, with (b) and (c) image locations indicated by dashed boxes. (b) Formation of aqueous droplets containing dextran and methylene blue within a continuous sunflower oil stream (dyed red). (c) Separation of aqueous dextran-methylene blue droplets from emulsion into a continuous aqueous stream.

Figure 3.12a shows the emulsion that was formed within the T-junction device for aqueous methylene blue solution and the sunflower oil flow rates of 3 ml/h and 5 ml/h, respectively. The water-in-oil emulsion was then transferred to the emulsion separation device where the aqueous droplets were extracted into the water stream with 97 ± 4 vol.% efficiency. Emulsion separation is shown in Figure 3.12b, where the satellite droplet that was unable to be separated into the aqueous stream is 86.1 µm in diameter.
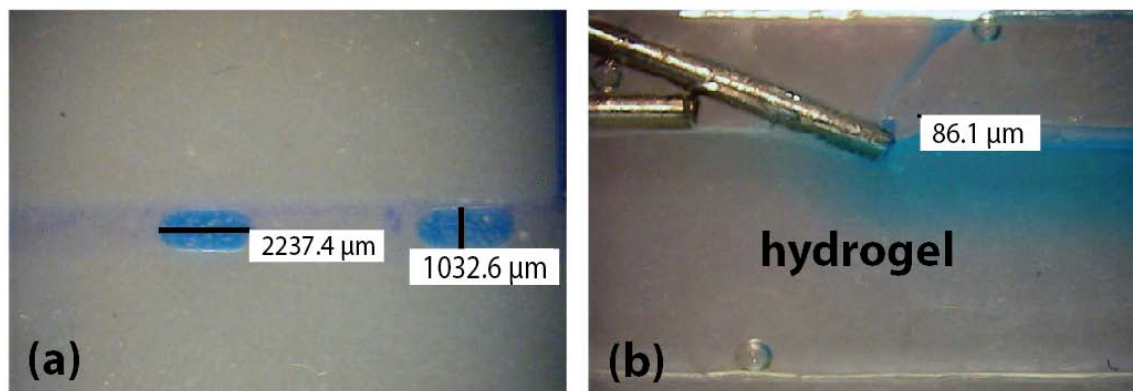
Figure 3.12. Formation of aqueous droplets containing methylene blue within a continuous oil stream. (b) Separation of aqueous methylene blue droplets from emulsion into a continuous aqueous stream.

The importance of the emulsion inlet needle location was investigated. When the inlet needle was moved away from the hydrogel-water stream interface the water droplets were unable to cross the water-oil interface. Instead, the aqueous droplets moved along the interface within the oil stream. When the needle was moved to the hydrogel-water interface, aqueous droplets were able to pass into the water stream although the separation efficiency was significantly lower. Inserting the emulsion inlet needle partially into the hydrogel layer allowed to the needle tip to be modified with a thin layer of hydrogel. It is believed that this modification as well as the location of the inlet needle at the hydrogel water interface allows for efficient emulsion separation by disrupting the oil film surrounding the water droplets. Once the oil boundary layer surrounding each aqueous droplet is disrupted the droplet is free to migrate into the continuous aqueous phase.

3.4.1.2 Mineral oil/aqueous emulsions

The emulsion separation method was applied to an aqueous/oil pair with a relatively high interfacial tension in order to demonstrate the range of interfacial tensions for which these devices can be successfully used. Mineral oil was selected for the oil phase and aqueous methylene blue solution was selected for the aqueous phase resulting in an interfacial tension of 41 ± 2 mN/m. It was observed that at higher interfacial tensions the interface between the oil and aqueous streams became more well-defined. The aqueous: oil flow rate ratio, and thus the aqueous droplet size, was varied as shown in Table 3.4. The water flow rate was maintained at 15 ml/h for all trials with mineral oil.

Table 3.4. Aqueous solution low rates and aqueous: oil flow rate ratios for emulsion formation devices. Droplet lengths (mm) for aqueous solution as dispersed phase in mineral oil.

Dispersed aqueous phase solute	Flow rate (ml/h)	Aqueous: oil flow rate ratio	Droplet length (mm)
Methylene blue	3	0.6	2.6
	10	2.5	7.9

Mineral oil and water are immiscible. In order to better visualize the stabilized co-current laminar flow within the separation device, Figure 3.13 shows droplets of the methylene blue solution being separated from mineral oil which has been dyed red. The aqueous droplets flow directly into the continuous aqueous stream in the separation device with little visible retention of the aqueous droplets in the dyed oil stream.
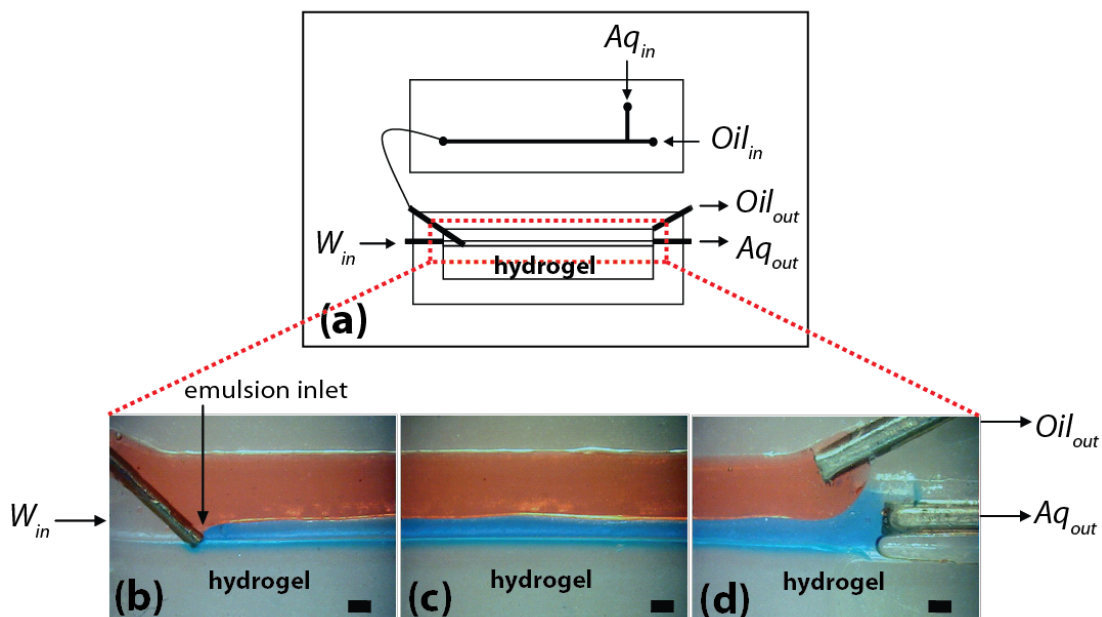
Figure 3.13. (a) Schematic of emulsion formation and separation devices with dashed box showing the location of images (b), (c), and (d). Co-current laminar flow of mineral oil and water allowing for the separation of a water-in-oil emulsion (scale bars: 800 μm) is shown in emulsion separation device. (b) Inlet. (c) Center. (d) Outlet.

Figure 3.14 shows the mineral oil/methylene blue emulsion that formed within the T-junction emulsion formation device at oil and aqueous flow rates of 3 ml/h and 5 ml/h, respectively. The separation device was able to separate the mineral oil/aqueous methylene blue emulsion with 97 ± 6 vol.% efficiency.
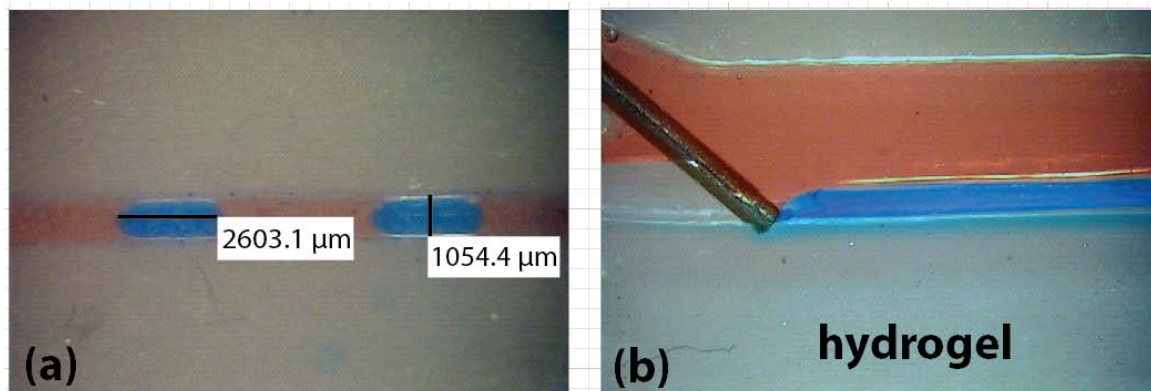
Figure 3.14. (a) Formation of aqueous droplets containing methylene blue within a continuous mineral oil stream. (b) Separation of aqueous methylene blue droplets from emulsion into a continuous aqueous stream.

These emulsion separation experiments demonstrate the robustness of this emulsion separation technique. The emulsion separation device is capable of separating water-in-oil emulsions with aqueous: oil flow rate ratios ranging from 0.4 to 2.5. This separation device is also able to separate emulsions with various hydrophilic solutes loaded into the aqueous phase resulting in interfacial tensions ranging from 9 mN/m to 41 mN/m.

3.4.2 Emulsion Separation Scale Up

For the emulsion separation scale up study, mineral oil containing sudan IV dye and water containing methylene blue dye were used to create an emulsion. Emulsion separation was demonstrated with the adjacent flow of deionized water.

3.4.2.1 Device Design

Due to the viscosity of the organic stream, further adjustments were made to the emulsion separation device in order to ensure good separation of the two fluids at the device outlet as emulsion and water flow rates changed. The primary difficulty that was encountered when attempting emulsion separation at higher flow rates was the contamination of the aqueous outlet stream with organic flow, resulting in an emulsion. Contamination of the aqueous stream outlet becomes more significant at higher flow rates. To prevent this contamination, the channel design was changed to move the organic and aqueous outlets farther apart. A second oil outlet was also added to facilitate removal of the oil stream. The photomask used to define the new emulsion separation device channel is shown in Figure 3.15 below.
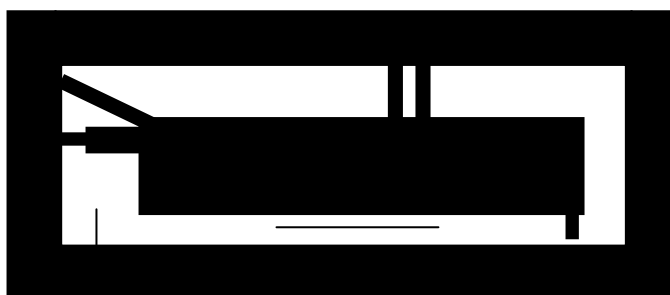
Figure 3.15. New emulsion separation device photomask design for scale up to the industrial level.

This design allowed for a small range of emulsion flow rates but as the emulsion inlet flow rate increased, an exponential increase in water flow rate was required to maintain the location of the aqueous-oil interface and avoid the formation of an emulsion. This situation is not desirable because it results in the use of large volumes of water for the

separation of small volumes of emulsion. In order to decrease the volume of water required to maintain the aqueous-oil interface, the aqueous outlet was crimped to decrease the effective needle diameter. The effect of crimping the needle outlet is very similar to the effect achieved by using a valve to regulate flow through the aqueous outlet needle.

Crimping of the aqueous outlet needle was replaced by a quarter turn ball valve in an attempt to quantify the regulation of aqueous outlet flow. Flow through the ball valve was controlled by the extent to which the valve handle was turned. The ball valve handle was turned to approximately 45° to regulate but not completely restrict flow. Due to the on-off nature of ball valves, this method of flow regulation was not reliable because a small adjustment in the valve handle resulted in a large difference in flow regulation. An ideal replacement for the ball valve would be a small scale, fine-tune metering valve. Because of the on-off nature of ball valves, the final device design used to achieve emulsion separation scale-up results was the crimped aqueous outlet needle design.

3.4.2.2 Scale Up Study

The goal of the emulsion separation scale-up project was to achieve effective emulsion separation at industrial scale flow rates to demonstrate the feasibility of this emulsion separation method for real world applications. Industrial scale throughput rates are defined as flow rates greater than 1 metric ton per year which is equivalent to flow rates greater than 2 milliliters per minute[20].

The emulsion separation device was scaled up to a width of three spacers, corresponding to a device width of 1.8 mm. Above this width, curing of the optical adhesive channel becomes challenging and delamination is common. The emulsion separation device was scaled up to a channel height of 10 mm. Above this height the increase in maximum emulsion flow rate per increase in height begins to plateau, as demonstrated in Figure 3.16.
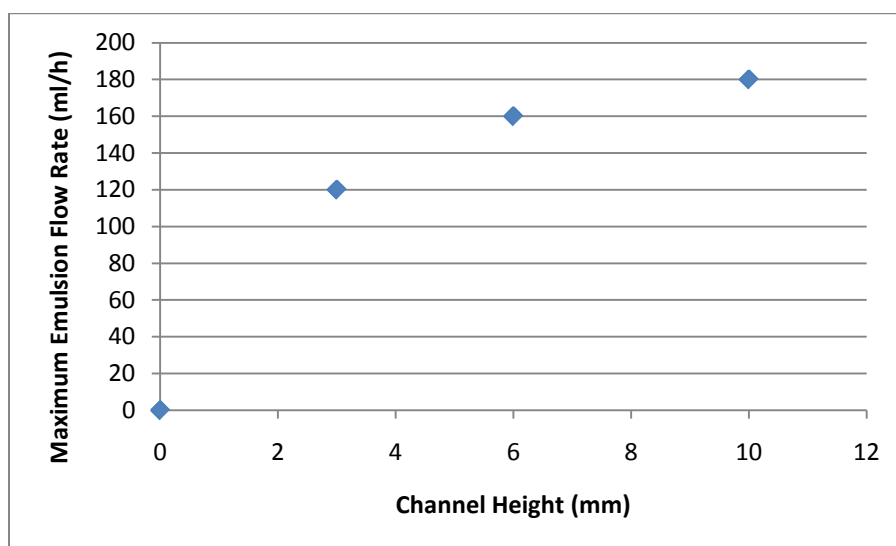

Figure 3.16. Maximum emulsion flow rate (ml/h) as a function of channel height (mm).

It would be of more value to focus efforts on increasing channel width since an increase in channel width in this range still has a linear increase on maximum emulsion flow rate, as shown in Figure 3.17. The device length has no impact on emulsion separation efficiency and so remained unchanged at 50 mm.
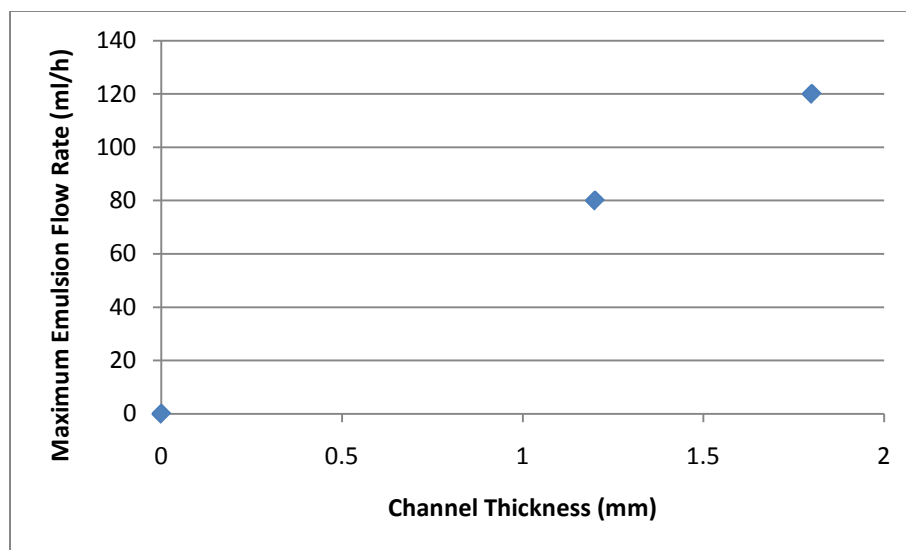
Figure 3.17. Maximum emulsion flow rate (ml/h) as a function of channel width

(mm).

The maximum theoretical channel size for this separation method was determined based on the Reynolds number and Weber number. The Reynolds number was set to 2000, the upper limit of laminar flow. The maximum hydraulic diameter was calculated to be approximately 12 cm. The Weber number was set to 1, the value above which the interface between the two phases becomes unstable and the interface becomes wavy. The maximum hydraulic diameter was calculated to be approximately 24 cm. Based on these calculations, the upper limit of laminar flow set the maximum channel dimensions for this separation method at a hydraulic diameter of 12 cm.

An average emulsion separation efficiency of 85% was achieved over all channel dimensions. An emulsion separation efficiency of 83% was achieved at emulsion flow rates up to 80 ml/h in an emulsion separation device with channel dimensions (width ×

height $\times$ length) of 1.2 mm $\times$ 3 mm $\times$ 50 mm. A device with these dimensions was defined as the base case and scale-up was initiated from these dimensions. Emulsion separation at the maximum emulsion flow rate within the base case is shown in Figure 3.18. The upper limit of emulsion separation was defined as the point when the incoming emulsion could no longer be separated with greater than 80% efficiency, when adjacent flow of the two immiscible liquids was no longer stable, or when an emulsion was being created at the outlet of the emulsion separation device. The observed trend was that with increasing device cross-sectional area, the emulsion flow rates the device was able to sustain while maintaining acceptable emulsion separation efficiency increased. Calculations of Reynolds numbers show that a larger cross-sectional area leads to a decrease in Reynolds number for a set flow rate. This emulsion separation method is more efficient at lower Reynolds number because of a more significant velocity profile in the aqueous phase which results in a greater driving force for the droplet to enter the aqueous phase.
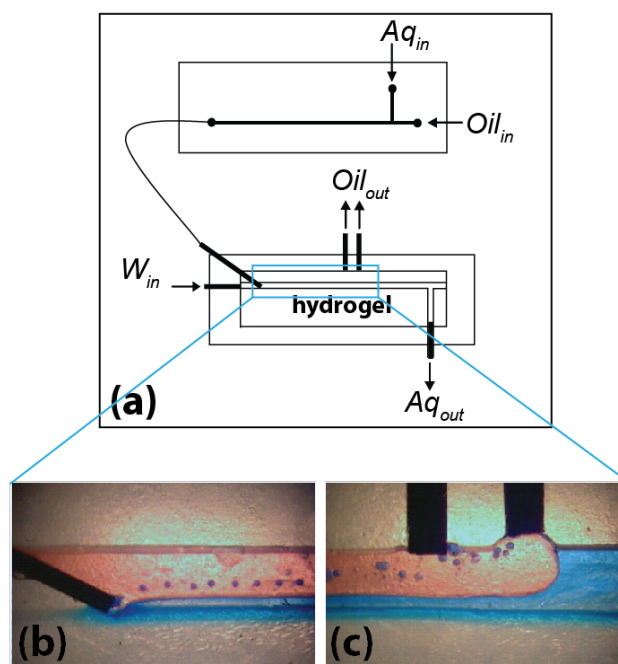
Figure 3.18. Emulsion separation within a channel 1.2 mm in width, 3 mm in height, and 50 mm in length. The emulsion flow rate was 30 ml/h. (a) Schematic of emulsion formation and separation devices with the locations of (b) and (c) outlined by the blue box. (b) Inlet of emulsion separation device. (c) Oil outlet of emulsion separation device (b).

The maximum emulsion flow rate was found to be 180 ml/h in an emulsion separation device with channel dimensions of 1.8 mm $\times$ 10 mm $\times$ 50 mm. Effective emulsion separation was no longer possible above this flow rate due to pressure build up within the emulsion formation device which caused tubing to dislodge from the emulsion formation device and caused delamination of the emulsion formation device. Furthermore, at flow rates above 180 ml/h it became increasingly difficult to achieve consistent emulsion separation. Slight adjustments to the emulsion separation system resulted in

large volumes of aqueous flow entering the oil stream which resulted in poor emulsion separation and the formation of an emulsion at the outlet of the device. At all other device dimensions, the maximum emulsion flow rate was determined based on the emulsion separation decreasing to below 80% efficiency. Table 3.5 summarizes the maximum flow rates achieved and the average emulsion separation efficiency at each device size.

Table 3.5. Summary of emulsion separation scale-up results. Maximum emulsion flow rate (ml/h) and average emulsion flow rate as a function of device dimensions.

Device Dimensions width × height × length (mm)	Maximum Emulsion Flow Rate (ml/h)	Average Emulsion Separation Efficiency (%)
$1.2 \times 3 \times 50$	80	83.4
$1.8 \times 3 \times 50$	120	84.2
$1.8 \times 6 \times 50$	160	85.8
$1.8 \times 10 \times 50$	180	84.9

The Reynolds, capillary, and Weber numbers were calculated for the system at the maximum emulsion flow rate to characterize the flow within the channel. The average Reynolds number was 4.22, demonstrating flow within the laminar regime. The average capillary number was 2.23×10^{-3}, showing the dominance of interfacial forces resulting in parallel flow to decrease interfacial area. The average Weber number was 1.41×10^{-3}, demonstrating the stability of the interface between the two immiscible fluids.

3.5 References

(1) Derkach, S. R. Rheology of Emulsions. *Advances in Colloid and Interface Science.* **2009**, 151, 1-23.

(2) Schultz, S.; Wagner, G.; Urban, K.; Ulrich, J. High-Pressure Homogenization as a Process for Emulsion Formation. *Chemical Engineering Technology.* **2004**, 27, 361-368.

(3) Engl, W.; Backov, R.; Panizza, P, Controlled production of emulsions and particles by milli- and microfluidic techniques. *Current Opinion in Colloid & Interface Science*. **2008**, 13, 206-216.

(4) Xu, J. H.; Li, S. W.; Tan, J.; Luo, G. S. Correlations of droplet formation in T-junction microfluidic devices: from squeezing to dripping. *Microfluidics and Nanofluidics.* **2008**, 5, 711-717.

(5) Okushima, S.; Nisisako, T.; Torii, T.; Higuchi, T. Controlled Production of Monodisperse Double Emulsions by Two-Step Droplet Breakup in Microfluidic Devices. *Langmuir*. **2004**, 20, 9905-9908.

(6) Chen, W.; Peng, J.; Su, Y.; Zheng, L.; Wang, L.; Jiang, Z. Separation of oil/water emulsions using Pluronic F127 modified polyethersulfone ultrafiltration membranes. *Separation and Purification Technology.* **2009**, 66, 591-597.

(7) Becker, J. R. *Crude Oil: Waxes, Emulsion, and Asphaltenes*; PennWell Publishing Company: Oklahoma, 1997.

(8) Noyes, R. *Unit Operations in Environmental Engineering*. Noyes Publications: New Jersey, 1994.

(9) Mason, S. L.; May, K.; Hartland, S. Drop size and concentration profile determination in petroleum emulsion separation. *Physicochemical and Engineering Aspects.* **1995**, 96, 85-92.

(10) Ehrfeld, W; Hessel, V; Lowe, H. *Microreactors: New Technology for Modern Chemistry;* Wiley-VCH: Germany, 2000.

(11) Fletcher, P. D. I.; Haswell, S. J.; Pombo-Villar, E.; Warrington, B. H.; Watts, P.; Wong, S. Y. F.; Zhang, X. Micro reactors: principles and applications in organic synthesis. *Tetrahedron.* **2002**, 58, 4735-4757.

(12) Leamon, J. H.; Link, D. R.; Egholm, M.; Rothberg, J. M. Overview: methods and applications for droplet compartmentalization of biology. *Nature Methods.* **2006**, 3, 541-543.

(13) Shchukin, D. G.; Sukhorukov, G. B. Nanoparticle Synthesis in Engineered Organic Nanoscale Reactors. *Advanced Materials.* **2004**, 16, 671-682.

(14) Lorber, N.; Pavageau, B.; Mignard, E. Droplet-based Millifluidics as a New Miniaturized Tool to Investigate Polymerization Reactions. *American Chemical Society.* **2010**, 43, 5524-5529.

(15) Fidalgo, L. M.; Whyte, G.; Bratton, D.; Kaminski, C. F.; Abell, C.; Huck, W. T. S. From Microdroplets to Microfluidics: Selective Emulsion Separation in Microfluidic Devices. *Angewandte Chemie International Edition.* **2008**, 47, 2042-2045.

(16) Kralj, J. G.; Schmidt, M. A.; Jensen, K. F. Surfactant-enhanced liquid-liquid extraction in microfluidic channels with inline electric-field enhanced coalescence. *The Royal Chemical Society.* **2005**, 5, 531-535.

(17) Hung, S. H.; Lin, Y. H.; Lee, G. B. A microfluidic platform for manipulation and separation of oil-in-water emulsion droplets using optically induced dielectrophoresis. *Journal of Micromechanics and Microengineering.* **2010**, 20, 1-8.

(18) Angelescu, D. E.; Mercier, B.; Siess, D.; Schroeder, R. Microfluidic Capillary Separation and Real-Time Spectroscopic Analysis of Specific Components from Multiphase Mixtures. *Analytical Chemistry.* **2010**, 82, 2412-2420.

(19) Tetradis-Meris, G.; Rossetti, D.; Torres, C. P.; Cao, R.; Lian, G.; Janes, R. Novel Parallel Integration of Microfluidic Device Network for Emulsion Formation. *Industrial and Engineering Chemistry Research.* **2009**, 48, 8881-8889.

(20) Jonsson, M.; Johnson, B. Millichannel Reactors: A Practical Middle Ground for Production. *Chemical Engineering*. **2009**, 116, 44-50.

(21) Mcdonald, J. C.; Whitesides, G. M. Poly(dimethylsiloxane) as a Material for Fabricating Microfluidic Devices. *Accounts of Chemical Research.* **2002**, 35, 491-499.

(22) Harrison, C.; Cabral, J. T.; Stafford, C. M.; Karim, A.; Amis, E. J. A rapid prototyping technique for the fabrication of solvent-resistant structures. *Journal of Micromechanics and Microengineering.* **2004**, 14, 153-158.

Chapter 4. Conclusions

4.1 Liquid-Liquid Extraction

This thesis demonstrated successful liquid-liquid extraction within micro- and milli-fluidic devices over a range of flow rates and solute concentrations. The system explored in this thesis used pentanone as the organic solvent, water as the extractant, and rhodamine 6G as the solute of interest. A math model was created to calculate the system's mass transfer coefficient based on device dimensions and the concentration of solutions entering and exiting the device. The mass transfer coefficient of the system demonstrated no statistically significant difference at various flow rates and concentrations. The theoretical mass transfer coefficient for the system was calculated for comparison based on the Stokes-Einstein equation and a modified correlation for laminar flow through a solid circular tube. Calculation of the theoretical mass transfer coefficient resulted in a value on the same order of magnitude as the experimental mass transfer coefficient, verifying the reliability of this method for mass transfer coefficient determination.

This microfluidic device achieved liquid-liquid extraction by the parallel laminar flow of two immiscible fluids; thus, no separation operation is required once extraction is complete. This eliminates a large portion of the time and monetary cost associated with liquid-liquid extraction. The novel component in this form of extraction is the use of a hydrogel for stabilizing co-current laminar flow. The use of a hydrogel layer allows for stabilization of parallel flows over larger length scales than traditional methods, such as the use of surface modification and guide structures.

4.2 Emulsion Separation

This thesis established the optimum device geometry to allow for effective emulsion separation. Mineral oil containing sudan IV dye and water containing methylene blue dye were used to create the emulsion within a microfluidic T-junction device. Water was supplied to the emulsion separation device to facilitate emulsion breaking. The emulsion separation device design was modified from initial design specifications to allow for better separation of the two phases at the device outlet. An additional organic outlet was added for efficient removal of the organic stream. The distance between the organic and aqueous outlets was increased to reduce the likelihood of contamination of the pure outlet streams. The aqueous outlet needle was surrounded by hydrogel to reduce the likelihood of oil contaminating the aqueous stream. Contamination of the aqueous stream becomes more significant at higher emulsion flow rates. The final modification, which had the largest impact on good separation at the device outlet, was crimping of the aqueous outlet needle which prevented the oil-water interface from migrating toward the aqueous outlet while maintaining a low water flow rate.

This thesis demonstrated the use of a milli-fluidic device for emulsion separation. Emulsion separation was accomplished with 85% efficiency. Emulsion separation was induced by interactions between the emulsion and the hydrogel layer as the emulsion entered the device. These interactions caused disruption of the oil boundary layer surrounding each aqueous droplet, allowing aqueous droplets to merge with the continuous aqueous stream. The initial device had channel dimensions of 1.2 mm in width, 3 mm in height, and 50 mm in length. With these dimensions, the device was able

to successfully separate the emulsion at emulsion flow rates up to 80 ml/h. This separation method was then scaled up to the industrial level to demonstrate feasibility in real world applications. The final scaled up device had channel dimensions of 1.8 mm in width, 10 mm in height, and 50 mm in length. With these dimensions, the device was able to successfully separate emulsions with a throughput of 180 ml/h, corresponding to 1.4 metric tons per year. This demonstrates that the separation method described in this thesis can be successfully applied at the industrial scale. An array of these milli-fluidic devices can be assembled for higher throughputs.

Chapter 5. Future Work

5.1 Liquid-Liquid Extraction

This thesis explored the use of micro- and milli-fluidic glass-on-glass devices for the parallel flow of two immiscible liquids and extraction of an amphiphilic dye molecule from the organic phase into the aqueous phase. The results of micro- and milli-fluidic LLE showed that as the device width increased, the extraction efficiency increased, doubling when the device width was doubled. An additional option for increasing extraction is to increase the channel width by increasing the number of spacers used to separate the two glass slides during device fabrication while reducing the channel height as much as possible. These adjustments will increase the interfacial area-to-volume ratio resulting in a greater degree of mass transfer per volume of solution processed. Current device fabrication methods allow for device widthes up to 1.8 mm, resulting in a hypothesized extraction efficiency of approximately 15% per milli-fluidic device with a 50 mm long channel. Separation efficiency can be further lengthening the channel which increases the contact area of the two immiscible phases.

To further increase the extraction efficiency of this system, droplet based liquid-liquid extraction should be performed within a microfluidic device with water as the continuous phase containing droplets of the organic phase and solute. The PDMS device used for emulsion droplet formation cannot be used in this case because the organic solvent could cause the PDMS to swell. Furthermore, the PDMS emulsion formation device would result in an emulsion where the organic solvent containing the solute is the continuous phase and water is the dispersed phase. Instead, a T-junction device should be made using optical adhesive and the photolithographic methods used to make the emulsion separation device. The emulsion formed by the droplet based extraction will then be transferred to the emulsion separation device for emulsion breaking and further extraction. The set up required to accomplish this separation is shown in Figure 5.1. By

combining the droplet based separation method with the emulsion separation device, the extraction efficiency should be significantly increased due to the increase in contact area between the two immiscible phases. Furthermore, during droplet based extraction, the internal circulation within each immiscible slug will decrease the diffusion path length to half the channel width making it much more effective for extraction than parallel flow of immiscible liquids[1]. Liquid-liquid extraction should be executed at the various concentrations and flow rates to prove the robustness of the system. The organic phase droplet size should be varied to determine if decreasing organic phase droplets from tubular slugs to spherical droplets with radii less than the channel radius affects the extraction efficiency. It is expected that as the droplet radius decreases to below the channel radius, the extraction will become more efficient since the diffusion path length is decreased. The mass transfer coefficient for the system should be calculated by combining a droplet based math model with the math model already established for parallel flow.
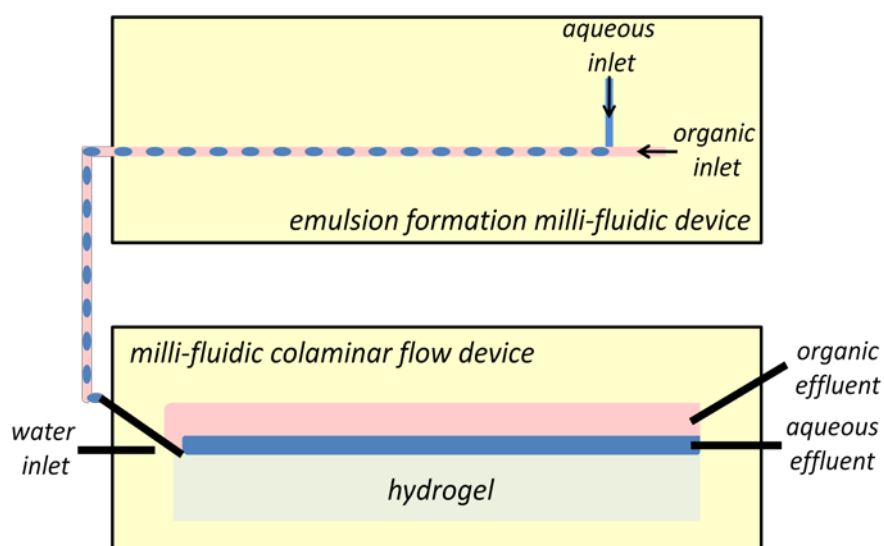
Figure 5.1. Droplet-based LLE combined with the co-current laminar flow device for emulsion separation and continued extraction.

The liquid-liquid extraction method explored in this thesis should be used for the extraction of larger biological molecules, such as proteins. One of the many advantages of this extraction method is that there is no need for a membrane to separate flow of the two immiscible fluids. This allows for the extraction of significant larger molecules than would be possible for other microfluidic extraction methods. The use of this liquid-liquid extraction method for the extraction of proteins would also demonstrate the robustness of this system for the extraction of a wide range of compounds.

5.2 Emulsion Separation

The milli-fluidic emulsion separation device was able to achieve emulsion separation with 85% efficiency. The droplets that were unable to be separated were satellite droplets created within the T-junction emulsion formation device. Emulsion separation is believed to be caused by disruption of the boundary layer surrounding each aqueous droplet. According to this logic, a decrease in the emulsion inlet needle inner diameter should be sufficient to separate the smaller emulsion droplets. The emulsion separation efficiency should be quantified at various needle diameters and compared to determine if a trend exists.

This thesis explored the use of a milli-fluidic separation device with the emulsion inlet located at the hydrogel-water interface for emulsion breaking. The upper limit of this device's processing capability was determined to demonstrate industrial feasibility by increasing device dimensions which allows for an increase in the emulsion inlet flow rate. An alternate method of emulsion separation scale up is to have emulsion separation occur in a parallel stack of devices. One emulsion inlet stream can be split into multiple streams and fed to various milli-fluidic devices. The arrangement of these devices into a microfluidic array would significantly increase the throughput of this emulsion separation method and further demonstrate industrial feasibility.

An additional method of emulsion separation scale up would be to have multiple emulsion inlet needles within one milli-fluidic device, as shown in Figure 5.2. This device geometry would maximize the throughput of each individual device while minimizing the space requirement. After proving the feasibility of each of the individual emulsion separation scale up methods, these methods could be combined to further demonstrate industrial scale feasibility.
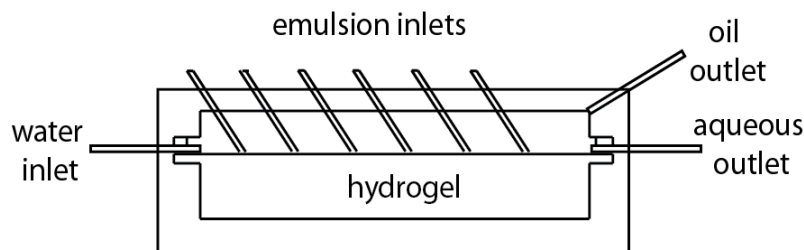
Figure 5.2. Alternate emulsion separation method with multiple emulsion inlet needles within one milli-fludic device.

The emulsion separation device should be tested on various emulsion systems to demonstrate the robustness of this separation method. The emulsion separation device described in this thesis could be applied for the separation of a salt water-motor oil emulsion, simulating the separation of the emulsion that results from an oil spill. Efficiency of separation could be quantified by the same method used in this thesis. This separation method could also be applied for the recovery of microreactor products. A reaction could be carried out to completion within an aqueous droplet in a continuous oil stream. The resulting emulsion could be separated using the method described in this thesis. The amount of product recovered could be quantified using a spectroscopy technique.

The scale-up of the emulsion separation device in this thesis was accomplished by crimping the aqueous outlet needle to offer some form of flow regulation. Although this method

was able to accomplish the end goal of determining the maximum emulsion flow rate to the device, it is difficult to quantify the degree of crimping which makes each experiment difficult to reproduce. A small scale, fine tune, metering valve could be used to accurately and reproducibly regulate flow. Once consistent, reproducible results have been achieved for emulsion separation, some rules of thumbs could be generated to predict flow rates and efficiencies for various emulsion flow rates, channel dimensions, and emulsion systems.

5.3 References

(1) Dessimoz, A.; Cavin, L.; Renken, A.; Kiwi-Minsker, L. Liquid-liquid two-phase flow patterns and mass transfer characteristics in rectangular glass microreactors. *Chemical Engineering Science.* **2008**, 63, 4035-4044.

Appendix A – Microfluidic Liquid-Liquid Extraction Images
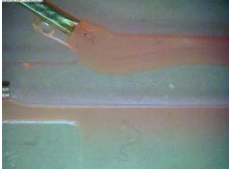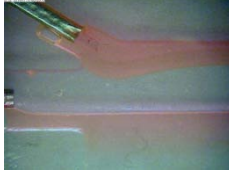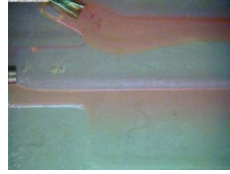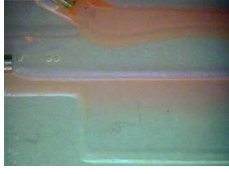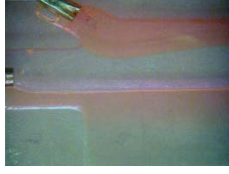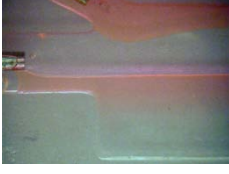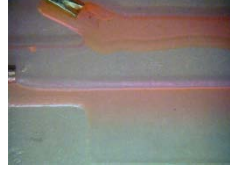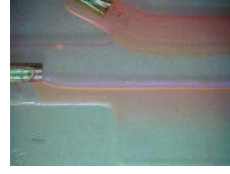
Pentanone flow rate held constant at 40 ml/h

Number at the top of each column is water flow rate in ml/h

Low Concentration

10	20	30	40

Middle concentration

10	20	30	40

High concentration

10	20	30	40

Appendix B – Milli-fluidic Liquid-Liquid Extraction Images

Pentanone flow rate held constant at 40 ml/h

Number at the top of each column is water flow rate in ml/h

Low Concentration

10	20	30	40

Middle Concentration

10	20	30	40

High Concentration

10	20	30	40
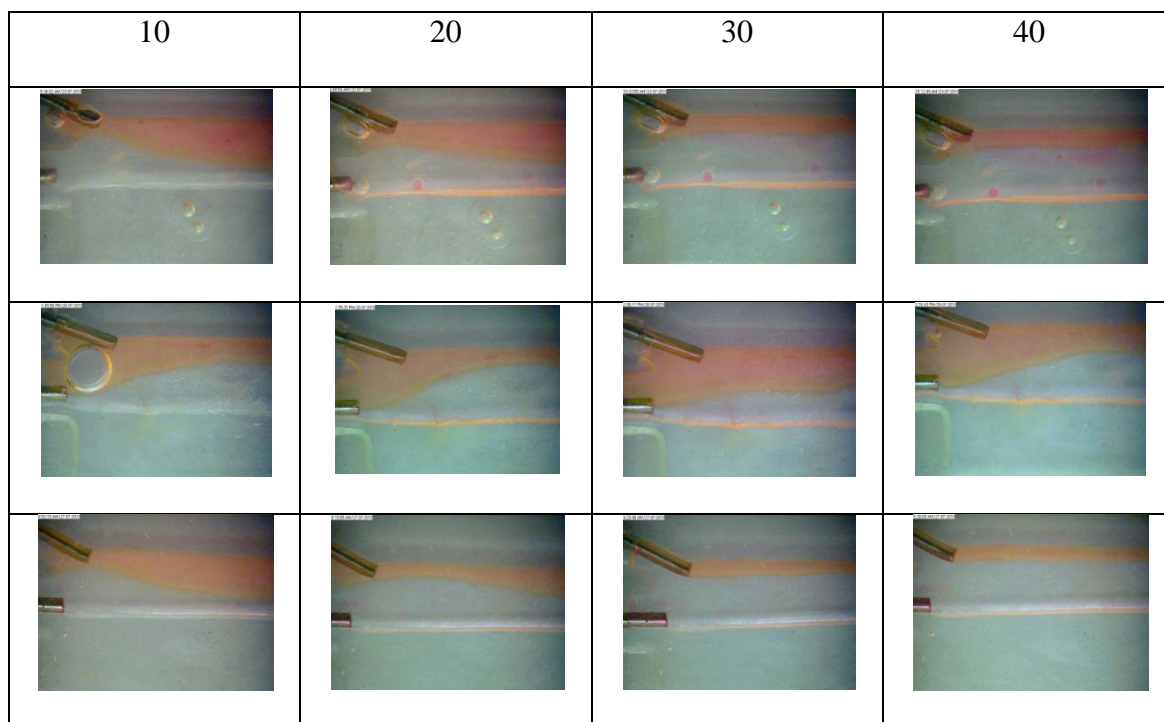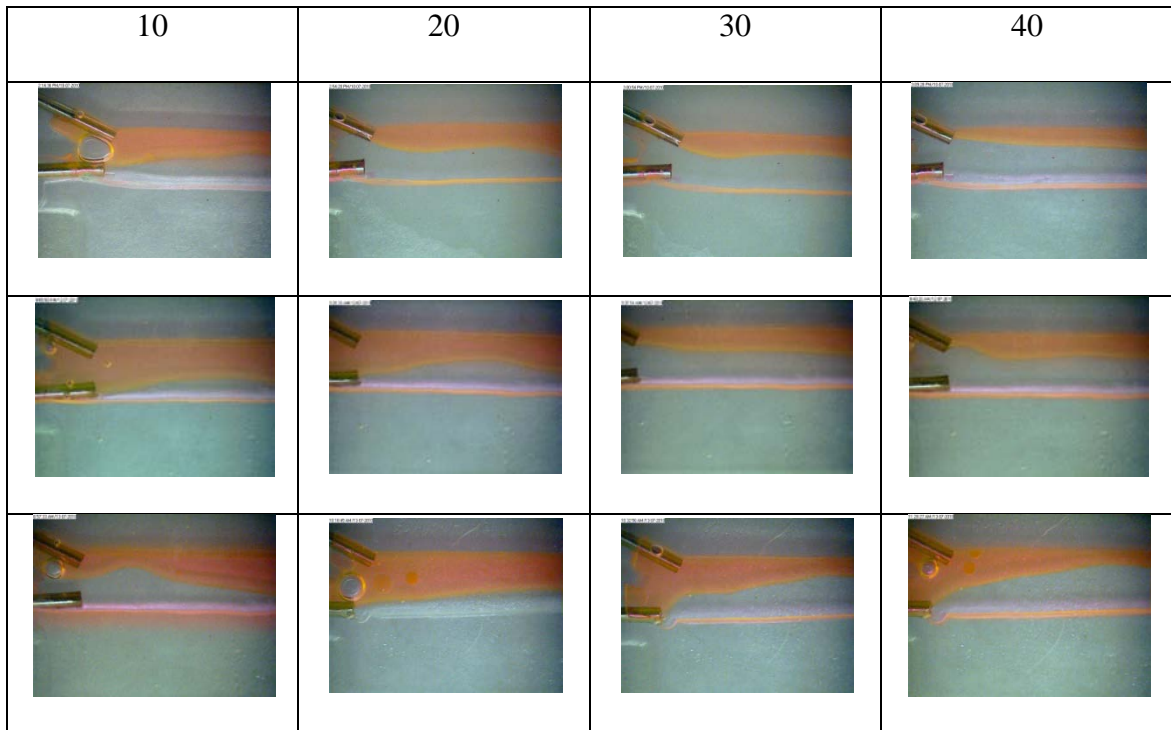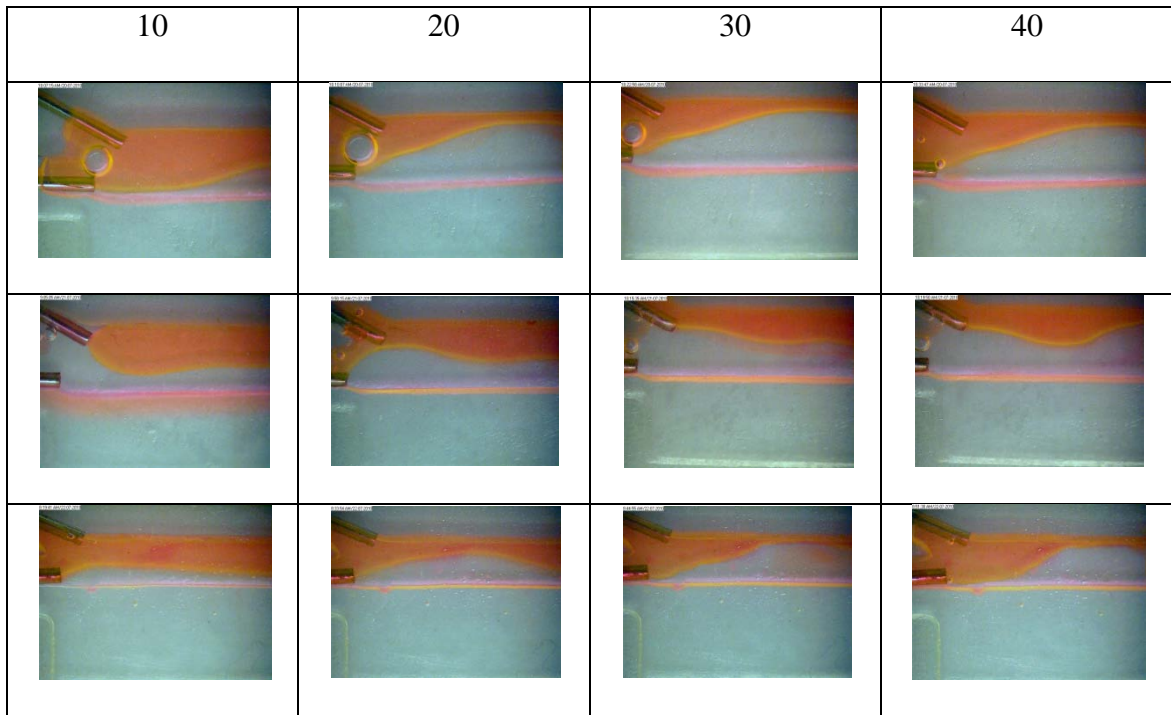
Appendix C - Matlab code for solving differential mass balance

FILE #1---ODE45 function file

```matlab
function ydot = newumm(z,y)

global J
global k
% duration of experiment (experimental run time)
t = 116;                    % s
% width of device
w = 0.12;                   % cm
% volume flow of pentanone stream
qp = 40/3600;               % cm^3/s
% volume flow rate of water stream
qw = 40/3600;               % cm^3/s

% constants for differential equations
alpha1 = k*w/qp;
alpha2 = k*w/qw;
ydot1 = -alpha1*(y(1) - y(2));            % dCp/dz differential equation
ydot2 = alpha2*(y(1) - y(2)) - J*w/qw;        % dCw/dz differential equation
ydot = [ydot1;ydot2];

global J
global k
J = minout(2)
k = minout(1)
mintot = mintot

[z,y]=ode45('newumm',zpan,y0);
```

FILE #2---minimization function file

```
function mintot = newummRCS(minout)

global zpan

% inlet concentration of rhodamine in pentanone
Cpo = 5.73*10^-4;              % g/cm^3
% inlet concentration of rhodamine in water
Cwo = 0;                   % g/cm^3
% initial conditions
y0 = [Cpo;Cwo];
% experimental outlet concentrations
Cwexp = 3.18*10^-6;
Cpexp = 5.36*10^-4;

global k
global J
k = minout(1);
J = minout(2);


[z,y]=ode45('newumm',zpan,y0);
finalz = length(z);
finalCp = y(finalz,1);
finalCw = y(finalz,2);

mintot = (finalCp-Cpexp)^2 +(finalCw - Cwexp)^2;
```

FILE #3---run file

```
%fminsearch only gives local solution so Dabinit and kinit have to be good
%guesses

% minout is a vector [k J]
% mintot is the difference between each exp outlet conc. and the final
% conc. on the graph

clear
close all
format long
global zpan

% inlet concentration of rhodamine in pentanone
Cpo = 5.73*10^-4;              % g/cm^3
% inlet concentration of rhodamine in water
Cwo = 0;                  % g/cm^3
% initial conditions
y0 = [Cpo;Cwo];
% range to integrate over (length of channel)
zpan = (0:0.01:5.44);
% diffusivity of rhodamine out of 30 vol% PEGDA hydrogel
Jinit = 1.18*10^-6;            % g/cm^2s
% mass transfer coefficient of jasmine extraction from benzene to water
kinit = 2.33*10^-3;                  % cm/s     k = 3*10^-4

minoutguess(1) = kinit;
minoutguess(2) = Jinit;

mintot1 = newummRCS(minoutguess);

[minout,mintot] = fminsearch('newummRCS',minoutguess);
```
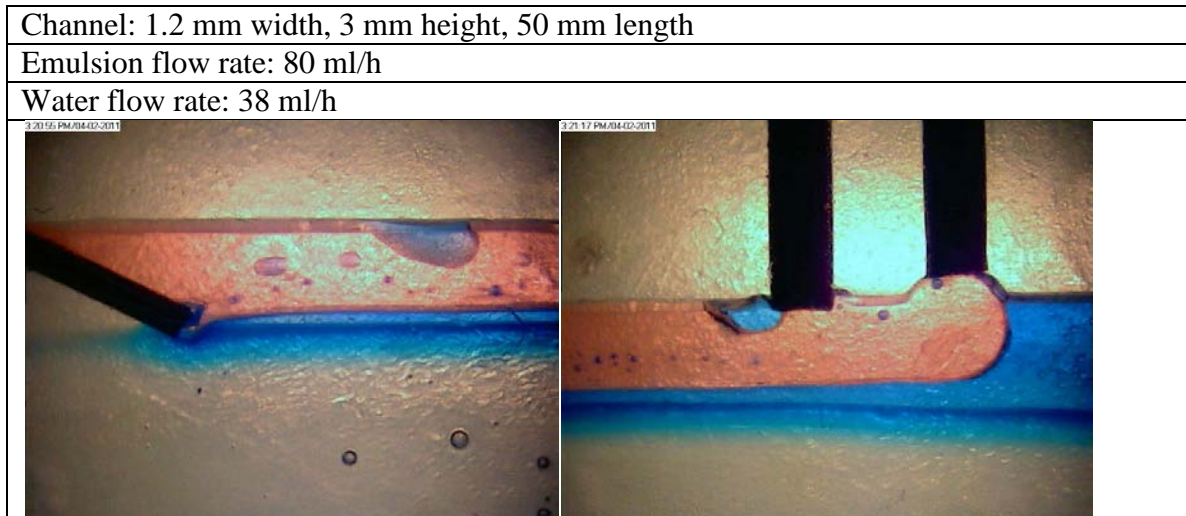
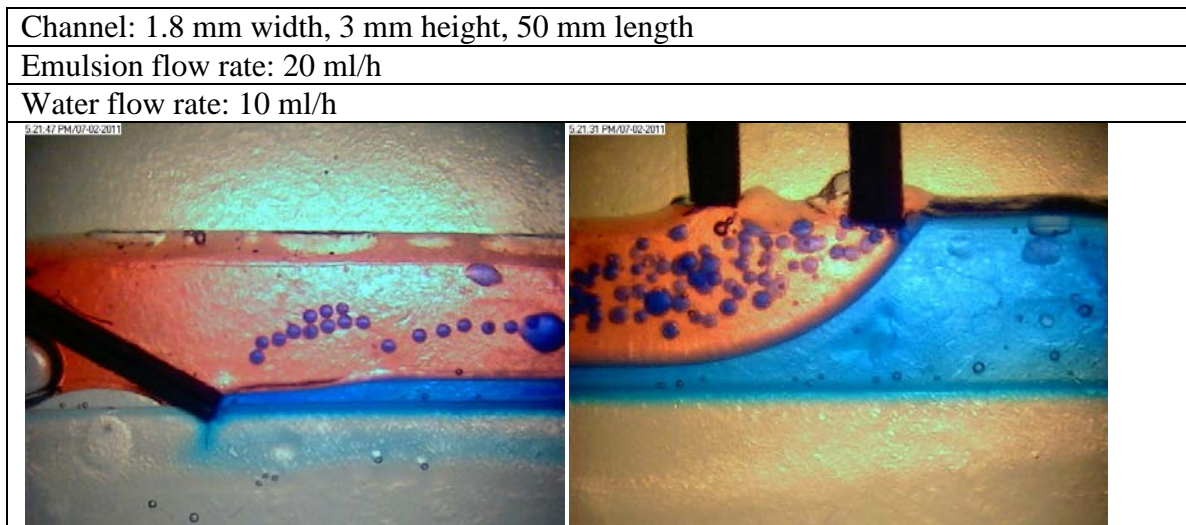## Appendix D – Emulsion Separation Scale Up Images
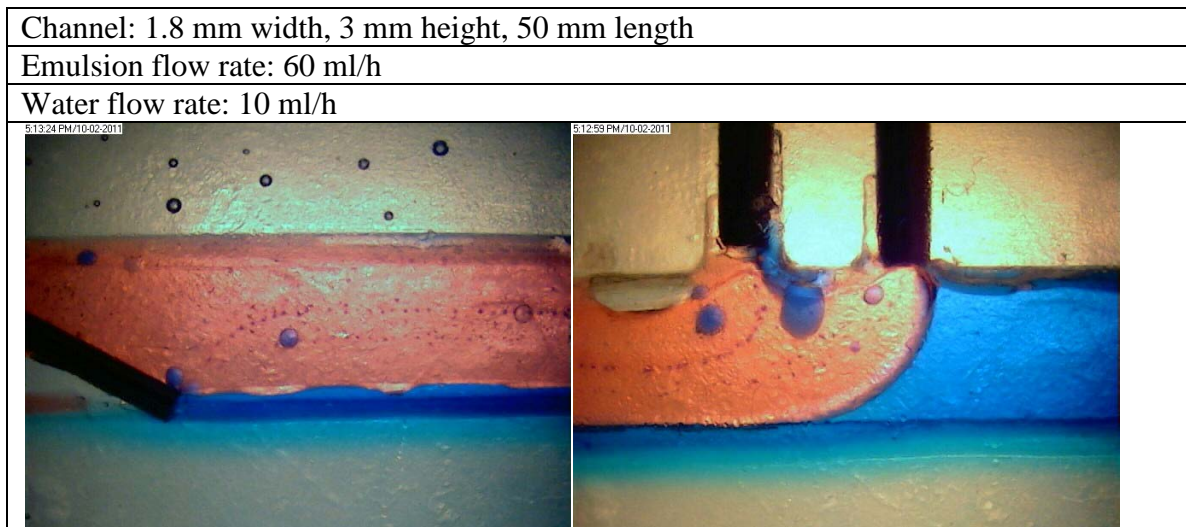
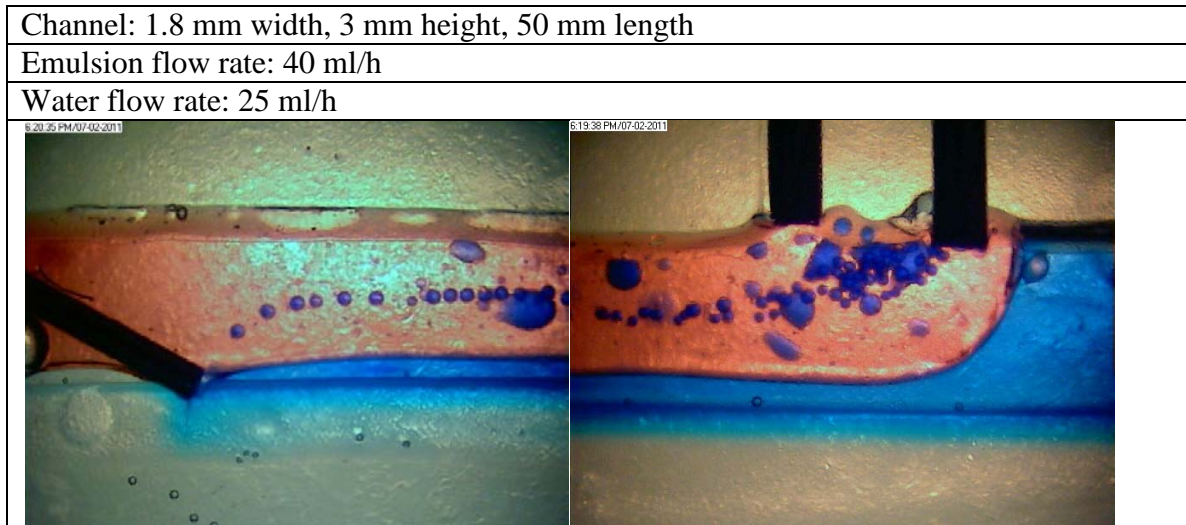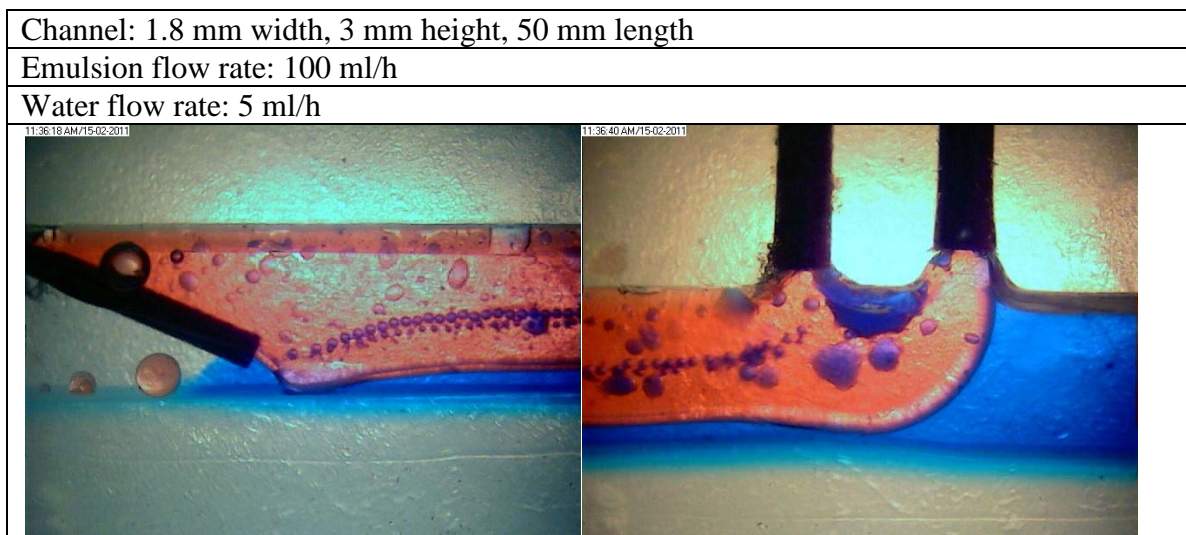Oil: aqueous flow rate ratio is 1 for all scale up trials
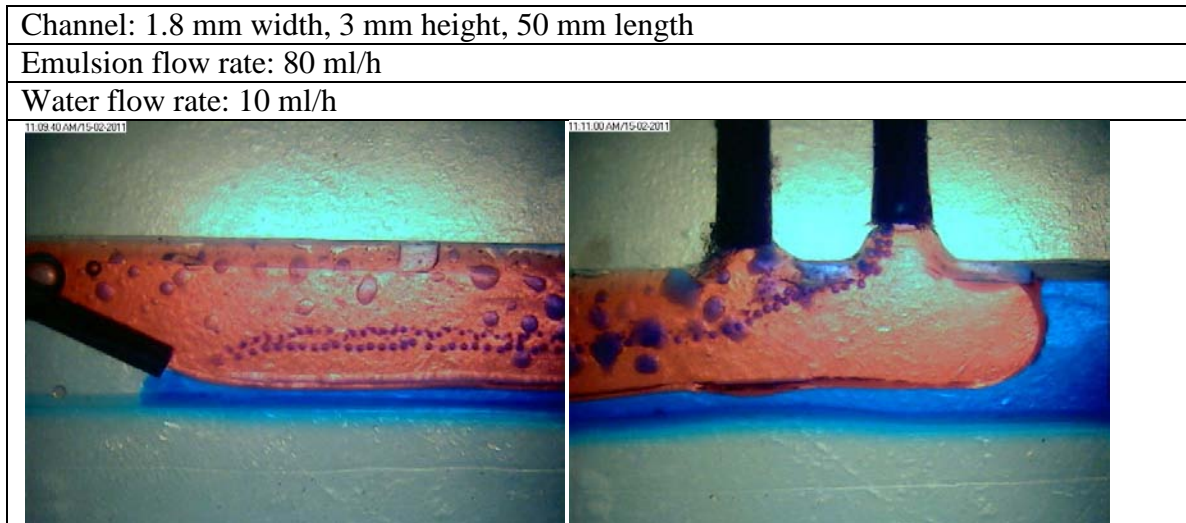
Channel: 1.2 mm width, 3 mm height, 50 mm length

Channel: 1.2 mm width, 3 mm height, 50 mm length
Emulsion flow rate: 2 ml/h
Water flow rate: 7 ml/h

Channel: 1.2 mm width, 3 mm height, 50 mm length
Emulsion flow rate: 50 ml/h
Water flow rate: 30 ml/h

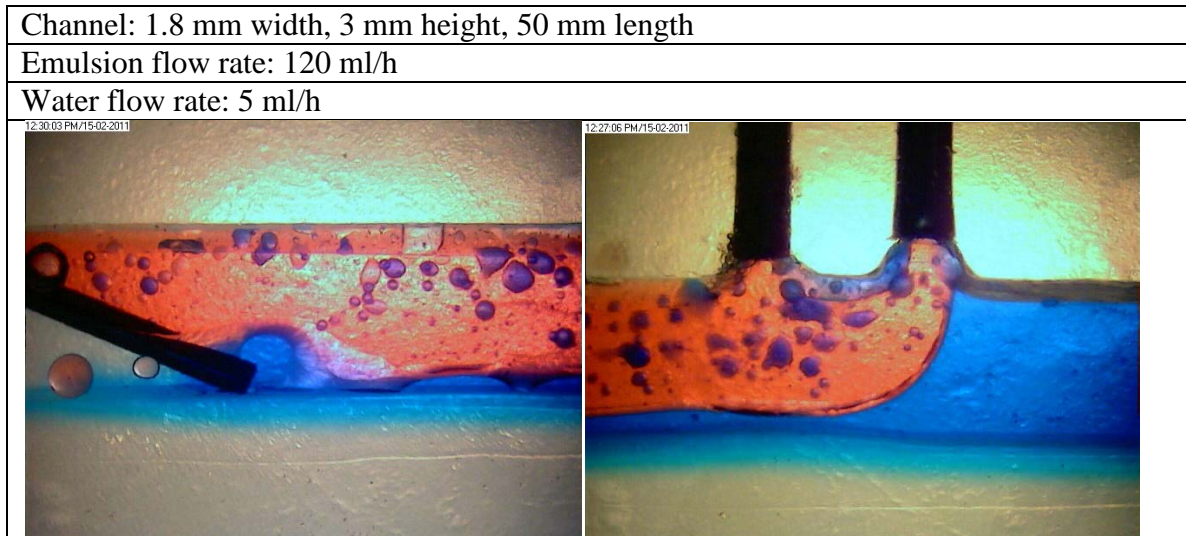| Channel: 1.2 mm width, 3 mm height, 50 mm length |
| --- |
| Emulsion flow rate: 80 ml/h |
| Water flow rate: 38 ml/h |
| |

Channel: 1.8 mm width, 3 mm height, 50 mm length
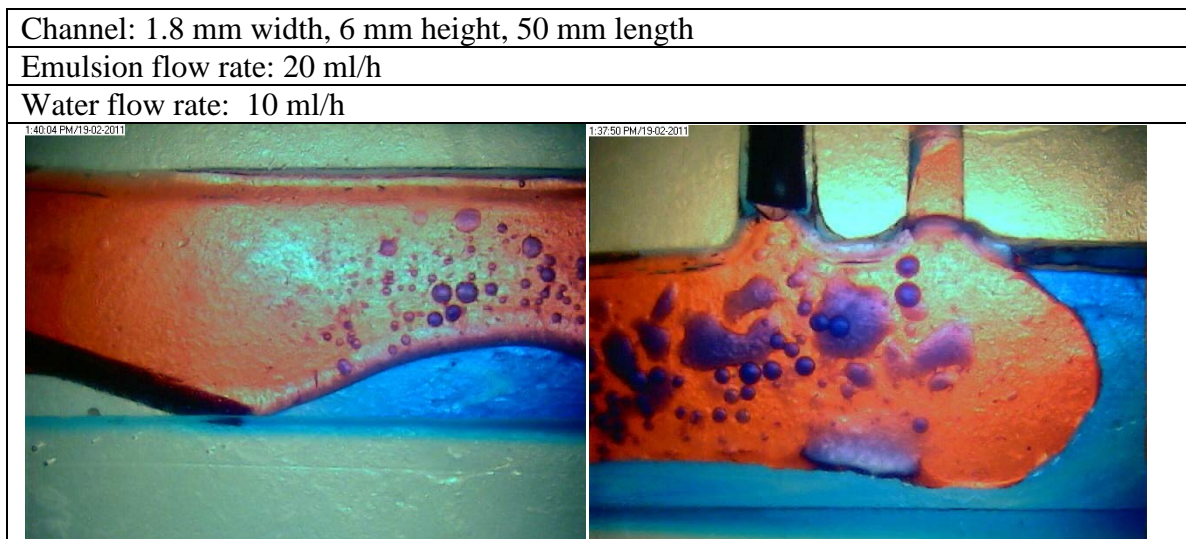
Channel: 1.8 mm width, 3 mm height, 50 mm length
Emulsion flow rate: 20 ml/h
Water flow rate: 10 ml/h

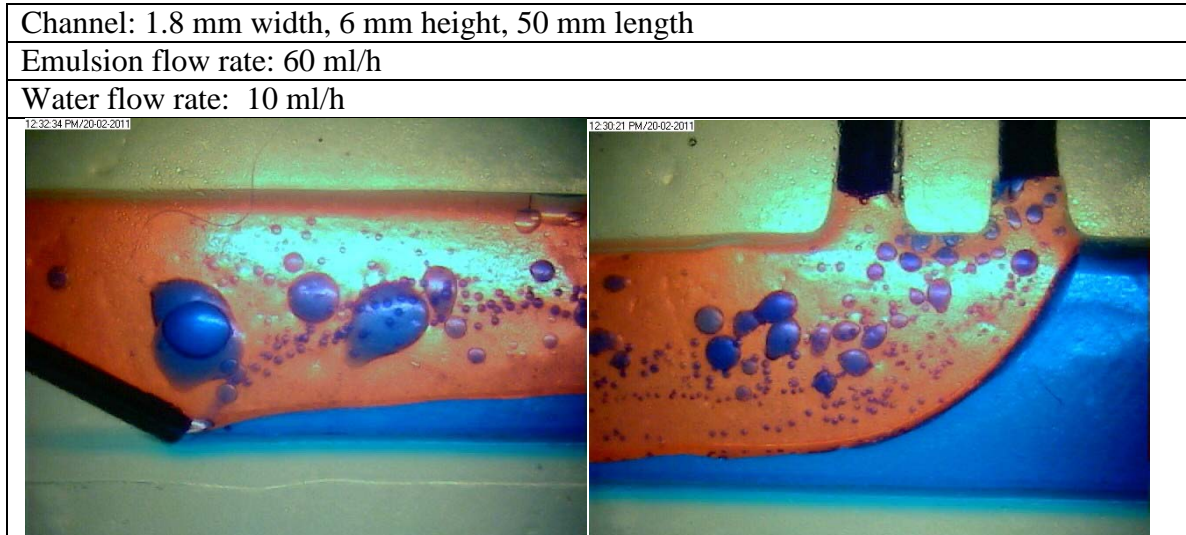| Channel: 1.8 mm width, 3 mm height, 50 mm length |
|---|
| Emulsion flow rate: 40 ml/h |
| Water flow rate: 25 ml/h |

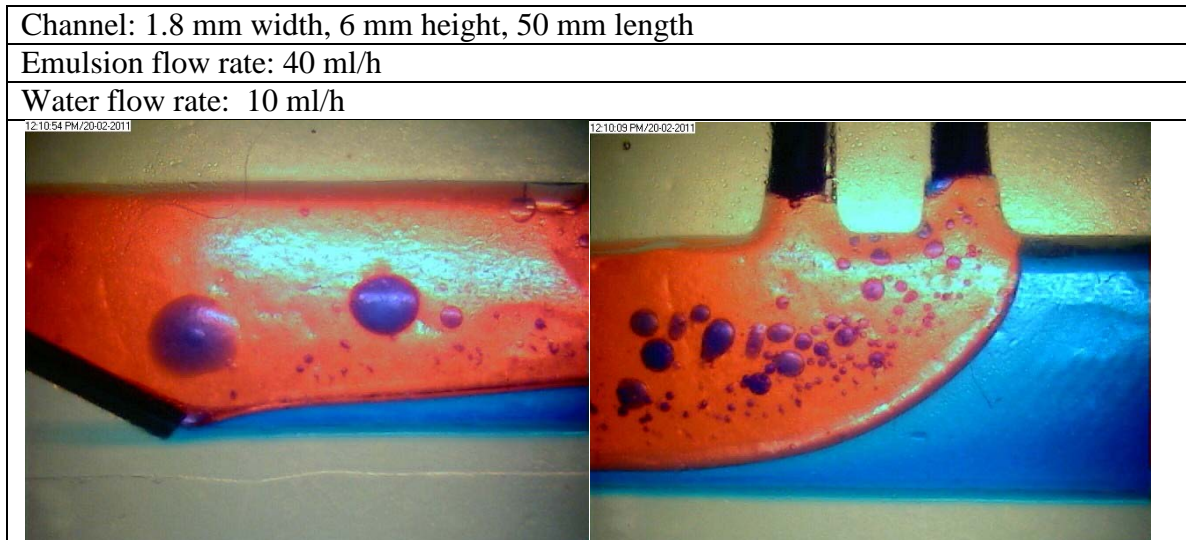| Channel: 1.8 mm width, 3 mm height, 50 mm length |
|---|
| Emulsion flow rate: 60 ml/h |
| Water flow rate: 10 ml/h |

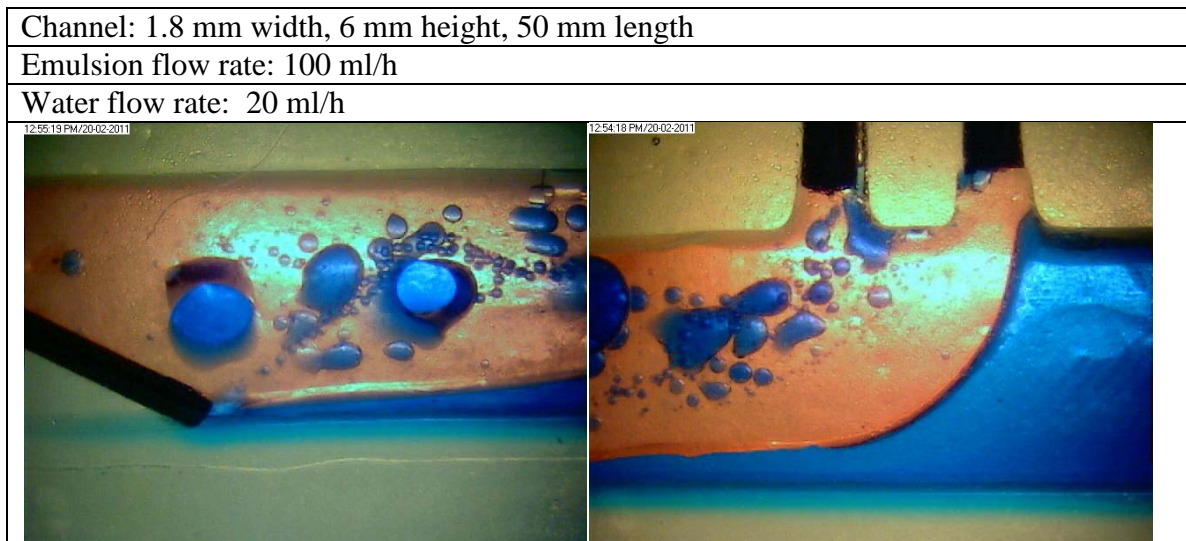| Channel: 1.8 mm width, 3 mm height, 50 mm length |
|---|
| Emulsion flow rate: 80 ml/h |
| Water flow rate: 10 ml/h |

Channel: 1.8 mm width, 3 mm height, 50 mm length
Emulsion flow rate: 100 ml/h
Water flow rate: 5 ml/h

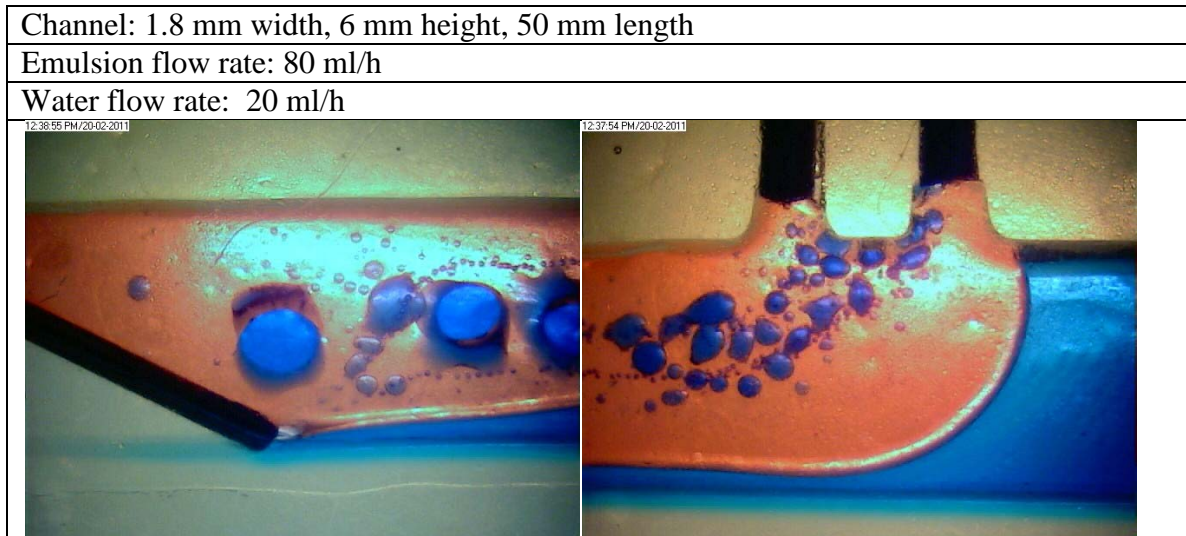| Channel: 1.8 mm width, 3 mm height, 50 mm length |
| --- |
| Emulsion flow rate: 120 ml/h |
| Water flow rate: 5 ml/h |

Channel: 1.8 mm width, 6 mm height, 50 mm length

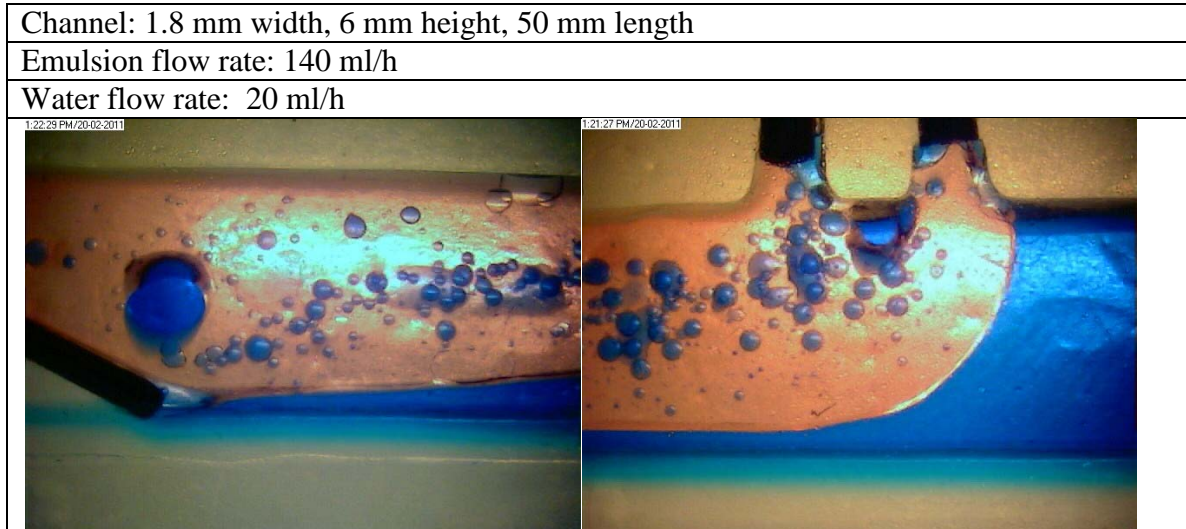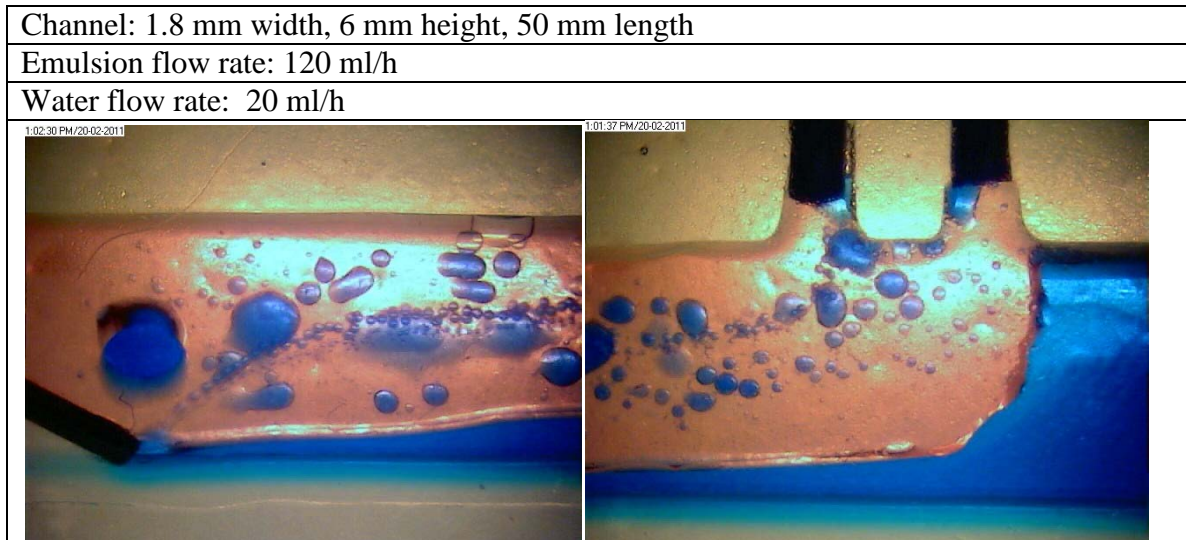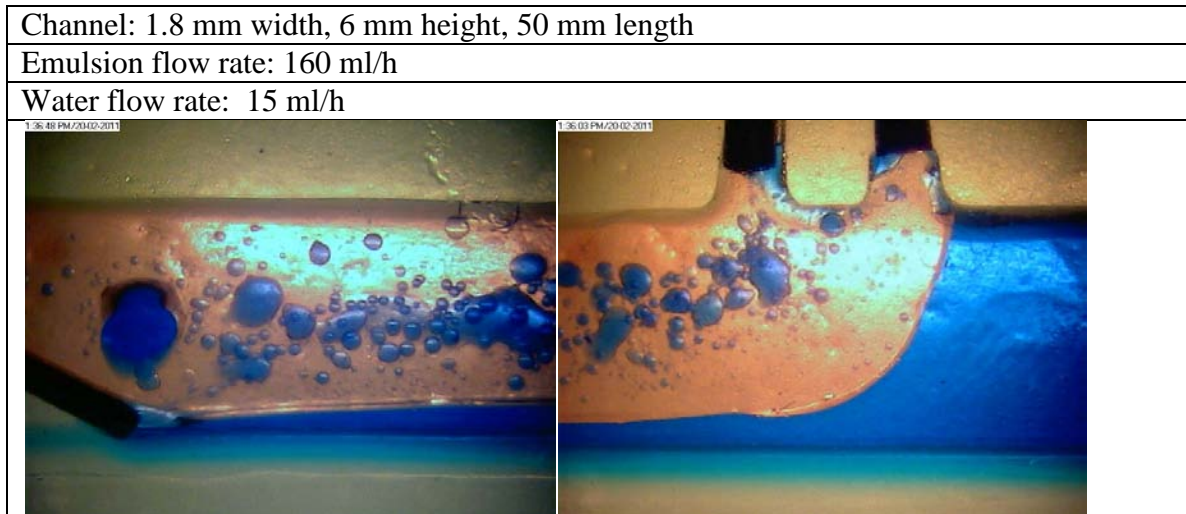| Channel: 1.8 mm width, 6 mm height, 50 mm length |
| --- |
| Emulsion flow rate: 20 ml/h |
| Water flow rate: 10 ml/h |

Channel: 1.8 mm width, 6 mm height, 50 mm length
Emulsion flow rate: 40 ml/h
Water flow rate: 10 ml/h

Channel: 1.8 mm width, 6 mm height, 50 mm length
Emulsion flow rate: 60 ml/h
Water flow rate: 10 ml/h

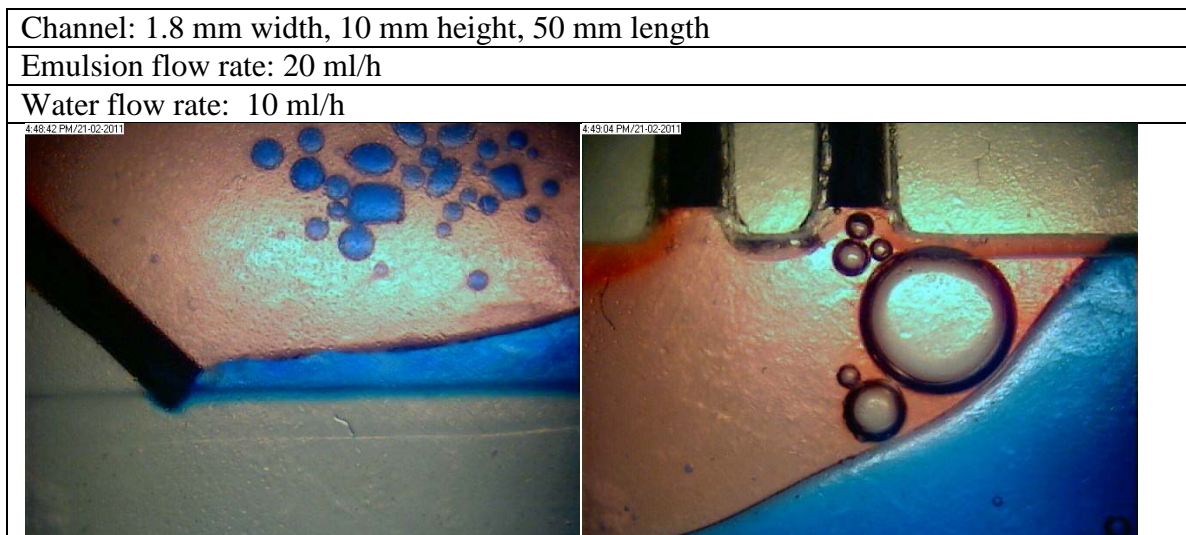| Channel: 1.8 mm width, 6 mm height, 50 mm length |
| --- |
| Emulsion flow rate: 80 ml/h |
| Water flow rate: 20 ml/h |

Channel: 1.8 mm width, 6 mm height, 50 mm length
Emulsion flow rate: 100 ml/h
Water flow rate: 20 ml/h

Channel: 1.8 mm width, 6 mm height, 50 mm length
Emulsion flow rate: 120 ml/h
Water flow rate: 20 ml/h

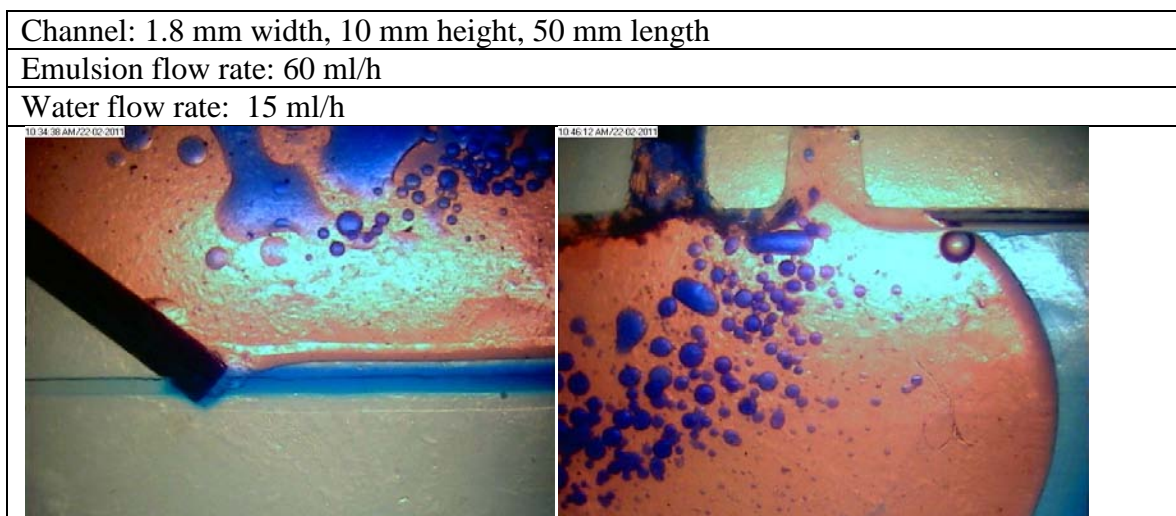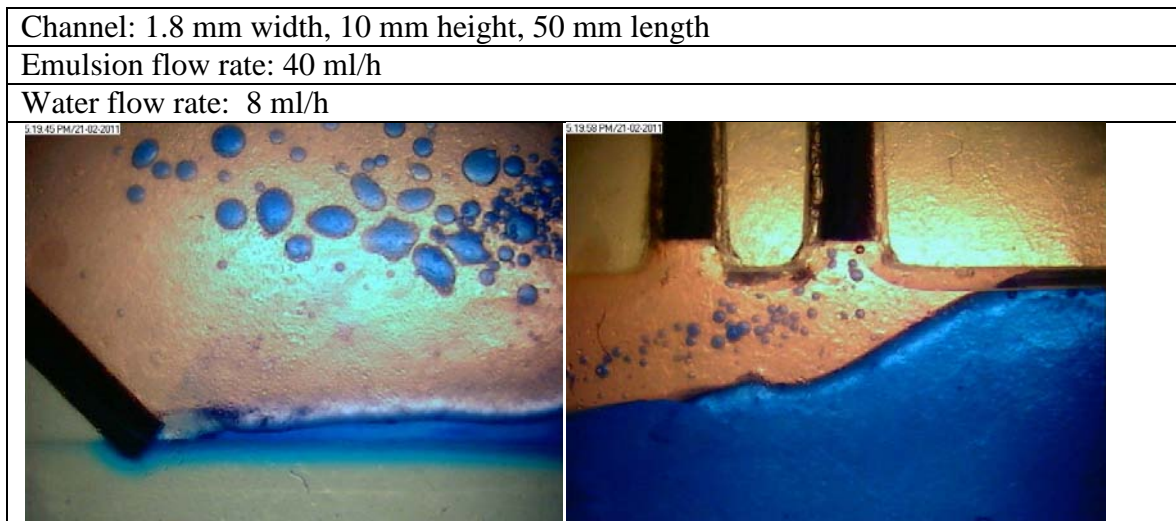| Channel: 1.8 mm width, 6 mm height, 50 mm length |
|---|
| Emulsion flow rate: 140 ml/h |
| Water flow rate: 20 ml/h |

Channel: 1.8 mm width, 6 mm height, 50 mm length
Emulsion flow rate: 160 ml/h
Water flow rate: 15 ml/h

Channel: 1.8 mm width, 10 mm height, 50 mm length
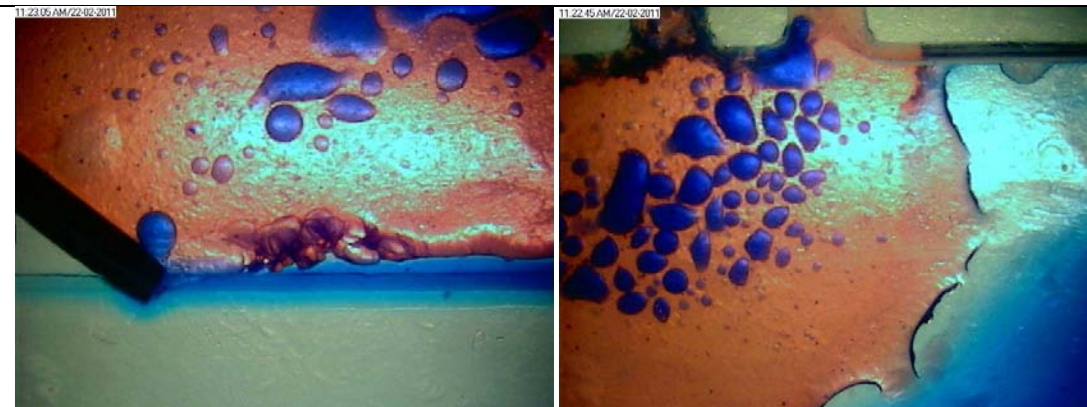
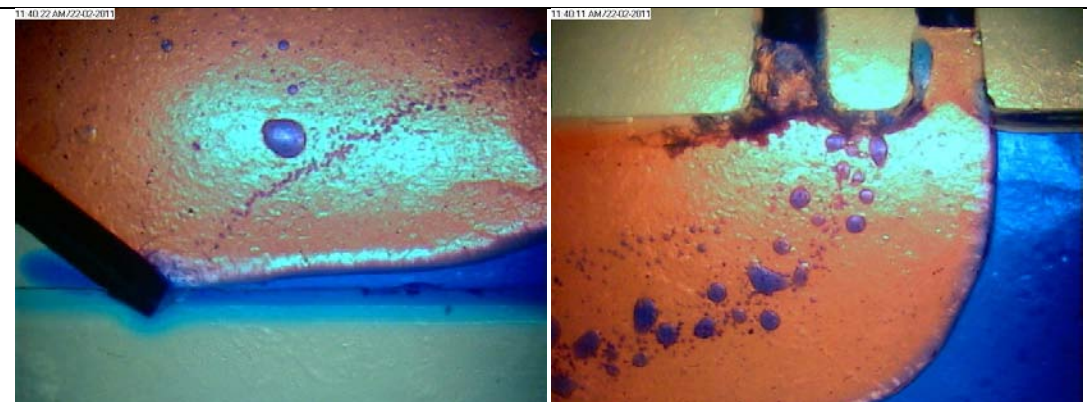| Channel: 1.8 mm width, 10 mm height, 50 mm length |
| --- |
| Emulsion flow rate: 20 ml/h |
| Water flow rate: 10 ml/h |
| |

Channel: 1.8 mm width, 10 mm height, 50 mm length
Emulsion flow rate: 40 ml/h
Water flow rate: 8 ml/h

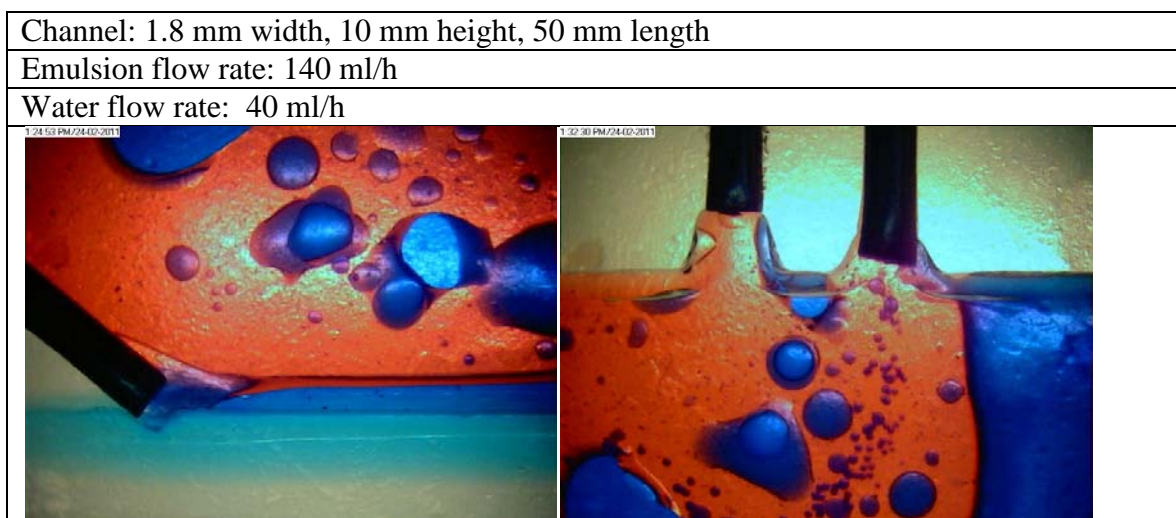| Channel: 1.8 mm width, 10 mm height, 50 mm length |
|---|
| Emulsion flow rate: 60 ml/h |
| Water flow rate: 15 ml/h |
| |

Channel: 1.8 mm width, 10 mm height, 50 mm length
Emulsion flow rate: 80 ml/h
Water flow rate: 15 ml/h

Channel: 1.8 mm width, 10 mm height, 50 mm length
Emulsion flow rate: 100 ml/h
Water flow rate: 5 ml/h

Channel: 1.8 mm width, 10 mm height, 50 mm length
Emulsion flow rate: 120 ml/h
Water flow rate: 20 ml/h

Channel: 1.8 mm width, 10 mm height, 50 mm length
Emulsion flow rate: 140 ml/h
Water flow rate: 40 ml/h

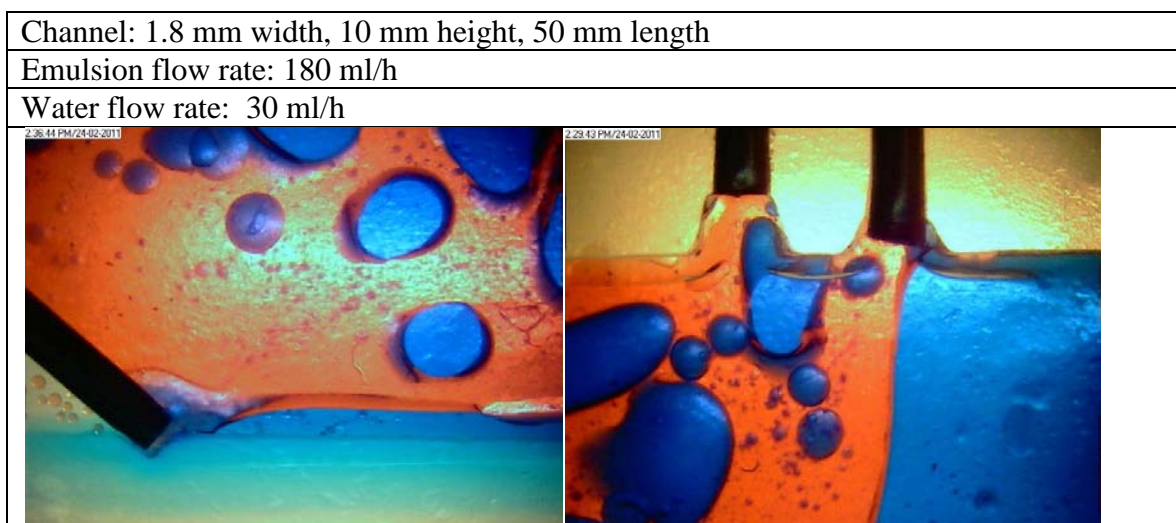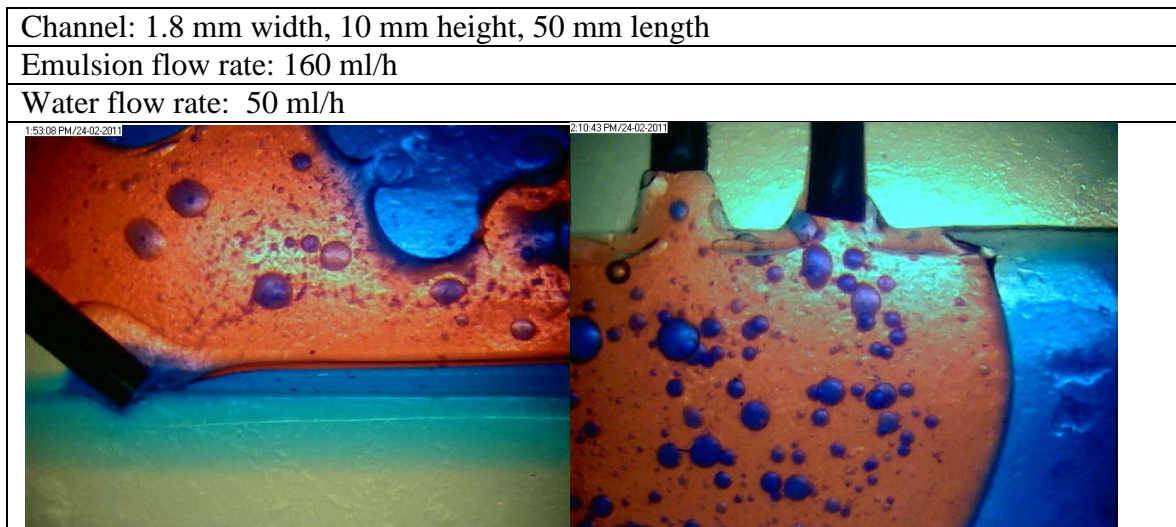| Channel: 1.8 mm width, 10 mm height, 50 mm length |
| Emulsion flow rate: 160 ml/h |
| Water flow rate: 50 ml/h |

| Channel: 1.8 mm width, 10 mm height, 50 mm length |
| Emulsion flow rate: 180 ml/h |
| Water flow rate: 30 ml/h |

Appendix E – Emulsion Separation Scale Up Data

1.2 mm channel width, 3 mm channel height, 50 mm channel length

Channel Width (mm)	Channel Height (mm)	Emulsion Flow Rate (ml/h)	Water Flow Rate (ml/h)	Efficiency	Average Efficiency
1.2	3	2	7	90.91	
1.2	3	2	7	90.91	90.91
1.2	3	2	7	90.91	
1.2	3	10	20	85.45	
1.2	3	10	20	71.82	84.55
1.2	3	10	20	96.36	
1.2	3	20	25	77.27	
1.2	3	20	25	79.55	76.45
1.2	3	20	25	72.53	
1.2	3	30	30	86.36	
1.2	3	30	30	76.83	82.68
1.2	3	30	30	84.85	
1.2	3	40	17	87.50	
1.2	3	40	17	81.33	86.01
1.2	3	40	17	89.20	
1.2	3	50	30	82.18	
1.2	3	50	30	81.21	82.04
1.2	3	50	30	82.73	
1.2	3	80	38	81.53	
1.2	3	80	38	82.95	80.91
1.2	3	80	38	78.25	

1.8 mm channel width, 3 mm channel height, 50 mm channel length

Channel Width (mm)	Channel Height (mm)	Emulsion Flow Rate (ml/h)	Water Flow Rate (ml/h)	Efficiency	Average Efficiency
1.8	3	20	10	77.27	
1.8	3	20	10	83.84	81.73
1.8	3	20	10	84.09	
1.8	3	40	25	87.19	
1.8	3	40	25	90.91	87.85
1.8	3	40	25	85.45	
1.8	3	60	10	85.23	
1.8	3	60	10	82.95	83.84
1.8	3	60	10	83.33	
1.8	3	80	10	84.09	
1.8	3	80	10	81.82	85.61
1.8	3	80	10	90.91	
1.8	3	100	5	84.09	
1.8	3	100	5	82.18	84.45
1.8	3	100	5	87.09	
1.8	3	120	5	79.55	
1.8	3	120	5	82.95	81.44
1.8	3	120	5	81.82	

1.8 mm channel width, 6 mm channel height, 50 mm channel length

Channel Width (mm)	Channel Height (mm)	Emulsion Flow Rate (ml/h)	Water Flow Rate (ml/h)	Efficiency	Average Efficiency
1.8	6	20	10	95.45	
1.8	6	20	10	87.50	91.29
1.8	6	20	10	90.91	
1.8	6	40	10	85.80	
1.8	6	40	10	84.09	85.80
1.8	6	40	10	87.50	
1.8	6	60	10	79.55	
1.8	6	60	10	81.82	82.58
1.8	6	60	10	86.36	
1.8	6	80	20	85.80	
1.8	6	80	20	80.68	85.80
1.8	6	80	20	90.91	
1.8	6	100	20	84.09	
1.8	6	100	20	88.18	87.73
1.8	6	100	20	90.91	
1.8	6	120	20	82.95	
1.8	6	120	20	85.23	84.85
1.8	6	120	20	86.36	
1.8	6	140	20	90.91	
1.8	6	140	20	85.06	84.42
1.8	6	140	20	77.27	
1.8	6	160	15	84.09	
1.8	6	160	15	87.50	84.09
1.8	6	160	15	80.68	

1.8 mm channel width, 10 mm channel height, 50 mm channel length

Channel Width (mm)	Channel Height (mm)	Emulsion Flow Rate (ml/h)	Water Flow Rate (ml/h)	Efficiency	Average Efficiency
1.8	10	20	10	86.36	
1.8	10	20	10	84.09	84.85
1.8	10	20	10	84.09	
1.8	10	40	8	84.09	
1.8	10	40	8	87.50	85.80
1.8	10	40	8	85.80	
1.8	10	60	15	88.64	
1.8	10	60	15	86.36	85.61
1.8	10	60	15	81.82	
1.8	10	80	15	78.98	
1.8	10	80	15	89.20	86.36
1.8	10	80	15	90.91	
1.8	10	100	5	81.82	
1.8	10	100	5	78.18	80.00
1.8	10	100	5	80.00	
1.8	10	120	20	84.09	
1.8	10	120	20	88.64	87.88
1.8	10	120	20	90.91	
1.8	10	140	40	85.06	
1.8	10	140	40	88.96	84.42
1.8	10	140	40	79.22	
1.8	10	160	50	87.50	
1.8	10	160	50	82.39	84.66
1.8	10	160	50	84.09	
1.8	10	180	30	89.39	
1.8	10	180	30	87.88	84.85
1.8	10	180	30	77.27	

Appendix F – Table of Contents for Emulsion Separation Videos

B2b. Outlet of emulsion separation device with oil flow rate: 20 ml/h, aqueous flow rate: 20 ml/h, water flow rate: 25 ml/h

B3a. Inlet of emulsion separation device with oil flow rate: 30 ml/h, aqueous flow rate: 30 ml/h, water flow rate: 10 ml/h

B3b. Outlet of emulsion separation device with oil flow rate: 30 ml/h, aqueous flow rate: 30 ml/h, water flow rate: 10 ml/h

C. Device dimensions of 1.8 mm × 3 mm × 50 mm with crimped aqueous outlet

C1a. Inlet of emulsion separation device with oil flow rate: 40 ml/h, aqueous flow rate: 40 ml/h, water flow rate: 10 ml/h

C1b. Outlet of emulsion separation device with oil flow rate: 40 ml/h, aqueous flow rate: 40 ml/h, water flow rate: 10 ml/h

C2a. Inlet of emulsion separation device with oil flow rate: 50 ml/h, aqueous flow rate: 50 ml/h, water flow rate: 5 ml/h

C2b. Outlet of emulsion separation device with oil flow rate: 50 ml/h, aqueous flow rate: 50 ml/h, water flow rate: 5 ml/h

C3a. Inlet of emulsion separation device with oil flow rate: 60 ml/h, aqueous flow rate: 60 ml/h, water flow rate: 5 ml/h

C3b. Outlet of emulsion separation device with oil flow rate: 60 ml/h, aqueous flow rate: 60 ml/h, water flow rate: 5 ml/h

D. Device dimensions of 1.8 mm × 6 mm × 50 mm with crimped aqueous outlet

D1a. Inlet of emulsion separation device with oil flow rate: 10 ml/h, aqueous flow rate: 10 ml/h, water flow rate: 10 ml/h

D1b. Outlet of emulsion separation device with oil flow rate: 10 ml/h, aqueous flow rate: 10 ml/h, water flow rate: 10 ml/h

D2a. Inlet of emulsion separation device with oil flow rate: 20 ml/h, aqueous flow rate: 20 ml/h, water flow rate: 10 ml/h

D2b. Outlet of emulsion separation device with oil flow rate: 20 ml/h, aqueous flow rate: 20 ml/h, water flow rate: 10 ml/h

D3a. Inlet of emulsion separation device with oil flow rate: 30 ml/h, aqueous flow rate: 30 ml/h, water flow rate: 10 ml/h

D3b. Outlet of emulsion separation device with oil flow rate: 30 ml/h, aqueous flow rate: 30 ml/h, water flow rate: 10 ml/h

D4a. Inlet of emulsion separation device with oil flow rate: 40 ml/h, aqueous flow rate: 40 ml/h, water flow rate: 20 ml/h

D4b. Outlet of emulsion separation device with oil flow rate: 40 ml/h, aqueous flow rate: 40 ml/h, water flow rate: 20 ml/h

D5a. Inlet of emulsion separation device with oil flow rate: 50 ml/h, aqueous flow rate: 50 ml/h, water flow rate: 20 ml/h

D5b. Outlet of emulsion separation device with oil flow rate: 50 ml/h, aqueous flow rate: 50 ml/h, water flow rate: 20 ml/h

D6a. Inlet of emulsion separation device with oil flow rate: 60 ml/h, aqueous flow rate: 60 ml/h, water flow rate: 20 ml/h

D6b. Outlet of emulsion separation device with oil flow rate: 60 ml/h, aqueous flow rate: 60 ml/h, water flow rate: 20 ml/h

D7a. Inlet of emulsion separation device with oil flow rate: 70 ml/h, aqueous flow rate: 70 ml/h, water flow rate: 20 ml/h

D7b. Outlet of emulsion separation device with oil flow rate: 70 ml/h, aqueous flow rate: 70 ml/h, water flow rate: 20 ml/h

D8a. Inlet of emulsion separation device with oil flow rate: 80 ml/h, aqueous flow rate: 80 ml/h, water flow rate: 15 ml/h

D8b. Outlet of emulsion separation device with oil flow rate: 80 ml/h, aqueous flow rate: 80 ml/h, water flow rate: 15 ml/h

E. Device dimensions of 1.8 mm × 10 mm × 50 mm with crimped aqueous outlet

E1a. Inlet of emulsion separation device with oil flow rate: 10 ml/h, aqueous flow rate: 10 ml/h, water flow rate: 10 ml/h

E1b. Outlet of emulsion separation device with oil flow rate: 10 ml/h, aqueous flow rate: 10 ml/h, water flow rate: 10 ml/h

E2a. Inlet of emulsion separation device with oil flow rate: 20 ml/h, aqueous flow rate: 20 ml/h, water flow rate: 8 ml/h

E2b. Outlet of emulsion separation device with oil flow rate: 20 ml/h, aqueous flow rate: 20 ml/h, water flow rate: 8 ml/h

E3a. Inlet of emulsion separation device with oil flow rate: 30 ml/h, aqueous flow rate: 30 ml/h, water flow rate: 15 ml/h

E3b. Outlet of emulsion separation device with oil flow rate: 30 ml/h, aqueous flow rate: 30 ml/h, water flow rate: 15 ml/h

E4a. Inlet of emulsion separation device with oil flow rate: 40 ml/h, aqueous flow rate: 40 ml/h, water flow rate: 15 ml/h

E4b. Outlet of emulsion separation device with oil flow rate: 40 ml/h, aqueous flow rate: 40 ml/h, water flow rate: 15 ml/h

E5a. Inlet of emulsion separation device with oil flow rate: 50 ml/h, aqueous flow rate: 50 ml/h, water flow rate: 5 ml/h

E5b. Outlet of emulsion separation device with oil flow rate: 50 ml/h, aqueous flow rate: 50 ml/h, water flow rate: 5 ml/h

E6a. Inlet of emulsion separation device with oil flow rate: 60 ml/h, aqueous flow rate: 60 ml/h, water flow rate: 20 ml/h

E6b. Outlet of emulsion separation device with oil flow rate: 60 ml/h, aqueous flow rate: 60 ml/h, water flow rate: 20 ml/h

E7a. Inlet of emulsion separation device with oil flow rate: 70 ml/h, aqueous flow rate: 70 ml/h, water flow rate: 40 ml/h

E7b. Outlet of emulsion separation device with oil flow rate: 70 ml/h, aqueous flow rate: 70 ml/h, water flow rate: 40 ml/h

E8a. Inlet of emulsion separation device with oil flow rate: 80 ml/h, aqueous flow rate: 80 ml/h, water flow rate: 50 ml/h

E8b. Outlet of emulsion separation device with oil flow rate: 80 ml/h, aqueous flow rate: 80 ml/h, water flow rate: 50 ml/h

E9a. Inlet of emulsion separation device with oil flow rate: 90 ml/h, aqueous flow rate: 90 ml/h, water flow rate: 30 ml/h

E9b. Outlet of emulsion separation device with oil flow rate: 90 ml/h, aqueous
flow rate: 90 ml/h, water flow rate: 30 ml/h